# Regulation and Function of CD70 and its Clinical Relevance in Clear Cell Renal Cell Carcinoma

**Dissertation**
zur Erlangung der naturwissenschaftlichen Doktorwürde
(Dr. sc. nat.)

vorgelegt der
Mathematisch-naturwissenschaftlichen Fakultät
der Universität Zürich
von

**Melanie Ruf**

aus Deutschland

Promotionskomitee

Prof. Dr. Burkhard Becher (Vorsitz)
Prof. Dr. Holger Moch (Leitung der Dissertation)
Dr. Peter Schraml
Prof. Dr. Bernd Wollscheid
Prof. Dr. Lukas Sommer

Zürich 2015

*meiner Familie*

# Content

1 Abbreviations ..... 1

2 Summary ..... 3

3 Zusammenfassung ..... 4

4 Introduction ..... 6

4.1 Renal cell carcinoma is the most frequent malignancy of kidneys ..... 6

4.1.1 RCC subtypes are classified by their morphologic appearance ..... 7

4.1.2 Diagnosis, prognosis and treatment of RCC ..... 9

4.2 The Von Hippel-Lindau gene is frequently inactivated in ccRCC ..... 11

4.2.1 HIF stabilization due to inactivated pVHL drives tumorigenesis in ccRCC ..... 11

4.2.2 HIF controls metabolic reprogramming in ccRCC ..... 12

4.3 Biomarkers for RCC ..... 13

4.3.1 New biomarker candidates by ccRCC-specific surfaceome identification ..... 14

4.4 Expression and function of CD70, a tumor necrosis factor ligand ..... 14

4.4.1 Aberrant CD70 expression in cancers ..... 16

5 Objectives ..... 19

6 Results ..... 20

6.1 CD70 is regulated by pVHL and enhances sCD27 release in ccRCC ..... 20

6.1.1 CD70 is frequently expressed in primary ccRCC and ccRCC metastasis ..... 20

6.1.2 CD70 is highly glycosylated in RCC cell lines ..... 22

6.1.3 CD70 expression and *VHL* mutation status in ccRCC tissues and cell lines. ..... 23

6.1.4 CD70 expression is regulated by the pVHL/HIF axis in RCC tissue and cell lines .. 26

6.1.5 CD70 expression is directly regulated by HIF ..... 29

6.1.6 CD70 is not regulated by hypermethylation of its promoter in RCC ..... 30

6.1.7 The CD70 receptor, CD27, is strongly expressed in RCC infiltrating lymphocytes 32

6.1.8 $CD27^{+}$ lymphocytes preferentially infiltrate CD70-expressing tumors which correlates with worse patient outcome ..... 33

6.1.9 PBMCs trigger the release of sCD27 in a CD70-dependent manner ..... 34
6.1.10 Soluble CD27 levels are elevated in sera of patients with CD70-expressing RCC. 35
6.1.11 Chronic CD70 /CD27 interaction in RCC leads to T cell exhaustion ..... 37
6.2 PTPRJ is negatively regulated by the pVHL/HIF axis in RCC ..... 41
6.3 The tumor progression suppressor TGF-βRIII increases with tumor progression in the sera of RCC patients ..... 42
7 Discussion ..... 44
7.1 CD70 is regulated by the pVHL/HIF axis in ccRCC ..... 44
7.1.1 The high and frequent expression of CD70 in ccRCC is unique among RCC and other solid tumors ..... 44
7.1.2 CD70 is linked to the *VHL* mutation state ..... 45
7.1.3 CD70 is regulated by the pVHL/HIF axis in ccRCC ..... 46
7.1.4 HIF acts as a transcription factor, activating the expression of CD70 ..... 47
7.1.5 CD70 expression is not regulated by hypomethylation of its promoter in RCC ... 47
7.1.6 CD70 posttranslational modification is potentially organ-specific ..... 47
7.2 $CD27^+$ tumor infiltrating lymphocytes in CD70-expressing ccRCCs ..... 48
7.2.1 CD70 attracts $CD27^+$ tumor infiltrating lymphocytes in RCC ..... 48
7.2.2 Continuous CD70/CD27 interaction promotes tumor progression in ccRCC ..... 48
7.2.3 CD27 does not induce RCC cell proliferation *in vitro* ..... 49
7.2.4 CD27 does most likely not mediate apoptosis of TILs of RCC *in vivo* ..... 49
7.2.5 Continuous T cell activation leads to T cell exhaustion ..... 49
7.3 CD70/CD27 interaction triggers the release of sCD27 ..... 51
7.4 PTPRJ is negatively regulated by the pVHL/HIF axis in RCC ..... 53
7.5 TGF-βRIII, a promising serum marker for tumor progression in RCC ..... 54
8 Conclusion ..... 55
9 Materials and Methods ..... 57
9.1 Patient material ..... 57

9.2 Immunohistochemistry ..... 58
9.3 *VHL* mutation analysis ..... 59
9.4 Gene expression analysis ..... 59
9.5 Cell lines ..... 59
9.6 Immunofluorescence ..... 60
9.7 Immunoblot analysis ..... 60
9.8 Transient transfections ..... 61
9.9 Quantitative real time-PCR ..... 62
9.10 Chromatin immunoprecipitation ..... 62
9.11 Luciferase gene reporter assay ..... 63
9.12 Molecular cloning ..... 64
9.13 Bisulfite sequencing ..... 65
9.14 Determination of sCD27 in cocultures and sera of RCC patients ..... 65
9.15 Statistical and computational analyses ..... 66
10 Annex ..... 67
11 References ..... 89
12 Curriculum vitae ..... 103
13 Acknowledgements ..... 105

# 1 Abbreviations

| | |
|---|---|
| **2-OG** | 2-oxoglutarate |
| **3p** | shorter arm of chromosome 3 |
| **5'azaC** | 5-azacytidine |
| ***AKT*** | gene encoding protein kinase B |
| **ALCAM** | activated leukocyte cell adhesion molecule |
| **AMPK** | 5' adenosine monophosphate-activated protein kinase |
| **APC** | antigen-presenting cell |
| **AQUA** | automated quantitative analysis |
| **Asn** | Asparagine |
| **ATCC** | American type culture collection |
| **BATF** | basic leucine zipper transcription factor, ATF-like |
| **BHD** | Birt-Hogg-Dubé |
| **bHLH** | basic helix-loop-helix domain |
| **bp** | base pairs |
| **BSA** | bovine serum albumin |
| **CA-IX** | carbonic anhydrase 9 |
| **cc-pap** | clear cell papillary |
| **ccRCC** | clear cell renal cell carcinoma |
| **CD** | cluster of differentiation |
| **CD244** | natural killer cell receptor 2B4 |
| **CD57** | galactosylgalactosylxylosylprotein 3-beta-glucuronosyltransferase 1 |
| **cDNA** | complementary DNA |
| **ChIP** | chromatin immuno precipitation |
| **chromo** | Chromophobe |
| **c-Jun** | transcription factor |
| **CpG** | cytosine-phosphate-guanine |
| **CRP** | C-reactive protein |
| **CT** | computer scanning |
| **Cul2** | Cullin-2 |
| **DAPI** | 4',6-diamidino-2-phenylindole |
| **DMEM** | Dulbecco's modified Eagle's medium |
| **DNA** | deoxyribonucleic acid |
| **DTT** | dithiothreitol |
| ***E. coli*** | Escherichia coli |
| **E3** | ubiquitin ligase |
| **ECL** | Enhanced chemiluminescence |
| **EDTA** | ethylenediaminetetraacetic acid |
| **EGFR** | epidermal growth factor receptor |
| **ELISA** | enzyme-linked immunosorbent assay |
| ***EPAS*** | gene encoding HIF2α |
| **EPHA2** | ephrin type-A receptor 2 |
| **FH** | fumarate hydratase |
| **fi** | functional impact |
| ***FLCN*** | gene encoding folliculin |
| **FNIP** | protein binding to folliculin |
| **GFP** | green fluorescent protein |
| **Glut-1** | glucose transporter 1 |
| **HA** | influenza hemagglutinin |
| **HAF** | hypoxia-associated factor |
| **HCl** | hydrogen chloride |
| **HEK** | human embryonic kidney |
| **HGF-R** | hepatocyte growth factor receptor |
| **HIF** | hypoxia-inducible factor |
| **HRE** | hypoxia response element |
| **HRP** | horseradish peroxidase |
| **hypo** | hypoxia |
| **IFN** | interferon |
| **IGF2R** | insulin-like growth factor 2 receptor |
| **IHC** | immunohistochemistry |
| **IL** | interleukin |
| **IMP3** | U3 small nucleolar ribonucleoprotein |
| **kb** | kilo bases |
| **KCNJ5** | G protein-activated inward rectifier potassium channel 4 |
| **kDa** | kilo dalton |
| **Ki-67** | antigen KI-67 |
| **KLRG1** | Killer cell lectin-like receptor subfamily G member 1 |
| **kzNZK** | klarzelliges NZK |
| **LB** | lysogeny broth |
| **LKB** | serine/threonine kinase |
| **lof** | loss of function |
| ***MET*** | gene encoding hepatocyte growth factor receptor |
| **met** | metastatic |
| **miR** | microRNA |
| **MOPS** | 3-(N-morpholino)propansulfonic acid |
| **mRNA** | messenger RNA |
| **ms** | missense |
| **mTOR** | mammalian target of rapamycin |
| **MTORC** | mTOR complex |
| **MTT** | tetrazolium dye |
| **mut** | mutated |
| **MYC** | regulator gene |
| **NaCl** | sodium chloride |

| | |
|---|---|
| **NK** | natural killer |
| **NRC-1** | non-papillary renal carcinoma 1 |
| **N-TAD** | amino terminal TAD |
| **NZK** | Nierenzellkarzinom |
| ***OCT4*** | gene encoding octamer-binding transcription factor 4 |
| **OD** | optical density |
| **ODD** | oxygen-dependent degradation domain |
| **OH** | hydroxyl group |
| **P2P** | *PHD2* promoter construct |
| **p53** | tumor protein p53 |
| **pap** | Papillary |
| **PAS** | PER-ARNT-SIM |
| **PBMC** | peripheral blood mononuclear cells |
| ***PBRM1*** | gene encoding protein polybromo-1 |
| **PBS** | phosphate buffered saline |
| **PCR** | polymerase chain reaction |
| **PD1** | programmed cell death protein 1 |
| **PDGF** | platelet derived growth factor |
| **PDGFR** | PDGF receptor |
| ***PDK1*** | gene encoding pyruvate dehydrogenase lipoamide kinase isozyme 1 |
| **PD-L1** | programmed death-ligand 1 |
| **PHD** | prolyl hydroxylase |
| **PI3K** | phosphatidylinositol-4,5-bisphosphate 3-kinase |
| **PKB** | protein kinase B |
| **pM** | pathologic examination of a metastasis |
| **pN** | pathologic examination of a lymph node |
| **postOP** | after surgery |
| **PPIA** | peptidylprolyl isomerase A |
| **Pro** | Proline |
| **pT** | pathologic examination of a tumor |
| ***PTEN*** | gene encoding phosphatase and tensin homolog |
| **PTPRJ** | protein tyrosine phosphatase receptor J |
| **pVHL** | Von Hippel-Lindau protein |
| **qPCR** | quantitative real-time PCR |
| ***RASST1a*** | gene encoding Ras association domain-containing protein 1a |
| **Rbx1** | ring box protein 1 |
| **RCC** | renal cell carcinoma |
| **rcf** | relative centrifugal force |
| **RCGTC** | core sequence of a HRE |
| **Rheb** | Ras homolog enriched in brain |
| **rHRE** | reverse HRE |
| **RNA** | ribonucleic acid |
| **RPMI** | Roswell Park Memorial Institute medium |
| **rpm** | rounds per minute |
| **sCD27** | soluble CD27 |
| **SD** | standard deviation |
| ***SDH*** | gene encoding succinate dehydrogenase |
| **SDM** | site director mutator |
| **SDS** | sodium dodecyl sulfate |
| **SEER** | Surveillance, Epidemiology, and End Results Program |
| **Ser** | serine |
| **siRNA** | silencer RNA |
| **siScr** | siScramble |
| **Siva1** | apoptosis regulatory protein |
| **SNG-75** | CD70 targeting drug-conjugated antibody |
| **SRM** | small renal mass |
| **TAD** | transactivation domain |
| **TAE** | Tris base, acetic acid and EDTA. |
| **T-BET** | T-box transcription factor TBX21 |
| **TBS-T** | Tris-buffered saline containing Tween |
| **TCEB1** | gene encoding elongin C |
| **TCEP** | tris(2-carboxyethyl)phosphine |
| **TCR** | T cell receptor |
| **TFB** | transforming buffer |
| **TGF-βRIII** | transforming growth factor beta receptor 3 |
| **Thr** | threonine |
| **TIL** | tumor inflitrating lymphocytes |
| **TLR** | toll-like receptor |
| **TMA** | tissue microarray |
| **TNF** | tumor necrosis factor |
| **TNM** | tumor, lymphnode and metastasis |
| ***TP53*** | gene encoding tumor protein p53 |
| **TRACK** | transgenic model of cancer of the kidney |
| **TRAF** | TNF receptor-associated factor |
| **TSC** | tuberous sclerosis complex |
| **ub** | ubiquitin |
| **US** | United States |
| **VEGF** | vascular endothelial growth factor |
| **VEGFR** | VEGF receptor |
| ***VHL*** | Von Hippel-Lindau gene |
| **WNT** | signaling pathway |
| **wt** | wild type |

# 2 Summary

As treatment response for advanced renal cell carcinoma (RCC) is still limited, biomarkers to diagnose and predict the applicability of drugs are needed. The deregulation of the Von Hippel-Lindau protein (pVHL)/hypoxia-inducible factor (HIF) axis is a hallmark of clear cell RCC (ccRCC). Consequently, protein products of HIF-regulated genes are considered potential therapeutic targets of this tumor type. In a previous work mass spectrometry analysis of RCC cell lines was used to define the ccRCC protein surfaceome. The expression pattern of these proteins was further validated on mRNA level. The overall objective of my PhD project was to select and analyse potential candidates of the RCC surfaceome for clinical applications. We focused our interest on the mechanism of the aberrant and frequent upregulation of CD70 in ccRCC. Since the discovery of the frequent overexpression of CD70 ccRCC in 2005, therapeutic antibodies targeting CD70 were developed, which are already under clinical evaluation. However, studies elucidating the regulation of the CD70 expression in RCC and the consequences of the constant interaction of CD70 with its unique receptor CD27 within the tumor microenvironment, are lacking. Immunohistochemical analyses of 667 RCC revealed elevated CD70 protein expression in 80% of primary tumors and metastases of ccRCC and in 32% of papillary RCC. We have found that in ccRCC abundant and frequent CD70 expression is directly driven by HIF. By analyzing *VHL* mutations, mRNA and protein expression patterns of pVHL, HIFα and several HIF targets in RCC tissues and cell lines, we found that CD70 upregulation is linked to the inactivation of pVHL. Reexpression of pVHL in pVHL-deficient cell lines as well as silencing of HIFα lead to attenuated CD70 expression, whereas transient overexpression of HIFα and hypoxia lead to increased CD70. Gene promoter analyses revealed that HIF directly binds to specific hypoxia response elements within the promoter of *CD70* thereby activating its transcription. Furthermore, $CD27^+$ lymphocytes preferentially infiltrate CD70-expressing ccRCCs, which seems to be linked to a more aggressive biological behavior. Coculturing of RCC cell lines with peripheral blood mononuclear cells induced significant increase of soluble CD27 levels in the presence of CD70. This may explain the high soluble CD27 levels observed in the sera of patients with CD70-expressing ccRCC infiltrated by $CD27^+$ lymphocytes, thus suggesting soluble CD27 as diagnostic tool for ccRCC patient monitoring.

# 3 Zusammenfassung

Aufgrund des begrenzten Behandlungserfolgs von fortgeschrittenem Nierenzellkarzinom (NZK), bedarf es Biomarkern zur Diagnose und Prognose der Anwendbarkeit von Medikamenten. Die Aufhebung der „Von Hippel-Lindau-Protein (pVHL)/ Hypoxie-induzierbarer Faktor (HIF)"-Achse ist ein Merkmal des klarzelligen NZK (kzNZK). Daraus ergibt sich die Möglichkeit, dass Gene, die von HIF gesteuert werden als therapeutische Ziele für diese Tumorart genutzt werden können. In einer früheren Arbeit wurde das Oberflächenproteom des kzNZK durch eine massenspektrometrische Analyse definiert. Das Expressionsmuster dieser Proteine wurde weiterhin auf mRNA-Ebene validiert. Das Hauptanliegen meines PhD-Projektes lag in der Auswahl und Analyse potentieller Kandidaten des NZK-Oberflächenproteoms für deren klinische Anwendbarkeit. Wir richteten unser Interesse auf die Ursache der häufigen und fehlgeleiteten Überexpression von CD70 im kzNZK. Seit der Entdeckung der hohen und häufigen CD70-Expression im kzNZK im Jahre 2005 wurden CD70-zielgerichtete therapeutische Antikörper entwickelt, die schon klinisch getestet werden. Dennoch gibt es keine Studien, die veranschaulichen, wodurch die kontinuierliche Hochregulierung von CD70 im NZK gesteuert wird und was die Folgen der konstanten Interaktion von CD70 mit seinen einzig bekannten Rezeptor CD27 für die nahe Umgebung des Tumors sind. Immunhistochemische Analysen von 667 NZK ergaben eine erhöhte CD70-Expression in 80% der Primärtumoren und Metastasen des kzNZK und in 32% des papillären NZK. Wir haben herausgefunden, dass die hohe und häufige Expression von CD70 im kzNZK direkt durch HIF angetrieben wird. Durch die Analyse der *VHL*-Mutationen, der mRNA- und Protein-Expressionsmuster von pVHL, HIFα und verschiedener HIF-gesteuerter Gene in NZK-Gewebe und -Zelllinien, haben wir entdeckt, dass CD70 mit der Inaktivierung von pVHL verknüpft ist. Die Wiederexpression von pVHL in pVHL-defizienten Zelllinien als auch das Gen-Silencing von HIFα führten zu einer Abschwächung der CD70-Expression, wohingegen eine vorübergehende Überexpression von HIFα und Hypoxie CD70 erhöhten. Genepromoter-Analysen legten dar, dass HIF direkt an spezifische Hypoxie-Antwort-Elemente innerhalb des Promoters von *CD70* bindet und dadurch dessen Transkription auslöst. Des Weiteren infiltrieren $CD27^+$ Lymphozyten bevorzugt CD70-expreimierende kzNZK, was mit einem vermehrt aggressiven biologischen Verhalten zusammenzuhängen scheint. Kokultivierung von NZK-Zelllinien mit mononukleären Zellen des periphären Blutes induzierten einen signifikanten Anstieg der gelösten CD27-Menge an Anwesenheit von CD70. Dies könnte die

Ursache der erhöhten gelösten CD27-Mengen im Blutserum von Patienten mit CD70-exprimierenden NZK, die von $CD27^+$ Lymphozyten infiltriert sind, sein. Deshalb ist der Einsatz von gelöstem CD27 als diagnostisches Instrument für die kzNZK-Patientenbeobachtung denkbar.

# 4 Introduction

## 4.1 Renal cell carcinoma is the most frequent malignancy of kidneys

Renal cell carcinoma (RCC) is the most frequent malignancy of adult kidneys (87%) and accounts for 2-3% of all cancers [1, 2]. The remainder are 11% urothelial carcinomas of the renal pelvis and rare others (2%) [3]. Being the 9th most common cancer in men, RCC occurs about twice as often in men than in women, being the 14th most common cancer [4, 5]. With 6,910 cases more than three years before the incidence of RCC has risen to 65,150 new estimated cases in the US in 2013 [6, 7]. With 30-40% patients dying due to the disease [3], RCC ranks as the 16th most common cause of death from cancer [4]. Despite the increase of RCC in the last decades, the incidence has peaked and the mortality rate has stabilized in highly developed countries [4, 8] (Fig. 1A). Seventy percent of RCC occur in more developed countries from Europe, North America and Australia, of which Czech Republic is the country with the highest incidence [9]. The incidence of RCC increases consistently with age, peaking at 60-70 years and reaching a plateau at age 70-75 [5] (see also fig. 1B). Risk factors are smoking, obesity, hypertension and germline mutations in specific genes [10]. Smoking increases the risk by 50% in male and by 20% in female [11]. Obesity increases the risk by 24% in male and 34% in female [12]. In familial cases (2-5% of all cases) mutations in 19 genes, e.g. Von Hippel-Lindau gene (*VHL*), *PBRM1*, *PTEN*, molecular target of rapamycin (*MTOR*) and *TP53*, have been discovered to be significantly relevant [13]. Consumption of fruits and vegetables can decrease the risk [14]. Despite improved imaging techniques and 50% incidental diagnosis, 20-30% of patients already present with metastatic RCC at the time of diagnosis [15]. Additional 20% of patients will relapse after nephrectomy [16].

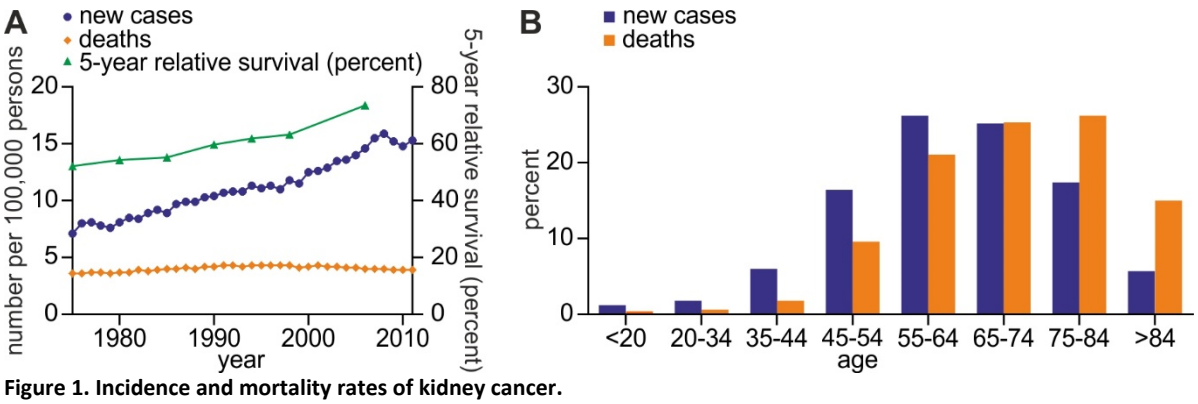


**Figure 1. Incidence and mortality rates of kidney cancer.**

A) Number of new cases and deaths of kidney cancer per 100,000 persons and 5-year relative survival age-adjusted and based on the US population. B) Percent of new cases and deaths of kidney cancer by age group. Source: SEER Cancer Statistics Factsheets: Kidney and Renal Pelvis Cancer. National Cancer Institute. Bethesda, MD, http://seer.cancer.gov/statfacts/html/kidrp.html

### 4.1.1 RCC subtypes are classified by their morphologic appearance

A renal tumor was documented for the first time in 1613 [3]. Since then the classification of RCCs is continuously evolving [17]. RCC can be distinguished by histopathologic features and underlying gene mutations [13]. The World Health Organization divides RCC in three major histological entities: 75-80% clear cell RCC (ccRCC), 10-15% papillary RCC and 4-5% chromophobe RCC [3, 18] (Fig. 2 and table 1). Most syndromes are sporadic, only 3-5% are familial and result from autosomal dominant mutations [19, 20]. Most genes are involved in regulating cellular metabolism leading to the "Warburg effect" [21]. Each of the known kidney cancer genes is involved in pathways that respond to metabolic stress as energy, nutrient, iron and oxygen sensing (Fig. 3A).

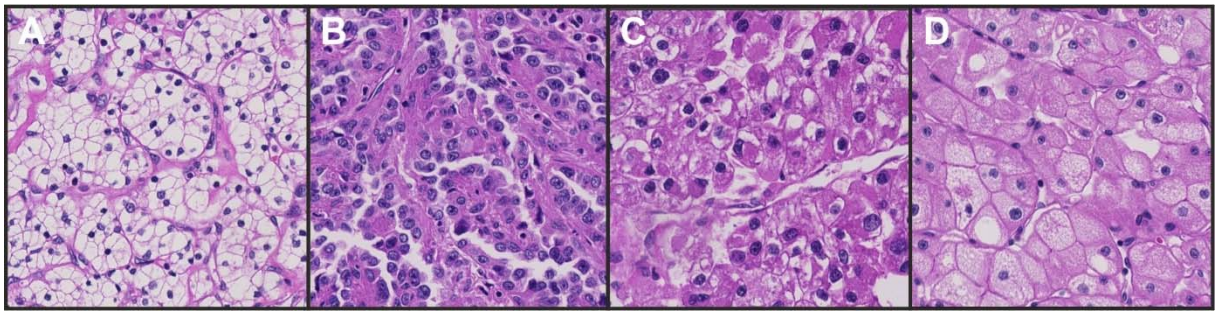


**Figure 2. Histology of the major RCC subtypes.**

A) Hematoxylin and eosin tained ccRCC, B) papillary RCC type 1, C) papillary RCC type 2 and D) chromophobe RCC. 40x magnification.

**Table 1. RCC major subtypes.** Adapted from Bhatt and Finelli, 2014; Moch, 2013 and Lopez-Beltran *et al.*, 2009 [3, 17, 22].

| RCC subtype | Inci-dence | Development | Cell/tissue characteristics | Growth pattern | Prognosis | Cell of origin | Genes for familial type | Protein |
|---|---|---|---|---|---|---|---|---|
| clear cell | 75-80% | solitary, rare multicentric or bilateral | clear cytoplasm due to high glycogen and lipid content | solid, tubular, cystic, rare papillae | aggressiveness according to grade, stage and sarcomatoid change | proximal tubule | *VHL* (3p25 deletion) | pVHL |
| papillary | 10-15% | multicentric, bilateral or solitary | type 1 (basophilic) or type 2 (eosinophilic) | tubulo-papillary, solid | Aggressiveness according to grade, stage and sarcomatoid change | proximal tubule | *MET* (7p31): type 1 *FH* (1q42): type 2 | MET HGF-R fumarate hydratase |
| chromophobe | 4-5% | solitary | pale or eosinophilic granular cytoplasm | solid | 10% mortality | intercalated cells of distal nephron and collecting tubule | *BHD* (17p11) | folliculin |

All kidney tumors of the clear cell type are considered malignant, independent of the size [23]. Clear cell RCC metastasizes late, even after 10 years and to unusual sites [22]. Most appear as solitary neoplasms [24] with a yellow surface due to high lipid content, which is dissolved during histologic processing, creating a clear cytoplasm surrounded by a cell membrane [25]. Genotyping is the tool of choice for further differentiation. The most typical genetic alteration in ccRCC is chromosomal 3p deletion. Lost genes include *VHL*, *RASSF1α* and *NRC-1* [22]. The most common inherited syndrome is the Von Hippel-Lindau-syndrome [25]. The biallelic *VHL* inactivation on chromosome 3p occurs as an initiating event in more than 90% of ccRCCs [26]. The *VHL* protein is a component of oxygen and iron sensing pathway that regulates the hypoxia-inducible factor (HIF) [21]. Two key pathways are essential to the pathophysiology of ccRCCs: the hypoxia-inducible pathway associated with frequent mutations in the *VHL* suppressor gene and the mTOR signaling pathway [27] (Fig. 3A, B).

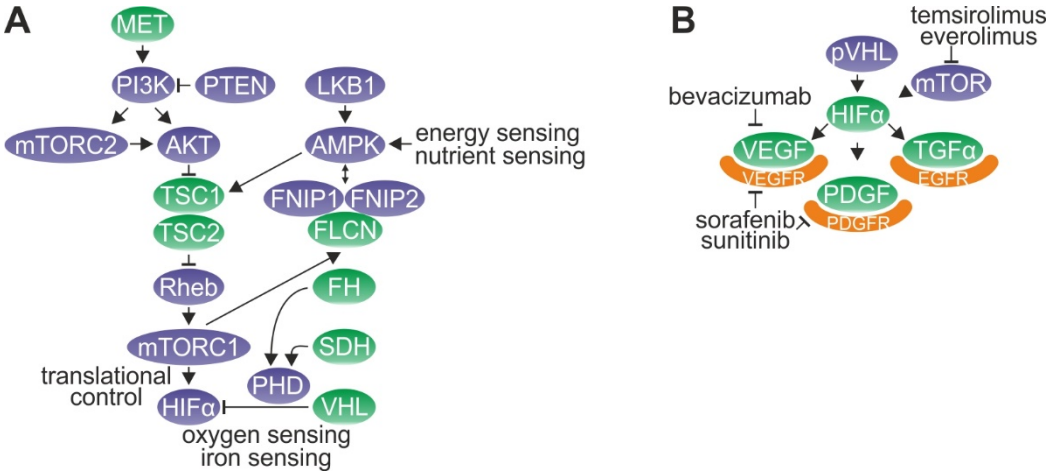


**Figure 3. Kidney cancer pathways and targeted treatment options.**

A) Adapted from Linehan *et al.*, 2010b [28]. The kidney cancer genes *MET* (receptor tyrosine kinase), *TSC1*, *TSC2* (tuberous sclerosis complex 1 and 2), *FLCN* (or *BHD*: folliculin), *FH* (fumarate hydratase), *SDH* (succinate dehydrogenase) and *VHL* are involved in energy, nutrient, oxygen and iron sensing (green). B) Adapted from Linehan *et al.*,2010b [28]. mTOR and the HIF-targets VEGF or their receptors VEGFR and PDGFR are therapy targets for RCC.

Papillary RCC is characterized by epithelial cells forming papillae and tubules [22]. There are variable proportions of papillae [23]. Papillae contain a fibrovascular core with aggregates of foamy macrophages [29]. Type 1 papillary RCC, previously termed as basophilic, appears more often multifocal and its papillae are covered by small cells with scanty cytoplasm arranged in a single layer. The tumor cells of type 2 papillary RCC, previously termed as eosinophilic, have a higher nuclear grade, eosinophilic cytoplasm and stratified nuclei [30]. Hereditary papillary

RCC is characterized by mutations in the proto-oncogene *MET*, which is is rare in the sporadic type [31]. Hepatocyte growth factor (HGF)-MET signalling affects the LKB1-AMTK energy sensing pathway [21] (Fig. 3A). The earliest karyotypic changes of the sporadic type are trisomy or tetrasomy of chromosome 7, trisomy of chromosome 17 and loss of chromosome 4 [32, 33].

Chromophobe RCC derives from intercalated cells of the collecting duct and consists of huge, pale cells with reticulated cytoplasm and prominent cell membrane [23]. Altered mitochondria and loss of multiple chromosomes (1, 2, 6, 10, 13, 17, 21, X, Y) are characteristic [34]. The FLCN (or BHD, folliculin) pathway is affected in the hereditary type of chromophobe RCC [21] (Fig. 3A). Since benign oncocytomas have only rearrangements in 11q13 or partial losses of chromosomes 1, 14, X, Y, they are considered to be the origin of chromophobe RCCs [35].

### 4.1.2 Diagnosis, prognosis and treatment of RCC

The number of incidentally diagnosed RCCs have risen because of improved imaging techniques [3]. CT scanning remains the standard test for diagnosis. Eighty to eighty-five percent of small renal masses (SRM) of more than 4 cm are RCCs per definition [36]. In addition, biopsies have gained diagnostic accuracy of more than 80% [37]. Together, these advanced diagnostic tools made it possible that more low-grade RCCs with low malignant potential are being found [3].

In RCC many parameters have been tested for prognostic significance, but only a few achieved widespread acceptance [38, 39]. The tumor, nodes and metastasis (TNM) staging differentiates patients with tumor thrombi from those with local nodal disease [40]. Although TNM staging is still the most powerful prognostic indicator for RCC [38], it is not optimal for predicting the long term course of the disease. The overall concordance rate is 58-73% and not significant for papillary RCC [41]. Fuhrman grading is being used for all RCC subtypes, but seems not to be the appropriate grading system for non-clear cell types [42]. A more recent factor, the invasion of the sinus fat tissue, is associated with a more aggressive tumor [43]. In addition, patient performance status, tumor burden (number of metastatic sites, anemia and disease-free intervals), proinflammatory markers (C-reactive protein (CRP) and

thrombocytosis) and treatment-related factors can discriminate patients having a favourable, intermediate and poor prognosis [44].

**Table 2. Pathological TNM classification of RCC.** Adapted from Moch *et al.*, 2009 [38].

| staging | classification | tumor size/extension |
|---|---|---|
| localized RCC | pT1a | tumor ≤4 cm, limited to kidney |
| | pT1b | tumor >4 cm and ≤7 cm, limited to kidney |
| | pT2 | tumor >7 cm, limited to kidney |
| locally advanced RCC | pT3 | tumor extends into major veins or invades adrenal or perinephric tissues but not beyond Gerota fascia |
| | pT3a | perinephric or sinus fat or adrenal extension |
| | pT3b | renal vein or vena cava involvement below diaphragm |
| | pT3c | vena cava involvement above diaphragm |
| | pT4 | vena cava involvement above diaphragm |
| regional lymph nodes | pNx | regional lymph node cannot be assessed |
| | pN0 | no regional lymph node metatases |
| | pN1 | metastases in one regional lymph node |
| | pN2 | metastases in more than one regional lymph node |
| distant metastases | pMx | distant metastases cannot be assessed |
| | pM0 | no distant metastases |
| | pM1 | distant metastases |

Curative treatment of noninvasive cancers confined to the kidney (localized RCCs) can be achieved by nephrectomy. Besides this, active surveillance can be used for patients, who are unfit for surgery or have a limited life expectancy [3]. Nephron-sparing (partial) nephrectomy is the standard treatment for pT1 (≤7 cm) tumors to preserve renal function, prevent chronic kidney disease and reduce overtreatment of benign tumors. More cardiovascular events and higher mortality are associated with radical nephrectomy [45]. However, it remains the standard treatment of larger tumors (>pT2). Thermal ablation presents an alternative for only selected patients, whose renal tumors are not in close proximity to susceptible organs. Ten percent of RCCs invade the venous system [3]. The treatment of advanced kidney cancer is a big challenge. Surgery prolongs survival in the absence of positive lymph node or distant metastasis [46, 47]. Positive lymph nodes reduce the 3-year overall survival from 66% to 12% [48]. Adjuvant cytokines (high dose interleukin (IL)-2) failed to show survival benefit. Data of targeted therapies are currently awaited [49]. The prognosis of metastatic RCC was less than 10% until targeted therapies were introduced [50]. These therapies affect mTOR or the downstream targets of pVHL pathway (VEGF, VEGFR, PDGFR). Bevacicumab is an antibody targeting VEGF, whereas sunitinib, sorafenib and axitinib are small-molecule receptor tyrosine kinase inhibitors targeting VEGFR and PDGFR. Small-molecules inhibiting mTOR are temsirolimus and everolimus [28] (Fig. 3B). Compared to IFNα or placebo they show a significant increase in survival [3, 51, 52]. However, these treatments have significant toxic side effects and response is only seen in a subgroup of patients.

## 4.2 The Von Hippel-Lindau gene is frequently inactivated in ccRCC

Von Hippel-Lindau syndrome patients develop capillary hemangioblastomas in the central nervous system and the retina, pancreatic and inner ear carcinomas [25]. Several hundred small foci of clear cell tumors and cysts in the kidney are precursor lesions of ccRCC. In almost all sporadic cases (92%) *VHL* is also biallelically altered [53], either by homozygous 3p loss, by mutations or by hypermethylation of the remaining allele in heterozygous cases [26]. This indicates that this tumor suppressor gene is centrally involved in the development of ccRCC [25]. pVHL acts as an adaptor protein to recruit effector proteins to their target proteins. Thereby it regulates HIFα for its proteolytic degradation [54], microtubule stability [55], the maintenance of the primary cilium [56], the activation of p53 [57], neuronal apoptosis [58], epithelial-mesenchymal transition [59], cellular senescence [60] and aneuploidy [61], secretion of extracellular components [62], growth factor receptor internalization [63], WNT signaling [64], ubiquitination of RNA polymerase II [65], degradation of β2-adrenergic receptors [66] and activity of nuclear factor (NF)-κB [67]. Deregulation of these processes leads to tumorigenesis and tumor progression [25]. It was shown that pVHL-deficiency alone is not sufficient to initiate tumor formation [68], therefore it is speculated that additional affected genes must be included. Genomic scale technologies elucidated that there are distinct molecular subclasses of ccRCC predicting patients' survival [13]. Different ccRCC entities are defined by mutations, amplifications, deletions and hypermethylation of different genes, as well as mRNA and microRNA expression to different extents.

### 4.2.1 HIF stabilization due to inactivated pVHL drives tumorigenesis in ccRCC

pVHL is as the recognition subunit of the E3 ligase complex consisting of elongin C and B, Rbx1 and Cul2, that targets HIF1 and 2α for oxygen-dependent, ubiquitin-mediated proteolytic degradation. Loss of pVHL function results in the constitutive stabilization of HIF1 and 2α leading to the induction of HIF-transcriptional targets [25] (Fig. 4). Recently, it was shown that out of the remaining 8% of ccRCCs with intact pVHL, 42% harbor biallelic inactivated elongin B gene (*TCEB1*) [26]. The high frequency implicates that HIF activation is an important oncogenic driving force in ccRCC, which is supported by data showing that HIF2α is necessary for tumor growth [69] and HIF1α is sufficient to induce ccRCC formation [70]. HIF1α is predominantly expressed in early lesions, whereas HIF2α, promoting tumor development, is higher expressed in advanced lesions of kidneys of Von Hippel-Lindau syndrome patients [69]. The shift towards

HIF2α in the HIF1α/HIF2α balance during the progression of ccRCC may be caused by biallelic genetic alterations in the *HIF1α* locus [71], differential posttranscriptional and posttranslational modifications of HIF1 and 2α [25], proteins, that promote the distinct activity of HIF2α (hypoxia-associated factor (HAF) [72], mTOR [73]), microRNAs (miR-30a-9p; miR-30c-2-3p) [74] or the transcriptional silencing of HIF1α by HIF1 and 2α [75].

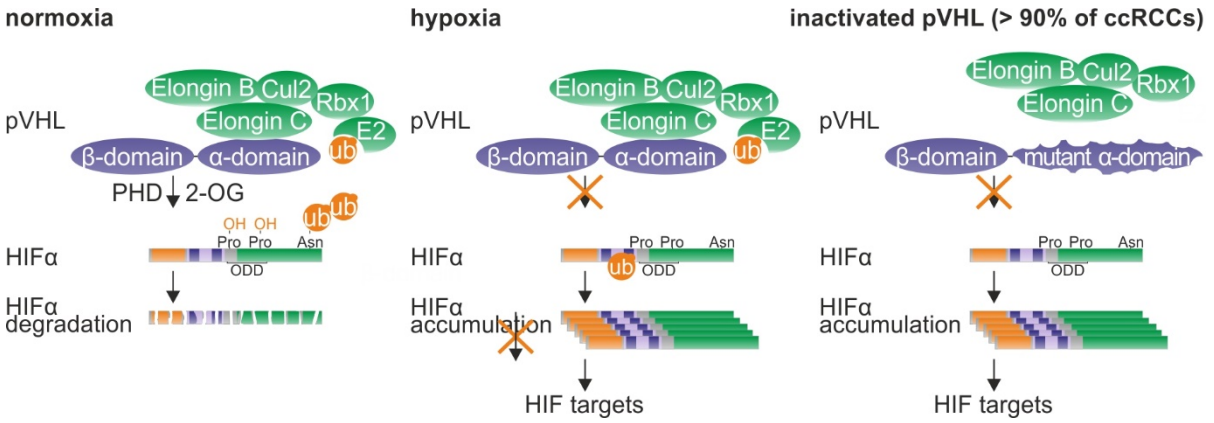


**Figure 4. The influence of pVHL on HIFα stabilization under normoxic, hypoxic and *VHL*-mutated conditions.**

Adapted from Linehan *et al.*, 2010a [21] and Keith *et al.*, 2012 [76]. Under normoxic conditions the pVHL E3 ubiquitin ligase complex, consisting of pVHL, Elongin B and C, cullin (Cul2), ring box protein 1 (Rbx1) and ubiquitin-conjugating enzyme (E2), targets HIFα for ubiquitin-mediated (ub) degradation using oxygen and 2-oxoglutarate (2-OG). Under hypoxic conditions or when pVHL lost its function the pVHL E3 ubiquitin ligase complex is unable to target and degrade HIFα. HIF-subunits consist of the DNA binding domain basic helix-loop-helix domain (bHLH, in orange), the protein-protein dimerization domain PAS (PER-ARNT-SIM, in blue) and the transactivation domain (TAD, in green). PHD can hydroxylate (OH) two specific proline residues (Pro) in the oxygen-dependent degradation domain (ODD). Asn= asparagine.

### 4.2.2 HIF controls metabolic reprogramming in ccRCC

HIFs are basic helix-loop-helix PER-ARNT-SIM (bHLH-PAS) proteins that form heterodimeric complexes. They are composed of an oxygen-labile α-subunit (HIF1, 2 or 3α) and a stable β-subunit (HIF1β) [76]. As a complex they can bind to hypoxia response elements (HREs) with the RCGTG core sequence. No additional sequences are required for HIF-binding. Many high-affinity sites are located at great distances from the genes they regulate. It is thought, that the range of HIF targets is determined by a cell-type-specific chromatin structure [77]. HIF activity is controlled through the stabilization of HIF1 and 2α. In the presence of oxygen HIF-specific prolyl-hydroxylases (PHDs) modify the HIFα-subunits, so that they can be degraded by the proteasome, mediated by pVHL [76]. Because the function of pVHL is lost in 92% of ccRCCs, prolyl-hydroxylated HIFα subunits cannot be bound by pVHL and targeted for ubiquitin-mediated proteolysis [78]. Increased expression of HIFα proteins in tumor cells actively drives tumor growth and progression by regulating the expression of crucial target genes. The

transcriptional specificity resides in the amino-terminal transactivation domain (N-TAD) of HIFα, which implicates that the interaction with different cofactors determine differential gene expression [79]. HIFα subunits were thought to have largely overlapping functions, but it became more a more obvious that they act sometimes opposingly through the regulation of unique targets, including *MYC* and *p53* [76].

The loss of function of pVHL in ccRCC stabilizes HIFα and leads to the activation of a series of genes, which encode proteins involved in angiogenesis, metabolism and cell cycle regulation. Among them are cell surface proteins, including VEGF and PDGF, which represent important therapy targets for ccRCC patients [80]. HIF controls metabolic reprogramming in RCC thereby enhancing the growth response to proliferative signals and ensuring the supply of precursors of anabolic metabolism [25, 81]. HIF activates the expression of glycolytic enzymes and glucose transporters. By the deprivation of pyruvate through the overexpression of pyruvate dehydrogenase kinase 1 and lactate dehydrogenase A, HIF mediates a Warburg-like metabolic shift in ccRCC [82]. HIF inhibits *MYC* thereby reducing mitochondrial respiration [83]. The increased pentose-phosphate pathway provides the tumor cell with NADPH and ribose-5-phosphate [84].

## 4.3 Biomarkers for RCC

Several potential predictive and prognostic biomarkers including circulating biomarkers (VEGF, VEGF-related proteins, cytokines and angiogenic factors and lactate dehydrogenase) and tissue-based biomarkers such as single-nucleotide polymorphisms have been identified for RCC, but none of them has entered clinical practice yet [85]. Tissue biomarkers need mostly invasive procedures and may be limited by tumor heterogeneity [86]. Blood biomarkers are susceptible to degradation by circulating proteases and nucleases [87]. Urine metabolites are a promising biomarker source, but may be difficult to use due to their heterogeneous nature [88].

Carbonic anhydrase 9 (CA-IX), a downstream effector of HIF1α, is a diagnostic biomarker for ccRCC [89]. Also the microRNA miR20 among others has shown to be higher in tissue and serum of patients with ccRCC [90]. Prognostic biomarkers for RCC are VEGF [91], *VHL* [92], HIF1α [93], CA-IX [94], a 4 microRNA expression signature [95], CRP [96], PD-L1 [97], Ki-67 [98], survivin [99], fascin [100], MET [101] and IMP3 [102].

### 4.3.1 New biomarker candidates by ccRCC-specific surfaceome identification

To improve diagnosis, prognosis and treatment of RCC patients, additional biomarkers, in particular cell surface proteins, would be of utmost importance.

In a previous work cell surface capturing technology was used to define the pVHL-dependent ccRCC protein surfaceome [103]. The expression pattern of 82 of these proteins was further validated using low-density arrays. We focused our interest on proteins that showed differential expression in ccRCC compared to normal kidney either on protein or on mRNA level as well as on proteins whose upregulation in RCC was already described before (Fig. 5). Among them are pVHL-associated and -independent ccRCC biomarker candidates.

| | | mRNA | | | | | protein | |
|---|---|---|---|---|---|---|---|---|
| | | tissue | | | cell lines | | | |
| | Gene name | ccRCC/ normal | pRCC/ normal | ccRCC/ pRCC | VHL-/ VHL19+ | VHL-/VHL30+ | VHL-/VHL+ | Full protein name |
| mRNA focus | TNFSF7/ CD70 | 189.03 | 14.19 | 13.32 | 1.92 | 1.81 | 0.24 | tumor necrosis factor ligand superfamily member 7 |
| | GABRD | 103.22 | 2.76 | 37.46 | 33.33 | 25.00 | 786-O | gamma-aminobutyric acid (GABA) A receptor, delta |
| | SCARB1 | 35.98 | 3.45 | 10.44 | 1.49 | 1.35 | 786-O, -19, -30 | scavenger receptor class B, member 1 |
| | KCNT1 | 1.11 | 15.53 | 0.07 | 3.13 | 0.61 | - | potassium channel, subfamily T, member 1 |
| | MAGEB6 | 15.40 | 1.24 | 12.39 | 1.72 | 5.88 | - | melanoma antigen family B, 6 |
| | CP | 13.93 | 0.38 | 37.14 | 5.26 | 3.03 | 786-O | ceruloplasmin (ferroxidase) |
| | SLC22A4 | 13.88 | 4.56 | 3.04 | 1.32 | 2.22 | 0.46 | solute carrier family 22 member 4 |
| | GPR149 | 13.72 | 2.16 | 6.34 | 0.93 | 1.45 | - | G protein-coupled receptor 149 |
| | CDH6 | 3.40 | 12.42 | 0.27 | 0.50 | 0.37 | 786-O, -19, -30 | cadherin 6, type 2, K-cadherin (fetal kidney) |
| protein focus | CD99 | 1.31 | 0.59 | 2.23 | 1.59 | 1.43 | 4.89 | CD99 |
| | SLC2A1 / GLUT1 | 2.21 | 0.26 | 8.55 | 2.77 | 2.94 | 4.71 | solute carrier family 2 |
| | ANPEP / CD13 | 0.48 | 1.13 | 0.42 | 0.59 | 1.72 | 3.65 | alanyl aminopeptidase |
| | DPP4 | 1.94 | 3.76 | 0.51 | 0.66 | 0.53 | 3.22 | dipeptidyl-peptidase 4 |
| | THBS1 | 0.55 | 0.17 | 3.34 | 0.50 | 1.43 | 2.83 | thrombospondin 1 |
| | ICAM1 | 1.36 | 0.69 | 1.97 | 1.89 | 1.56 | 2.26 | intercellular adhesion molecule 1 |
| | ITGA5 | 2.24 | 0.51 | 4.43 | 1.19 | 1.54 | 2.15 | integrin, alpha 5 |
| | AXL | 2.44 | 1.59 | 1.53 | 0.72 | 1.75 | 1.95 | AXL receptor tyrosine kinase |
| | SLC7A1 | 0.67 | 0.35 | 1.91 | 1.19 | 1.52 | 1.66 | solute carrier family 7 |
| | ⋮ | | | | | | | |
| literature focus | PTPRJ | 0.46 | 0.79 | 0.58 | 0.44 | 0.78 | 0.34 | receptor-type tyrosine-protein phosphatase eta |
| | ALCAM | 1.68 | 1.21 | 1.39 | 0.89 | 1.51 | 786-O, -19, -30 | activated leukocyte cell adhesion molecule |
| | MME / CD10 | 0.77 | 0.08 | 9.81 | 16.67 | 3.70 | 1.50 | neprilysin |
| | TGFBR3 | 0.48 | 0.21 | 2.26 | 1.39 | 1.37 | 786-O | transforming growthfactor, beta receptor III |
| | KDR/ VEGFRII | 5.20 | 0.21 | 24.45 | 0.05 | 0.00 | 786-O | kinase insert domain receptor |
| | EPHA2 | 0.67 | 0.67 | 1.01 | 0.62 | 0.99 | 786-O, -19, -30 | EPH receptor A2 |
| | M6PR / IGF2R | 0.84 | 9.00 | 0.94 | 0.90 | 0.70 | 786-O, -19, -30 | mannose-6-phosphate receptor |

**Figure 5. Biomarker candidates.**

Biomarker candidates which were further investigated are highlighted in blue.

## 4.4 Expression and function of CD70, a tumor necrosis factor ligand

One of the candidates, CD70, a member of the tumor necrosis factor ligand superfamily, caught particularly our interest because of its 189-fold upregulation in ccRCC compared to normal kidney on mRNA level.

CD70 is one of the ligands of the tumor necrosis factor (TNF) superfamily which is composed of 19 ligands and 30 receptors [104]. CD70 consists of 193 amino acids with an extracellular binding domain, a transmembrane segment, a short cytoplasmic domain and two potential *N*-linked glycosylation sites with a molecular mass of 50 kDa [105, 106] (Fig 6A). The homotrimeric type II membrane protein has been shown to exist only in the membrane-bound form and no recognizable motifs for cleavage from the cell surface have been found [106, 107].

Under normal conditions CD70 expression is tightly regulated and restricted to a small subset of antigen-stimulated B and T lymphocytes and mature dendritic cells [105, 108]. Low levels have also been detected on thymic medullar epithelial cells [109] and on a novel type of non-hematopoietic antigen presenting cells (APC) in the gut [110]. CD70 is upregulated upon Toll like receptor (TLR) signaling in dendritic cells and antigen-stimulation in T cells and remains on the surface for a few days [111, 112]. The expression of CD70 can on the one hand also be enhanced by cytokines, such as IL-1α, IL-12 and TNF-α, and on the other hand inhibited by IL-4 and IL-10 [111, 113].

The unique receptor for CD70 is the type I dimeric transmembrane glycoprotein CD27 (Fig. 6A). After interaction with its ligand CD70, it trimerizes and a truncated, soluble form of CD27 is cleaved and released by a membrane-bound protease [114, 115]. The soluble form is detectable in the serum of healthy individuals and is increased during immune activation by autoimmune diseases and viral infections [116]. CD27 is constitutively expressed on early thymocytes and $CD4^+$ and $CD8^+$ T cells and can also be upregulated following T cell activation [104, 117]. Upon T cell activation CD27 expression first increases, but is downregulated during several rounds of divisions and differentiation towards effector cells [117, 118]. Both, CD27 and CD70 are generally absent in non-lymphoid normal tissues including vital organs [106].

The primary function of TNF superfamily molecules is to regulate cell survival by positively influencing the T cell responses and mediating crosstalk between T cells and other cell types [104] (Fig. 6B). As a consequence of the ligation to CD70, a conserved motif in the cytoplasmic tail of CD27 binds to TNF receptor-associated factor (TRAF) 2 and TRAF5 and activates both the canonical and the non-canonical NF-κB pathway. In addition, CD27 activates the c-Jun kinase cascade [119]. Besides, it was shown that CD27 can bind to the apoptosis regulatory protein Siva1 and induce apoptosis. However, there is no concrete proof of the involvement

of Siva1 in CD27 signaling and the activated lymphocyte pool rather expands after ligation of CD27 to CD70 [106, 117, 120]. CD70 can act as a signal transducing receptor and induce the serine-threonine protein kinase/ protein kinase B (Akt1/PKB) pathway [117, 121].

The interaction of CD70 with its receptor CD27 promotes expansion and differentiation of memory and effector T cells as well as B cell expansion and plasma cell differentiation [104, 117]. It contributes to the formation of the effector cell pool by inducing proliferation and survival. Transgenic mouse models demonstrated that constitutive costimulation can induce severe immunopathology by chronic immune activation [117].

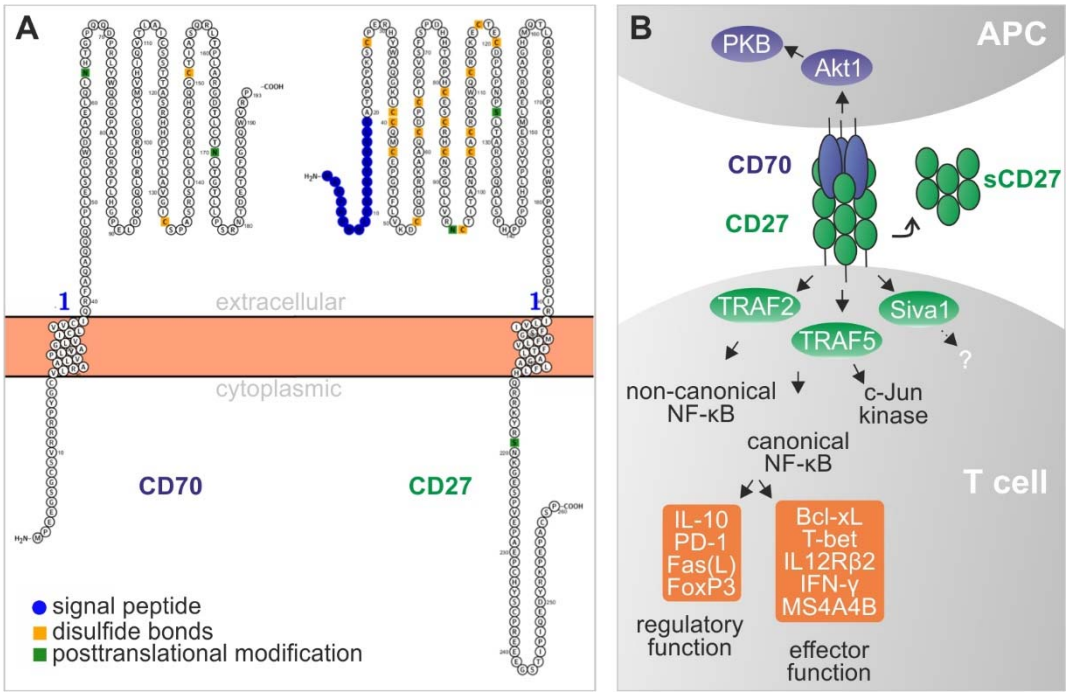


**Figure 6. CD70/CD27 signaling.**

A) CD70 and CD27 proteins visualized by Protter [122]. B) Adapted from Nolte *et al.*, 2009 [117]. CD70/CD27 signaling triggers the binding of CD27 to TRAF2 and 5 and activates thereby the non-canonical NF-κB, the canonical NF-κB and the c-Jun pathway. This induces effector and regulatory functions of T cells. In the CD70-expressing cell the Akt1/PKB cascade gets activated.

### 4.4.1 Aberrant CD70 expression in cancers

Aberrant expression of CD70 has also been described in the solid tumors nasopharyngeal carcinoma, thymic carcinoma, medulloblastoma, astrocytoma and glioblastoma as well as in the hematologic malignancies non-Hodgkin lymphoma and multiple myeloma (Table 3) [106]. The most frequent expression was reported in RCC [123-126], but the mechanism that leads to the upregulation of CD70 in this tumor type is unclear.

**Table 3. CD70 expression frequencies in cancer.**

Adapted from Grewal, 2008 [106].

| Hematological malignancies | CD70 expression frequencies % | Solid tumors | CD70 expression frequencies % (n) |
|---|---|---|---|
| Non-Hodgkin's lymphoma | | | |
| Diffuse large B cell lymphoma | 71% | Clear cell renal cell carcinoma [125] | 65% (59/91) |
| High grade B lymphoma | 58% | Papillary renal cell carcinoma [125] | 40% (9/23) |
| Follicular lymphoma | 33% | Glioblastoma [127] | not quantifiable |
| Mantle cell lymphoma | 25% | Astrocytoma [127] | not quantifiable |
| Chronic lymphocytic leukemia | 50% | Nasopharyngeal carcinoma [128] | 80% (16/20) |
| Hodgkin's disease | 96% | Thymic carcinoma [109] | 88% (7/8) |
| Waldenstrom's macroglobulinemia | 100% | | |
| Multiple myeloma | 63% | | |

Interestingly, CD70 expression is less prevalent in *VHL* non-related RCC subtypes. Studies elucidating the consequences of the constitutive expression of CD70 and its interaction with CD27 in ccRCC are rare and controversial. While some authors hypothesized that CD70 is involved in an immune escape mechanism of RCC by mediating apoptosis in lymphocytes [129], others suggested that CD70 rather triggers a phenotypic conversion of $CD27^+$ tumor infiltrating lymphocytes (TIL) into a more differentiated state [130]. A possible role for CD70/CD27 interaction in the regulation of tumor cell expansion and survival was suggested [117], since some evidences suggest, that it may allow the tumor to escape immune response by decreasing the effector T cell/ regulatory T cell ratio [131].

The constitutive expression of CD70 in multiple solid tumors paired with the restricted expression on normal cells makes CD70 an attractive target for antibody-based therapies without undesirable effects on non-CD70 expressing cells. Antibodies, that can deplete CD70-expressing tumor cells may be effective to remove CD70-expressing tumors [117]. It was shown that CD70 is rapidly internalized after binding to an antibody, so that the efficacy of drug delivery using CD70 as vehicle might be guaranteed [125, 132]. SNG-75 is an antibody-drug conjugate which is directed against CD70 and conjugated to monomethyl auristatin F, a microtubule-disrupting agent [133]. *In vitro* and *in vivo* antitumor activity and specificity has been demonstrated with CD70-expressing lymphoma, multiple myeloma, glioblastoma, pancreatic carcinoma and RCC models [133-135]. In a phase I clinical study SNG-75 demonstrated modest antitumor activity in both 39 metastatic RCC and 19 non-Hodgkin's lymphoma patients with manageable toxicity. Two (6%) partial responses and twelve (38%) stable disease outcomes in RCC could be achieved. Adverse events were fatigue, dry eyes, nausea and thrombocytopenia [136].

CD70 has been shown to be regulated by promoter-hypermethylation in CD70-expressing hematological malignancies [137-141], but in none of the solid tumors. Although a previous publication proposed a correlation between CD70 expression and CD70 methylation in breast cancer cell lines [142], recently no correlation in breast cancer tissue could be found [143]. This suggests the existence of other, not yet known, mechanisms in solid tumors leading to the upregulation of CD70.

Since the high and unique frequency of CD70 overexpression in ccRCC resembles the *VHL* mutation frequency being characteristic for this subtype, it might be conceivable that those two alterations of ccRCC could be connected with each other. Until now the impact of the constant stabilization of HIFα in ccRCC on the expression of CD70 was not examined. Moreover, studies elucidating the consequences of constant interaction of CD70 with its only known receptor CD27 expressed on T cells within the tumor microenvironment are lacking. For the application of the recently developed CD70-targeting drugs, it would be of interest if the CD70-expression on ccRCCs is previsable in the blood of patients.

# 5 Objectives

The overall objective of my PhD project was to select and analyse potential candidates of the RCC protein surfaceome for clinical applications. The analysis of the RCC surfaceome can be subdivided into three chapters. We focused our interest mainly on the mechanism of the aberrant and frequent upregulation of one of the candidates, CD70, in ccRCC. We also investigated the role of the interaction of CD70-expressing tumor cells and $CD27^+$ TILs in this tumor type.

- Primarily, we studied the impact of pVHL and HIF$\alpha$ on CD70 expression as well as the role of CD27-expressing TILs in ccRCC by
  (i) analyzing CD70 expression patterns in a large cohort of RCC tissues,
  (ii) investigating the interrelation of CD70 expression and the pVHL/HIF axis by *VHL* mutation analysis and *in vitro* experiments,
  (iii) determining CD27 mRNA and protein expression in TILs and its correlation with the CD70 expression status and
  (iv) examining the concentration of soluble CD27 (sCD27) in cocultures and sera of patients with CD70-positive and -negative tumors.
  (v) analyzing T cell exhaustion markers in CD70-expressing ccRCCs.

- Furthermore, a study about another RCC surface candidate, PTPRJ, investigating its pVHL/HIF-driven reduction in ccRCC was validated and extended [144].

- First insights about six other promising biomarker candidates (TGF-βRIII, CD10, AlCAM, VEGFRII, EPHA2 and IFG2R), which are upregulated in ccRCC have been gained by analyzing their concentrations in serum of RCC patients.

# 6 Results

In the following the results of my work studying CD70, PTPRJ and six additional proteins in ccRCC are shown.

## 6.1 CD70 is regulated by pVHL and enhances sCD27 release in ccRCC

### 6.1.1 CD70 is frequently expressed in primary ccRCC and ccRCC metastasis

Gene expression analysis of 116 RCC tissues [145] revealed that *CD70* was upregulated in primary and metastatic ccRCC (Fig. 7A). Using tissue micro arrays (TMAs) containing a total of 667 RCCs, we observed strong membranous CD70 protein expression in 78% of ccRCCs, but in only 32% of papillary RCC. Oncocytomas, chromophobe RCCs and normal kidneys were negative (Fig. 7B, C). Furthermore, 54 ccRCC brain metastases showed a similar CD70 expression frequency as observed in primary tumors. Notably, the strong CD70 expression seen in nine primary ccRCCs remained constant in their corresponding brain metastasis (Fig. 7D). Other primary solid tumors, as breast and lung cancer did not show any CD70 expression (Fig. 7E). Whereas CD70 expression was not associated with grade or stage in ccRCC, papillary RCC [146] showed an inverse correlation of CD70 with Fuhrman grade and nucleolar grade [147] (Fig. 8A, B). Moreover, the less aggressive subtype 1 of papillary RCC was more often CD70-positive than papillary RCC subtype 2 [148] (Fig. 8C).

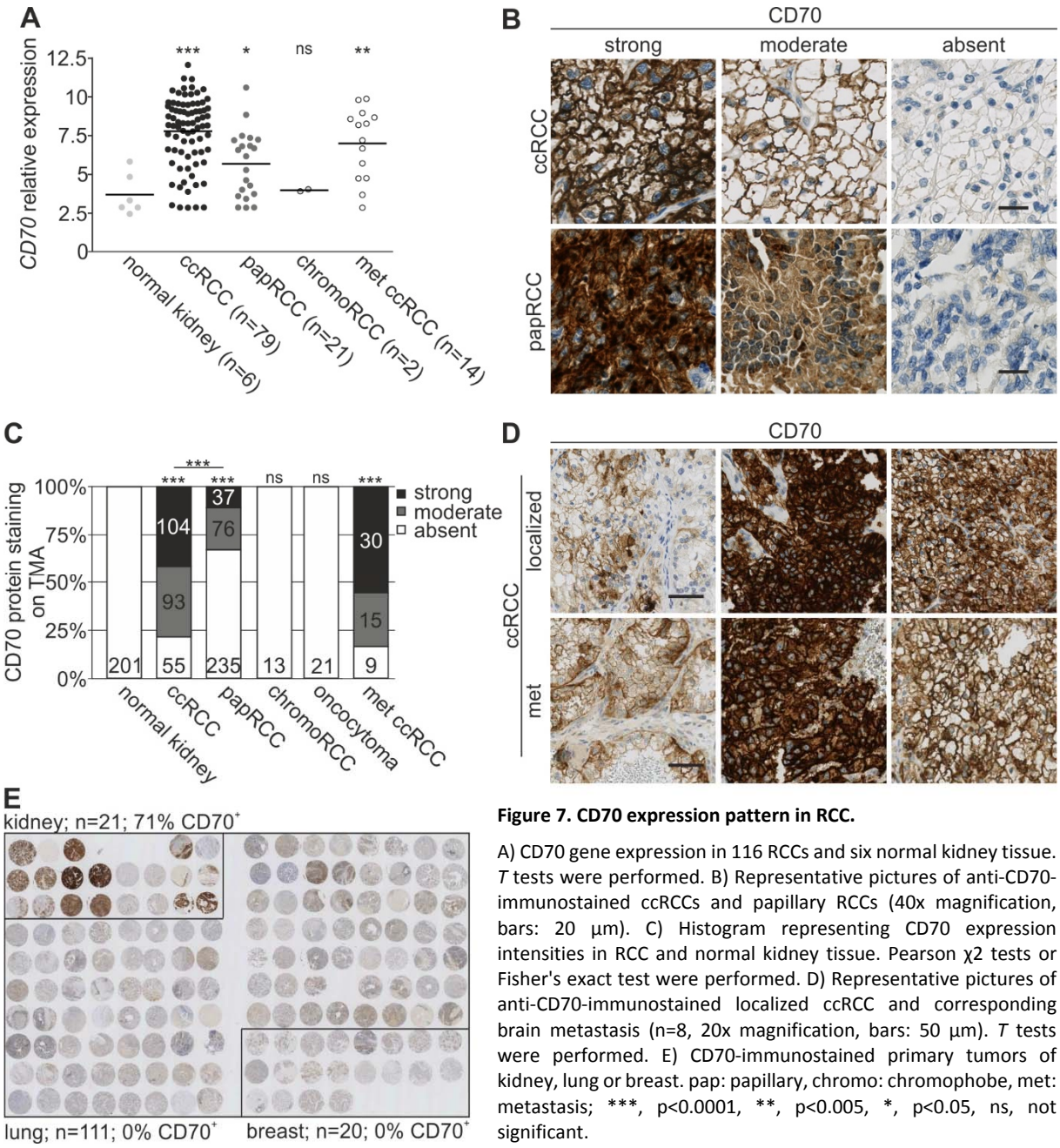


**Figure 7. CD70 expression pattern in RCC.**

A) CD70 gene expression in 116 RCCs and six normal kidney tissue. *T* tests were performed. B) Representative pictures of anti-CD70-immunostained ccRCCs and papillary RCCs (40x magnification, bars: 20 µm). C) Histogram representing CD70 expression intensities in RCC and normal kidney tissue. Pearson χ2 tests or Fisher's exact test were performed. D) Representative pictures of anti-CD70-immunostained localized ccRCC and corresponding brain metastasis (n=8, 20x magnification, bars: 50 µm). *T* tests were performed. E) CD70-immunostained primary tumors of kidney, lung or breast. pap: papillary, chromo: chromophobe, met: metastasis; ***, p<0.0001, **, p<0.005, *, p<0.05, ns, not significant.

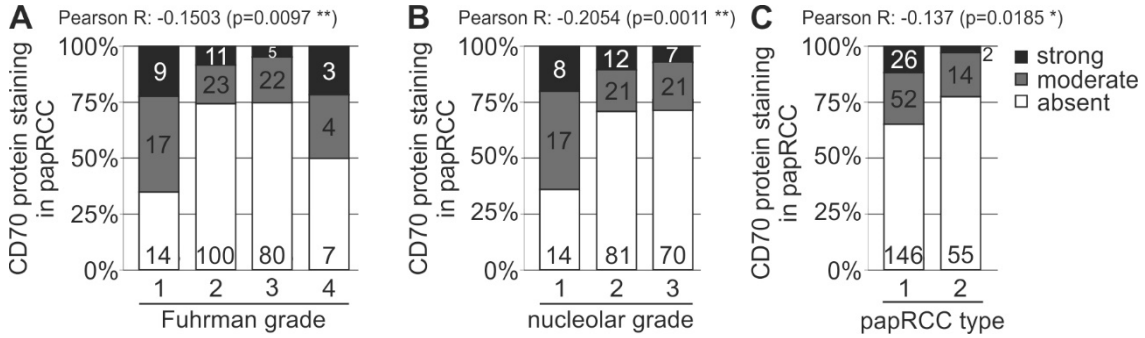


**Figure 8. Inverse correlation of CD70 with tumor grade and subtype in papillary RCC.**

A) Histogram representing CD70 expression in papillary RCCs subdivided according to A) Fuhrman grade, B) nucleolar grade and C) papillary subtypes. Pearson R correlation analyses are depicted.

### 6.1.2 CD70 is highly glycosylated in RCC cell lines

In Western blots of lysates of the two RCC cell lines 786-O and A498, CD70 appears in multiple bands (Fig. 9A, B), which was also described previously [126, 149]. To test the specificity of the CD70 antibody, we knocked down *CD70* in both A498 and 786-O cells with four different siRNAs. All bands except the one at 100 kDa were specific. The multiple banding pattern propably arises from differential glycosylation as CD70 is known to be a trimer which is heavily glycosylated on its extracellular domain [106].

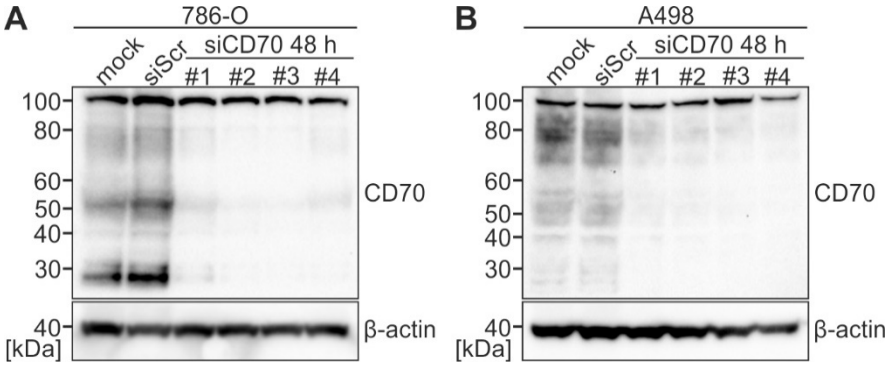


**Figure 9. Silencing of CD70 in 786-O and A498 cells.**

A) Western blot of CD70 in 786-O and B) A498 treated with siRNA targeting *CD70* (siCD70#1-4) or treated with siRNA control (siScr) for 48 hours (h).

The NetNGlyc 1.0 server predicts two *N*-glycosylation sites within the 193 amino acid sequence of CD70 by using artificial neural networks that examine the sequence context of Asn-Xaa-Ser/Thr sequons (where Xaa is not Pro) [150] (Fig. 10A). After removal of the *N*-glycans with peptide-*N*-glycosidase F (PNGase) CD70 was mainly reduced to its deglycosylated monomer of about 20 kDa (Fig. 10B). Notably, the extent of glycosylation of CD70 appears to be higher in RCC cells than in lymphoma cells (Fig. 10C). Raji cells originate from B cells, where CD70 is natively expressed [124]. Next, we wanted to investigate if the remaining bands after deglycosylation represent the dimeric and trimeric forms of CD70. The oligomers are held together by disulfide bonds [105], which might be too strong to be broken by the reducing conditions of the Western blot run. Additional pretreatment of the cell lysates with the strong reducing agent *tris*(2-carboxyethyl)phosphine (TCEP) changed the banding pattern of CD70 only slightly in the Western blot (Fig. 10D). Thus, the TCEP-treatment did either not reduce the disulfide bonds completely or the bands arise from another origin. Fluorescent staining of CD70 in whole uncut cells revealed, that it is localized in both the cytoplasm and the cell membrane of RCC cells (Fig. 11).

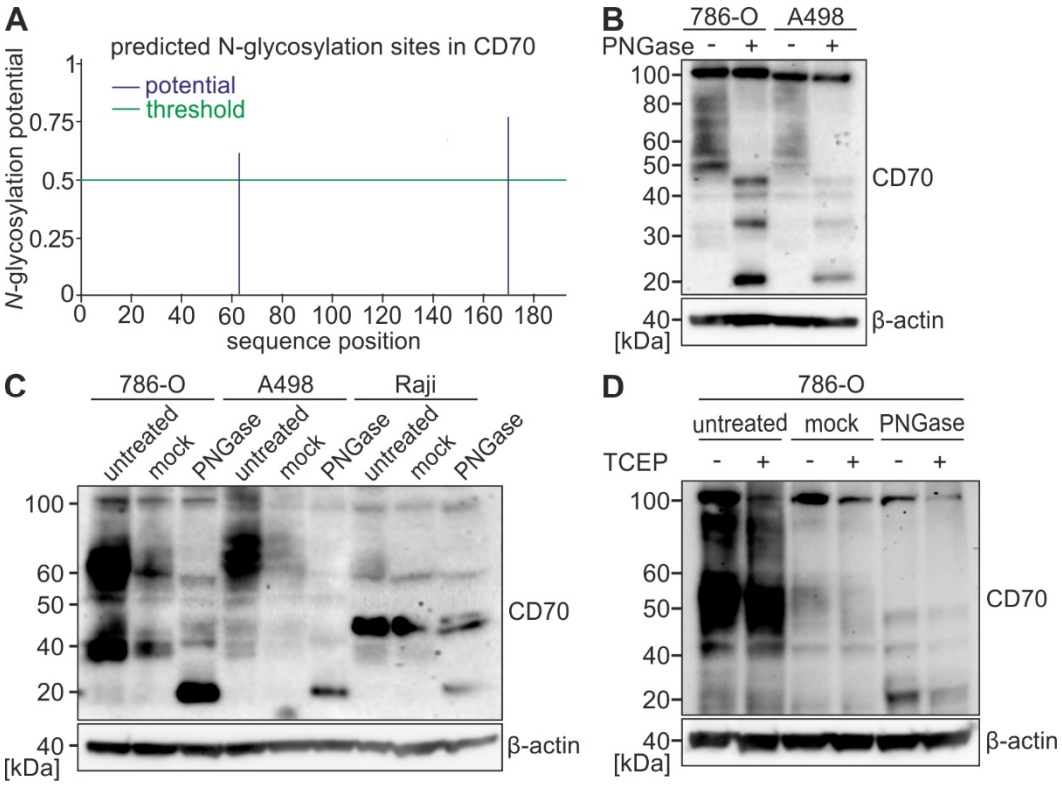


**Figure 10. CD70 is *N*-linked glycosylated.**

A) Predicted *N*-glycosylation sites within the CD70 amio acid sequence by the NetNGlyc 1.0 server. B) Western blot of 786-O and A498 lysates untreated and treated with PNGase. C) Western blot of 786-O, A498 and Raji lysates untreated, mock-treated and PNGase-treated. D) 786-O as in C) with and without TCEP-pretreatment.

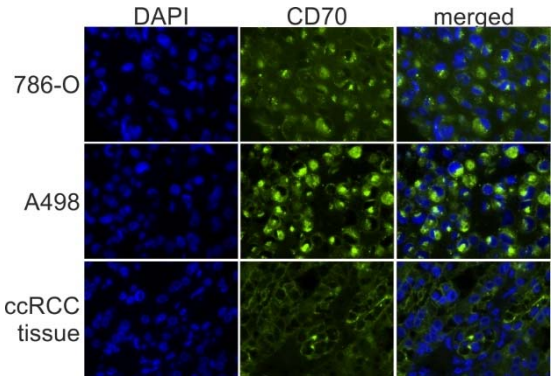


**Figure 11. CD70 is localized in the cytoplasm and the cell membrane.**

Fluorescent staining of CD70 and 4',6-diamidino-2-phenylindole (DAPI) in 786-O, A498 and ccRCC tissue (60x magnification).

### 6.1.3 CD70 expression and *VHL* mutation status in ccRCC tissues and cell lines.

*VHL* mutations are thought to affect pVHL's functional integrity in ccRCC. To test whether *VHL* mutations influence CD70 expression, we correlated the mRNA and protein expression patterns of CD70 with *VHL* mutation data in a series of ccRCCs, which were recently published by our group [151]. Although *VHL* wild type (wt) ccRCC may also have lost pVHL function due to hypermethylation of its gene promoter, we found an association of CD70 expression and mutated *VHL* (Fig. 12A, B). To test whether the missense mutations found in the *VHL* sequence

can impair the pVHL protein function, we used the software Site Director mutator (SDM), which predicts the effect of a missense mutation on the protein stability [151, 152]. CD70 expression was more frequent in tumors with *VHL* mutations, which predict impaired function of pVHL compared to tumors with *VHL* wt and *VHL* mutations not affecting the protein function (Fig. 12C).

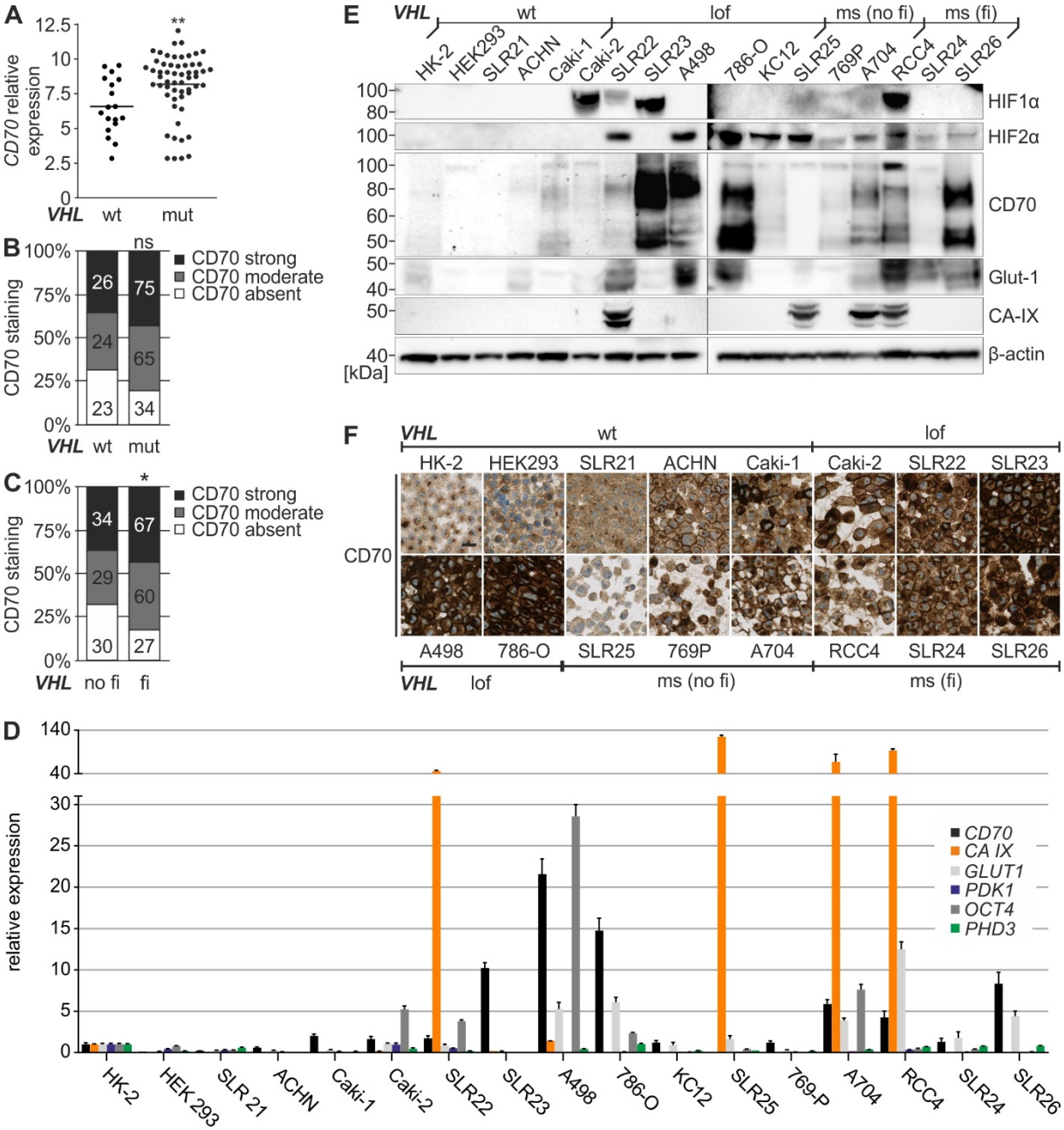


**Figure 12. CD70 is associated with the *VHL* mutation status.**

A) *CD70* gene expression in ccRCC tissue with mutated or wt *VHL*. **, p<0.001 by *t* test. B) Histogram representing CD70 expression intensities in ccRCCs with mutated or wt *VHL*. ns: not significant by Pearson $\chi^2$ test. C) CD70 expression intensities assigned to ccRCCs tissue with function of pVHL predicted to be impaired or not impaired. *In silico* analysis was done with SDM (http://mordred.bioc.cam.ac.uk/~sdm/sdm.php). *, p<0.05 by Pearson $\chi^2$ test. D) mRNA levels of *CD70*, the HIF1α-dependent genes *CA-IX* and *PDK1*, the HIF2α-dependent genes *GLUT1*, *OCT4* and *PHD3* , E) Western blot of HIF1α, HIF2α, CD70, CA-IX and Glut1 and F) cell microarray stained for CD70 (20x magnification, bar: 20 µm). The *VHL* mutation status is indicated as wt, loss of function (lof), missense (ms) with (fi) and without (no fi) functional impact on pVHL.

**Table 4. *VHL* and *HIF1α* mutation states in cell lines.**

| Name | Derived from | VHL status | Exon | mutation type | mutation consequence | SDM comment | HIF1α status adapted from Shen *et al.* [71]. |
|---|---|---|---|---|---|---|---|
| HK2 | proximal tubule | wt | | - | - | | - |
| HEK293 | embryonic | wt | | - | - | | - |
| SLR21 | clear cell carcinoma | wt | | - | - | | diploid |
| ACHN | adenocarcinoma | wt | | - | - | | - |
| Caki-1 | clear cell carcinoma | wt | | - | - | | - |
| Caki-2 | clear cell carcinoma | c.529A>T/p.Arg177X | 3 | point mutation | loss of function | | lost 1 allele |
| SLR22 | clear cell carcinoma | c.171_174del gcgg/p.Gly57GlyfsX7 | 1 | deletion | loss of function | | - |
| SLR23 | clear cell carcinoma | c. 263G>A/p.Trp88X | 1 | point mutation | loss of function | | haploid for some exons |
| A498 | epithelioid adenocarcinoma | c.426_429delTGAC/p.Val142ValfsX14 | 2 | deletion | loss of function | | homozygous deletion |
| 786-O | epithelioid adenocarcinoma | c.310delG/p.Gly104Alafsx55 | 1 | deletion | loss of function | | homozygous deletion |
| KC12 | clear cell carcinoma | *VHL*$^{-/-}$ | | biallelic deletion | loss of function | | - |
| SLR25 | clear cell carcinoma | c.233A>C/p.Asn78Thr | 1 | point mutation | missense | functionally not impaired | haploid for some exons |
| 769-P | epithelioid adenocarcinoma | c.539T>A/p.Ile180Asn | 3 | point mutation | missense | functionally not impaired | homozygous deletion |
| A704 | epithelioid adenocarcinoma | c.539T>A/p.Ile180Asn | 3 | point mutation | missense | functionally not impaired | lost 1 allele |
| RCC4 | clear cell carcinoma | c.194C>G/p.Ser65Trp * | 1 | point mutation | missense | functionally impaired | lost 1 allele |
| SLR24 | clear cell carcinoma | c.194C>G/p. Ser65Trp | 1 | point mutation | missense | functionally impaired | homozygous deletion |
| SLR26 | clear cell carcinoma | c.389T>A/p.Val130Asp | 2 | point mutation | missense | functionally impaired | homozygous deletion |

To confirm these findings *in vitro*, we sequenced the *VHL* gene in 17 RCC cell lines and combined it with the *HIF1α* mutation state from literature [71] (Table 4). *CD70* mRNA and protein levels were generally higher in RCC cell lines harboring *VHL* loss of function mutations (Caki-2, SLR22, SLR23, A498, 786-O and KC12) and *VHL* missense mutations predicted to affect the pVHL function (RCC4, SLR24 and SLR26). RCC cell lines with *VHL* missense mutations having no functional impact on the protein (SLR25, 769P and A704) and those with wt *VHL* (SLR21, ACHN, Caki-1, HK-2 and HEK293) showed no or only weak CD70 expression (Fig. 12D-F). CD70 expression was only observed in cell lines that either were positive for both HIF1α and HIF2α or were positive for at least one of them. CD70 was found to be upregulated more often HIF2α-expressing cell lines, since many of the *VHL*-mutated RCC cell lines have homozygous deletions in the *HIF1α* locus (Table 4). In most of the cell lines that express CD70 the HIF-targets Glut1 and CA-IX were also present (Fig. 12E). This was also true at mRNA level: the *CD70* expression was in line with the expression of *GLUT1* and *CA-IX*, but was not associated with the other HIF target genes *PDK1*, *OCT4* and *PHD3* (Fig. 12D).

### 6.1.4 CD70 expression is regulated by the pVHL/HIF axis in RCC tissue and cell lines

Only the reconstitution of full length pVHL, but not the reconstitution of the 19 kDa isoform ($pVHL_{19}$) lead to less CD70 protein in Western blots (Fig. 13A). In order to evaluate the impact of pVHL and HIF on CD70 expression in RCC, we performed Western blot (Fig. 13B) and qPCR analyses (Fig. 13C) of pVHL-deficient RCC cell lines 786-O and A498 and their stable transfectants reexpressing pVHL. Reconstituted pVHL lead to a decrease of *CD70* expression and the HIF targets *CA-IX*, *GLUT1*, *OCT4* and *PHD3*. TMA analyses demonstrated a significant association of CD70 expression and pVHL/HIF deregulation. CD70 expression was directly correlated with the expression of HIF1α (p=0.0136, Pearson R=0.1359) and HIF2α (p<0.0001, Pearson R=0.2833) as well as with the expression of the HIF targets CA-IX (p<0.0001, Pearson R=0.4267), Glut1 (p<0.0001, Pearson R=0.4093) and CD10 [103] (p<0.0001, Pearson R=0.3901). An inverse correlation was seen with pVHL (p=0.0144, Pearson R= −0.1398) and E-Cadherin [153] (p=0.0485, Pearson R= −0.1121). Next, we wanted to identify if pVHL drives the upregulation of CD70 via HIF in ccRCC. Silencing of *HIF2α* in 786-O and A498 exclusively

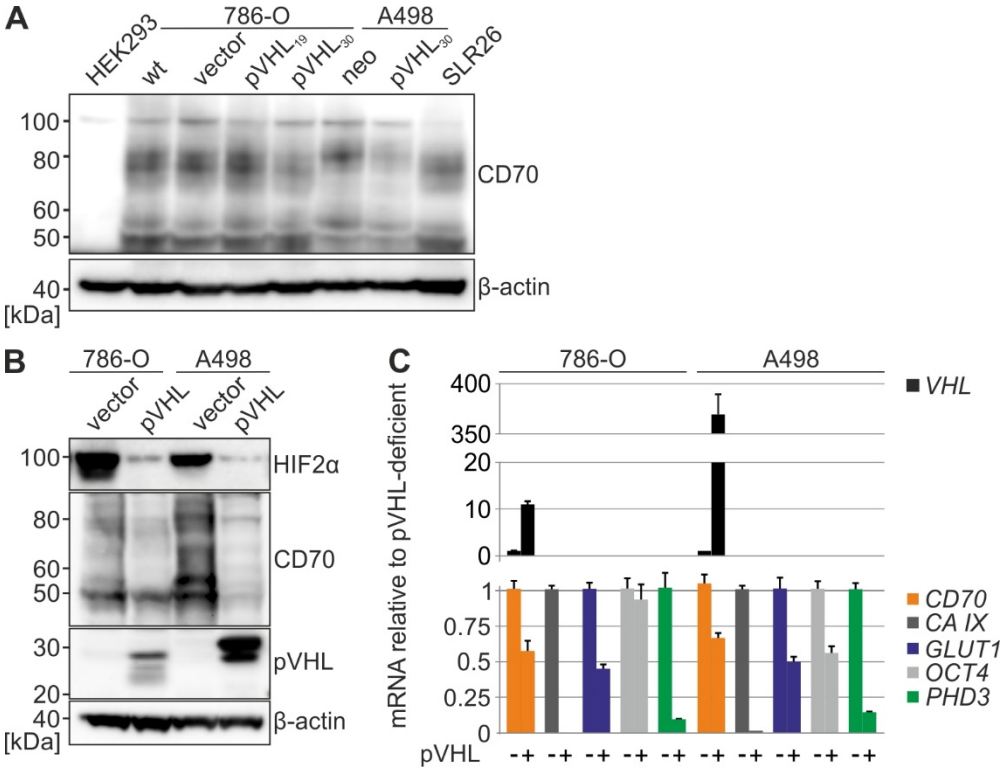


**Figure 13. CD70 expression is dependent on pVHL in RCC.**

A) Western blot of CD70 in the embryonic kidney cell line HEK293 and pVHL-deficient ccRCC cell lines 786-O and A498, which were reconstituted with either $pVHL_{19}$ or $pVHL_{30}$ isoform. B) Western blot of HIF2α, CD70 and pVHL in 786-O and A498 with reconstituted pVHL or empty vector. C) mRNA levels of *VHL, CD70, CA-IX, GLUT1, OCT4* and *PHD3* in 786-O and A498 with reconstituted pVHL relative to empty vector obtained by qPCR.

expressing HIF2α (but not HIF1α) lead to a decrease of *CD70* mRNA and protein expression (Fig. 14A-C). In SLR22 CD70 downregulation could only be achieved when both *HIF1α* and *HIF2α* were silenced (Fig. 14D).

Following transient overexpression of HIF1α and HIF2α in 786-O and A498 an increase of CD70 mRNA and protein levels was observed (Fig. 15A, B). Even in the pVHL-defective RCC cell lines SLR22 and SLR24 with low endogenous CD70 levels, upregulation of the latter was induced by overexpression of HIF2α (Fig. 15C, D). In pVHL-negative and -positive 786-O and A498 cells CD70 expression was continuously increasing under hypoxia within the first 12 hours (Fig. 15E, F). The transient transfection efficacy in 786-O cells had to be optimized before (Fig. 15G).

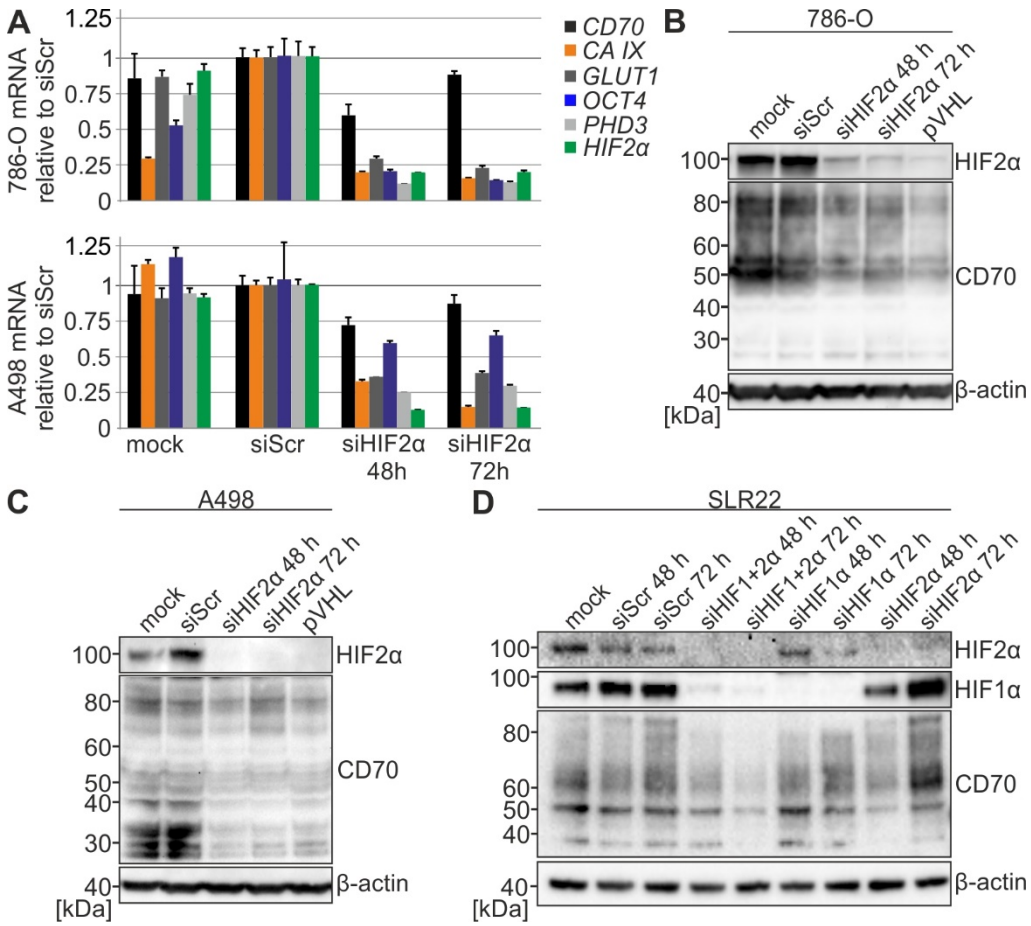


**Figure 14. CD70 expression is decreasing when HIF is silenced in RCC.**

A) mRNA levels of *CD70*, *CA-IX*, *GLUT1, OCT4*, *PHD3* and *HIF2α* relative to control siRNA (siScr= siScramble) obtained by qPCR in 786-O and A498, and B) Western blot of HIF2α and CD70 in 786-O and C) A498 after silencing of *HIF2α* for 48 hours (h) and 72 hours. D) Western blot of HIF1α, HIF2α and CD70 in SLR22 after silencing of *HIF1α*, *HIF2α* or both together for 48 hours (h) and 72 hours. D) was performed by A. Nowicka, Institute of Surgical Pathology, University Hospital Zurich.

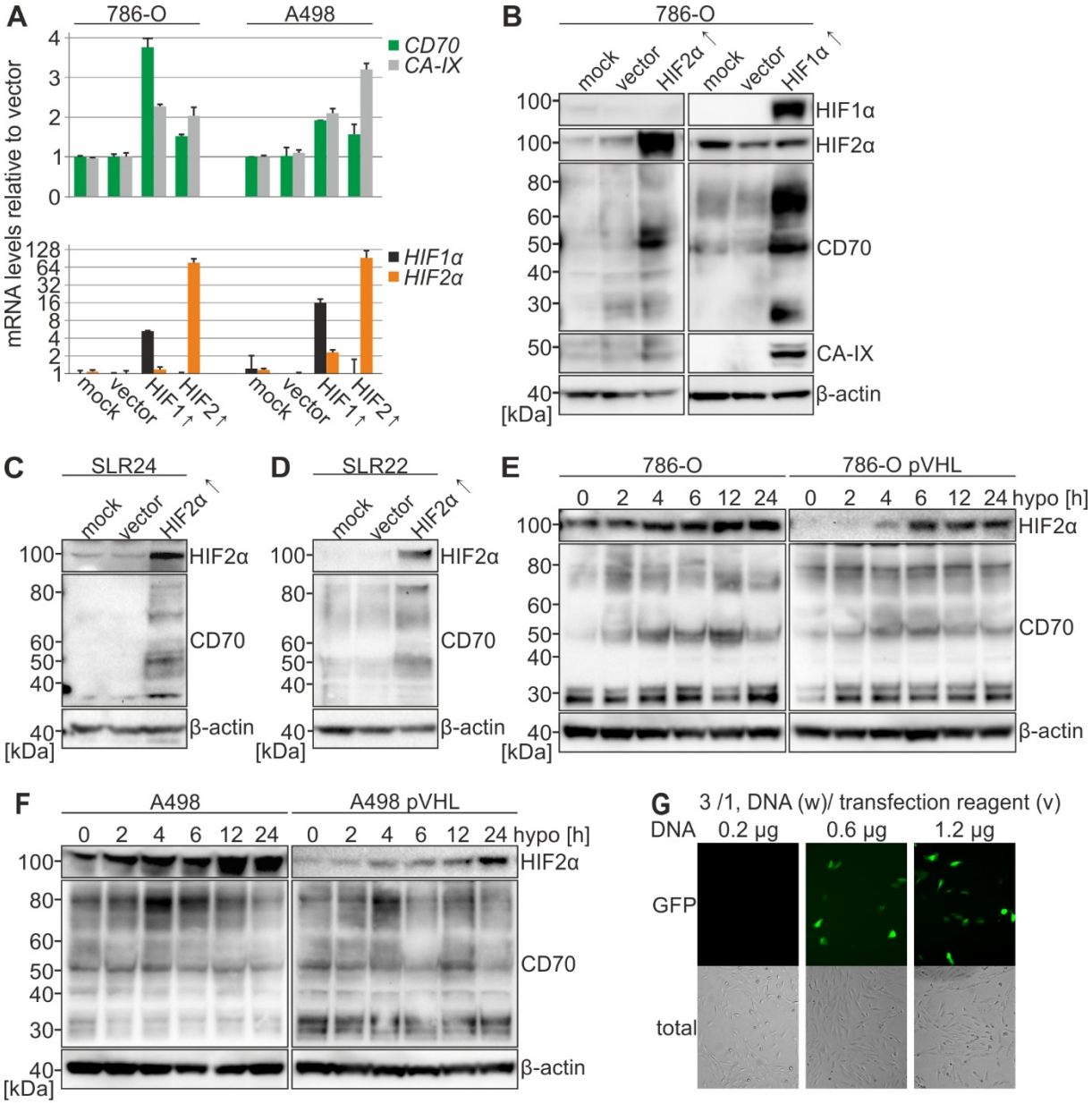


**Figure 15. Upregulation of HIF is accompanied by CD70 in RCC.**

A) mRNA levels of *CD70*, *CA-IX*, *HIF1α* and *HIF2α* relative to empty vector control (pcDNA3.1 (+)) obtained by qPCR and B) Western blot of HIF1α, HIF2α, CA-IX and CD70 in 786-O after transient overexpression of *HIF1α* and *HIF2α.* C) Western blot of HIF2α and CD70 in SLR24 and D) SLR22 after transient overexpression of *HIF2α.* E) Western blot of HIF2α and CD70 in 786-O and F) A498 with and without reconstituted pVHL incubated at 0.5% oxygen (hypo) for 0, 2, 4, 6, 12 and 24 hours (h). G) Optimization of transient protein overexpression in 786-O using green fluorescent protein (GFP). Error bars, SD (n=3).

### 6.1.5 CD70 expression is directly regulated by HIF

We performed ChIP with HIF2α-, HIF1α- and corresponding isotype control-antibodies (Fig. 16A, B) to elucidate if CD70 represents a potential HIF target. We investigated HIF's ability to bind to the eight potential HREs residing in 2.7 kb of the putative promoter of *CD70* (Fig. 16C). The reconstitution of pVHL in 786-O, A498 and RCC4 leads to a reduction of the direct binding of HIF2α and HIF1α to HRE3, 4 and 8 in the *CD70* promoter. No binding was observed for the negative control gene *KCNJ5* (encoding the G protein-activated inward rectifier potassium channel 4). *CD10* HRE2 served as positive control for HIF1α binding [103].

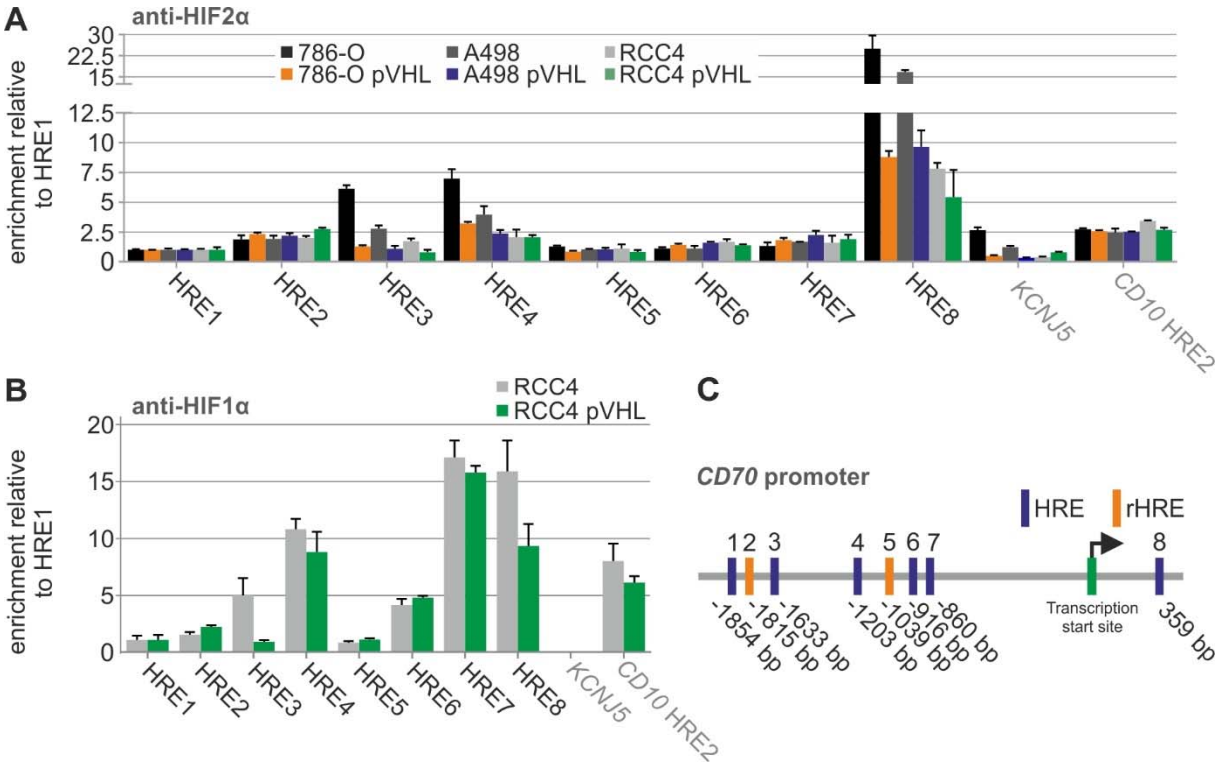


**Figure 16. HIF binds to the promoter of *CD70*.**

A) Binding of HIF2α and B) HIF1α at the *CD70* promoter relative to its isotype controls analyzed by ChIP. C) Schematic representation of the 2.7 kilo bases (kb) *CD70* promoter with the location of six HREs and two reverse HREs (rHRE). 1-8 indicate *in silico* identified HREs in the *CD70* promoter; *KCNJ5* served as negative and *CD10* HRE2 as positive control for HIF1α binding. bp= base pairs. Results are shown as ratios of the amplicons detected in 786-O, A498 or RCC4 pVHL-positive and negative relative to HRE1.

To confirm this finding we performed luciferase reporter gene assays. For this purpose, the DNA fragment containing the 5'-region of CD70 (−2000/+700) was inserted upstream of the luciferase gene. Compared to pVHL reexpressing A498 cells, the luciferase activity of the CD70 reporter gene construct was increased in A498 empty vector cells to the same extent as for the HIF target gene *PHD2* promoter construct (P2P) (Fig. 17A).The same effect was seen by overexpression of HIF2α in A498 and SLR22, but not by overexpression of its DNA binding

mutant [69] , which is unable to induce the expression of the CD70 protein product (Fig. 17B-D). By subdividing the *CD70* promoter into fragments containing the different HRE islands (Fig. 17E) we found, that the binding of HIF to HREs 4-7 and 8 indeed induced the transcriptional activity, whereas the binding to HREs 1-3 did not (Fig. 17F, G). These results suggest that HIF (with both HIF1α and 2α subunits) binds to three HREs within the *CD70* promoter (-1203; -860 and +359 bases from the *CD70* gene) thereby inducing the expression of CD70 in RCC.

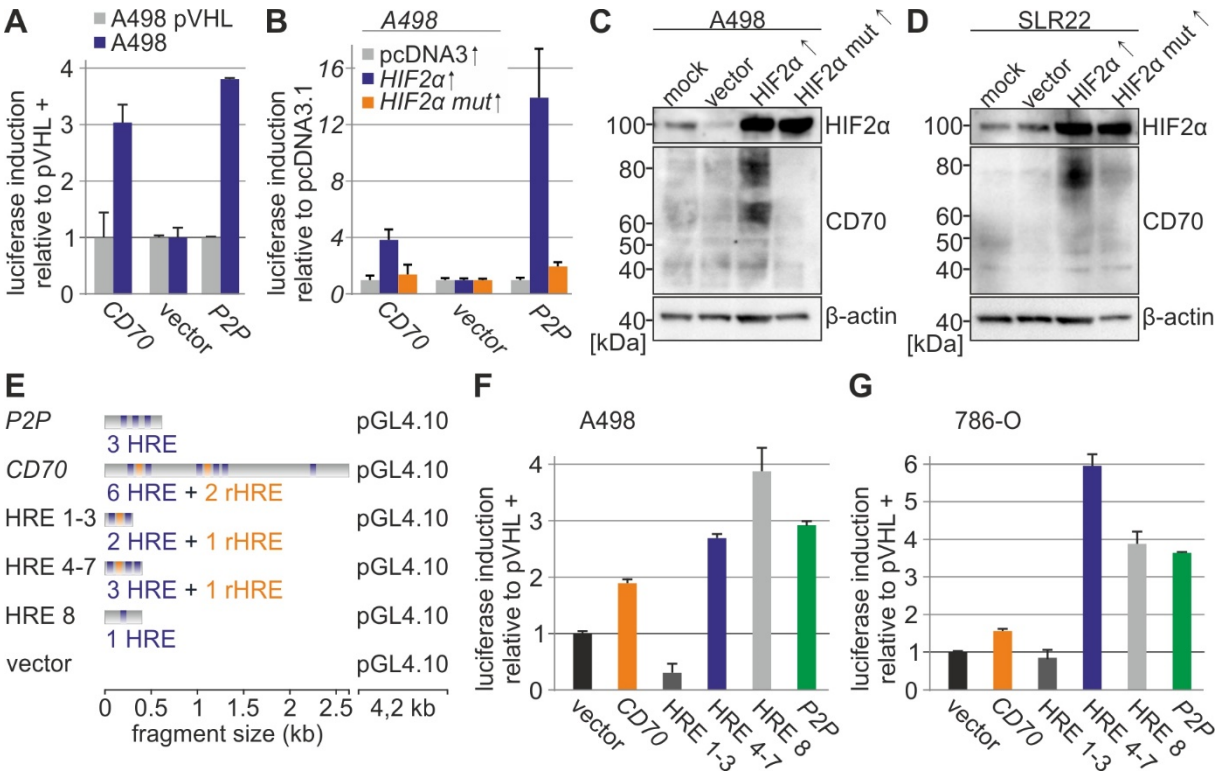


**Figure 17. HIF binding to the promoter of *CD70* induces its gene expression.**

A) Luciferase induction of the 2.7 kb promoter region of *CD70* in A498 empty vector relative to A498 reconstituted with pVHL. B) Luciferase induction of the 2.7 kb promoter region of *CD70* after overexpression of HIF2α or a DNA binding mutant of HIF2α in A498 relative to pcDNA3.1-transfected cells. C) Western blot of HIF2α and CD70 after transient overexpression of HIF2α or a DNA binding mutant of HIF2α in A498 and D) SLR22. E) Schematic illustration of the reporter constructs cloned into pGL4.10. *P2P* served as a positive control for the HIF activity. F) Luciferase induction of the different promoter regions of *CD70* in A498 empty vector and G) 786-O empty vector relative to cell line with reconstituted pVHL. (vector = empty luciferase reporter plasmid pGL4.10). Error bars, SD (n=3).

### 6.1.6 CD70 is not regulated by hypermethylation of its promoter in RCC

It was reported that the high expression of CD70 in various T cell affecting diseases is caused by demethylation of the *CD70* promoter [137-141]. To investigate if CD70 is also regulated by epigenetic changes in ccRCC in addition to the the pVHL/HIF axis, we analyzed the methylation status of the 11 cytosine-phosphate-guanine (CpG) islands within the promoter of *CD70* in

ccRCC. We performed bisulfite sequencing according to a published protocol [142] in four RCC cell lines with increasing CD70 expression levels and the epithelial kidney cell line HK-2 as negative control. Interestingly, there was a weak association of hypomethylation of CpGs to overexpression of CD70 in ccRCC cell lines (Fig. 18A). However, the inhibition of DNA methyltransferases with 5-azacytidine (5'azaC) lead to decreased CD70 expression in the ccRCC cell lines (Fig. 18B, C) which is in contrast to the results seen in breast cancer cell lines [142]. In addition, there was no association of CD70 expression with the methylation pattern of the *CD70* promoter seen in six paired normal and tumor tissues of RCC patients (Fig. 18D, E), suggesting that methylation plays a minor role in the gene regulation of CD70 in RCC.

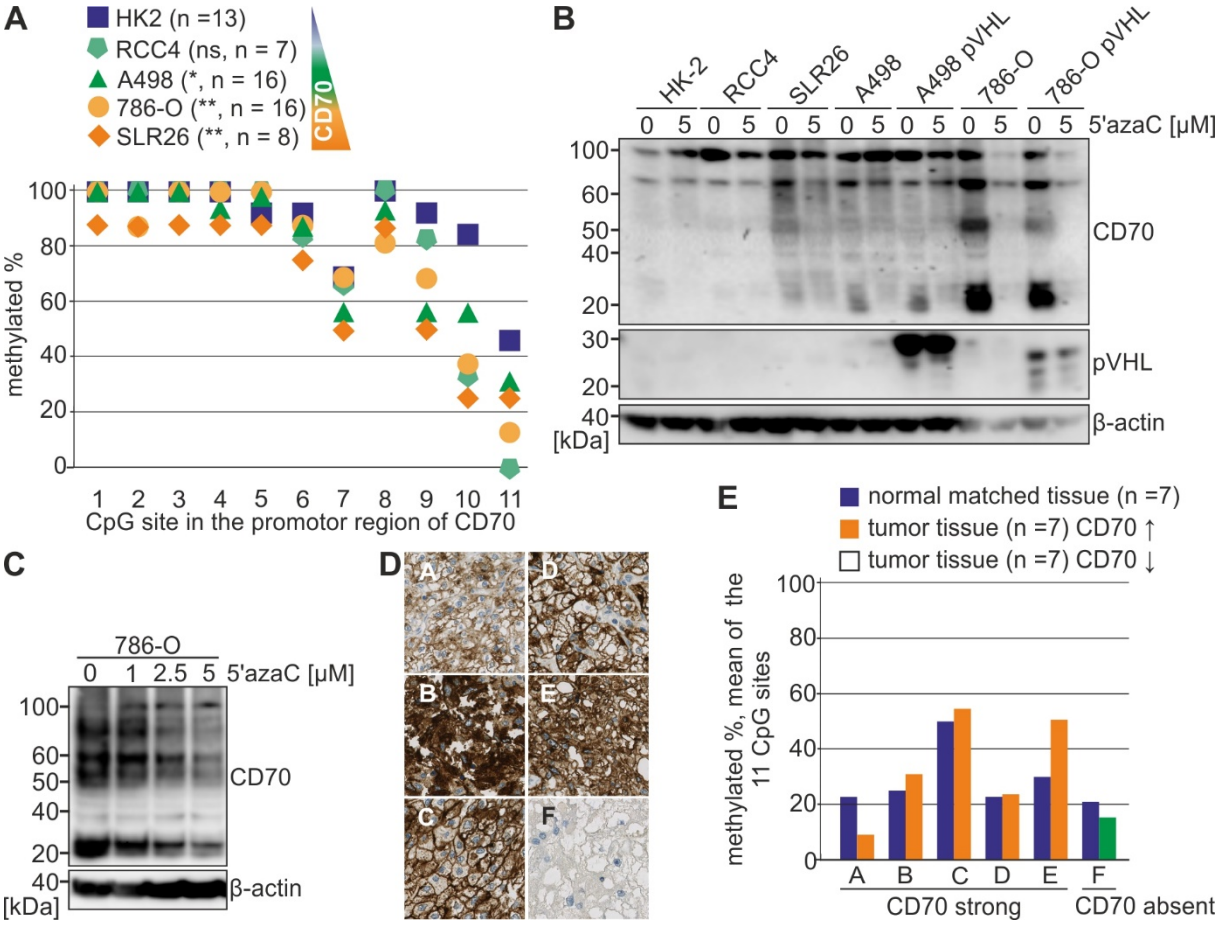


**Figure 18. CD70 promoter methylation in RCC and an epithelial kidney cell line.**

A) The genomic DNA from a series of RCC cell lines and HK-2 were treated with sodium bisulfite and a 240 bp sequence between positions -588 to -323 bp relative to the transcription start site was amplified by PCR. PCR products were cloned into pGEM®-T Easy vectors and the purified plasmid DNA of 7 to 16 independent clones was sequenced. The methylation status of the 11 CpG sites (X-axis) within this region was assessed and depicted as the mean methylation status (Y-axis). *T* test with HK-2 as reference was performed (** = p≤ 0.005, * = p≤0.05, ns = not significant). B) Western Blot of CD70 in HK-2 and several RCC cells after treatment with the DNA methyltransferase inhibitor (5'azaC). C) Titration of 5'azaC in 786-O. D) anti-CD70-immunostained tumors with different CD70 expression used for E) bisulfite sequencing.

### 6.1.7 The CD70 receptor, CD27, is strongly expressed in RCC infiltrating lymphocytes

It was previously reported that the receptor for CD70, CD27, is expressed in renal tubules and can be upregulated following ischemic renal injury [154]. We confirmed the expression in the tubules of all normal kidneys tested (Fig. 19A, B). In RCC we found CD27 much less frequently expressed. In addition to cytoplasmic staining and occasional nuclear staining in tumor cells several tumors had strongly positive infiltrates (Fig. 19C). Immunohistochemical (IHC) staining of RCC cell lines revealed a similar expression pattern as seen in the tumors. We decided to focus on CD27 expression on lymphocytes infiltrating RCCs for the following reasons: i) there was no consistence between the results obtained by IHC of the cell microarray and Western blots. ii) We could not silence the band appearing at the correct molecular weight for CD27 in the Western blot using four different siRNAs and iii) *CD27* mRNA levels from the gene expression data contrasted the protein expression levels seen in the different cell lines. iv) CD27 expression in ccRCC neither correlated with CD70 nor with pVHL expression and v) most importantly, TILs exhibited the highest CD27 expression levels.

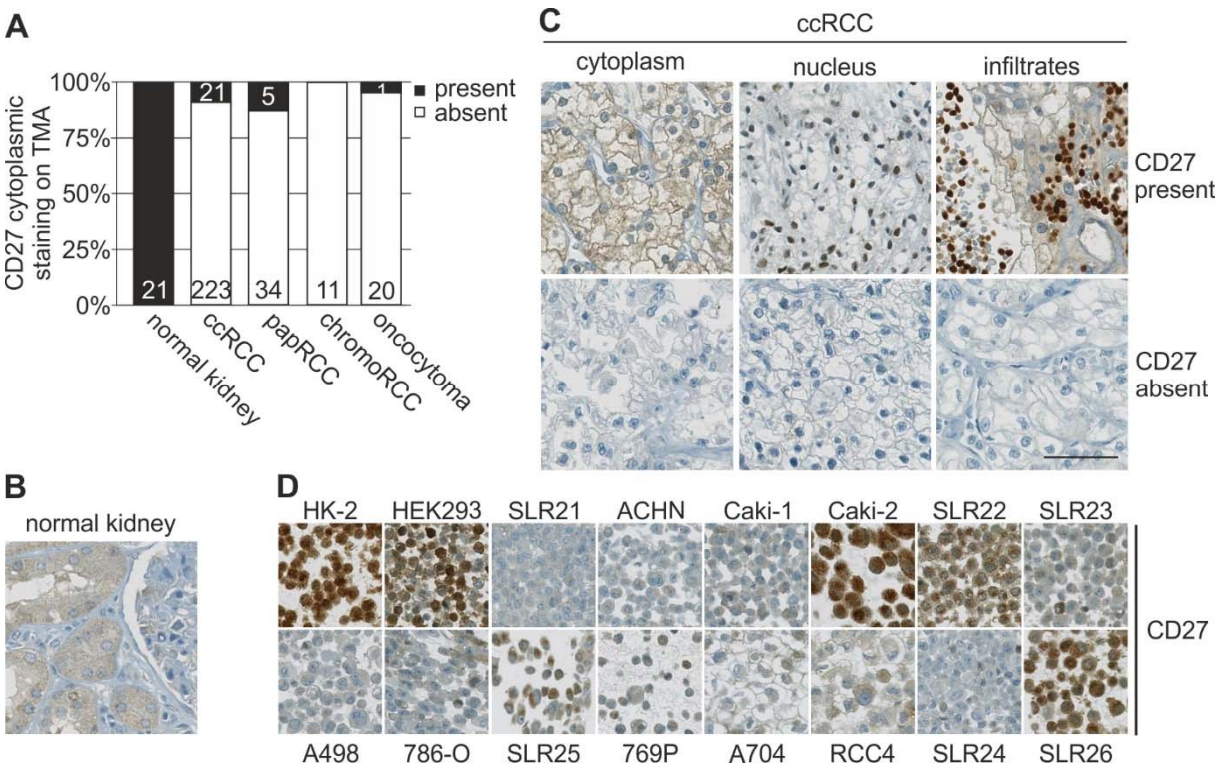


**Figure 19. CD27 expression pattern in RCC.**

A) Histogram representing CD27 expression frequencies in RCC and normal kidney tissue. B) Representative pictures of anti-CD27-immunostained renal tubules of normal kidney and C) ccRCCs (20x magnification, bars: 50 µm). D) Cell microarray stained for CD27 in different RCC cell lines (20x magnification). Pap: papillary, chromo: chromophobe.

### 6.1.8 CD27⁺ lymphocytes preferentially infiltrate CD70-expressing tumors which correlates with worse patient outcome

As the role of CD70/CD27 interaction in ccRCC is unknown, we next asked if there was an association between CD70-expressing tumor cells and CD27⁺ TILs. Recently, Wang *et al.* [130] showed that fresh renal tumors contained a significantly lower percentage of CD27-expressing T cells, less naive and central memory T cell subpopulations and in contrast more effector memory cells than the peripheral blood mononuclear lymphocytes (PBMCs) of the same patient. Furthermore, they suggested that this phenotypic conversion of the T cells is caused by high CD70 tumor expression. Our qPCR analysis of 47 ccRCCs selected from the TMA, which was immunostained against CD70, showed higher *CD27* mRNA expression in tumors with strong CD70 staining compared to tumors with lower CD70 expression (Fig. 20A).

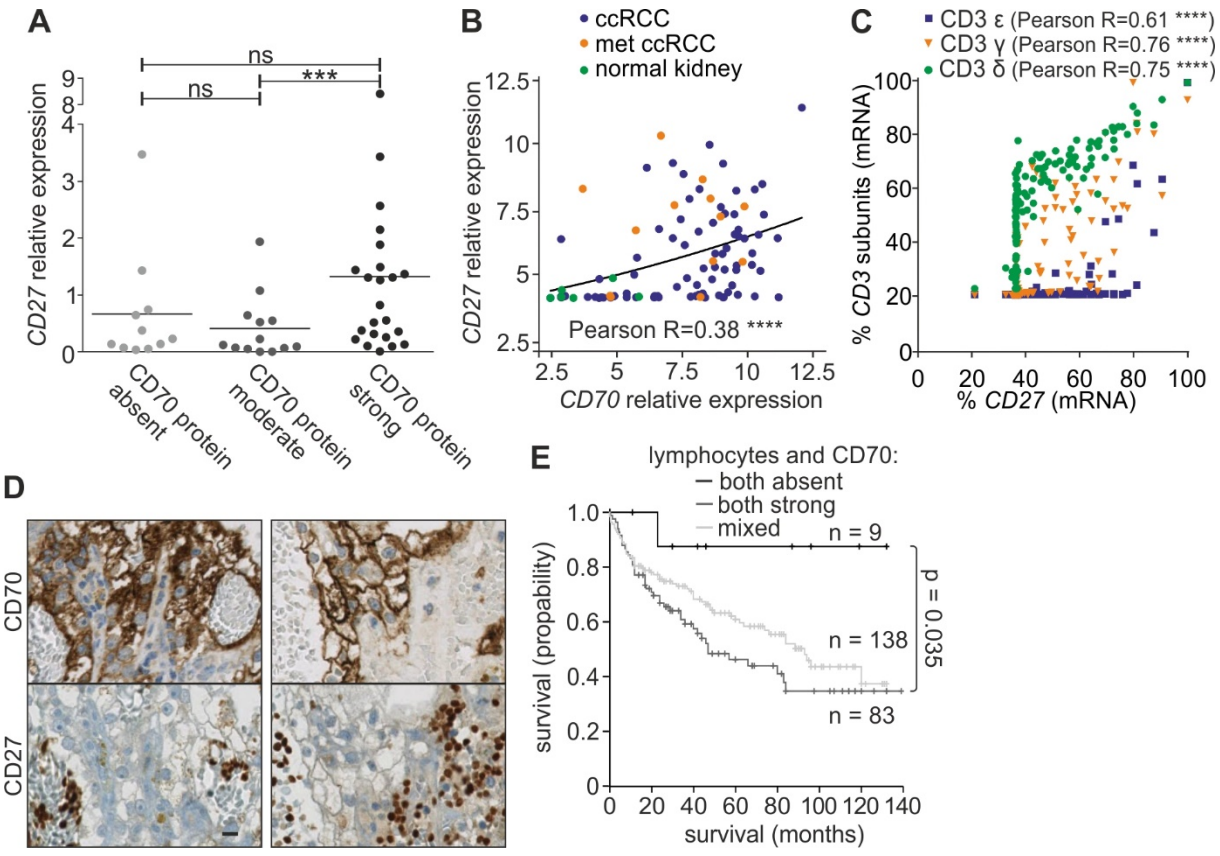


**Figure 20. Correlation between CD70 expression and CD27⁺ tumor infiltrating lymphocytes.**

A) *CD27* mRNA levels obtained by qPCR separated into ccRCCs showing no, moderate or strong CD70 tumor staining on TMA. ***, p<0.0001 by *t* test. B) *CD70* plotted against *CD27* mRNA levels of the gene expression data. Pearson R correlation analysis is depicted. (met: metastasis). C) *CD3* subunits (ε, γ and δ) plotted against *CD27* mRNA levels of the gene expression data. Results of Pearson R correlation analyses are depicted.D) Representative pictures of anti-CD70 and anti-CD27-immunostained ccRCCs of consecutive slides (40x magnification, bar: 100 µm). E) Kaplan-Meier plot of the overall survival of ccRCC patients defined by the CD70 expression accompanied by lymphocyte infiltration. Log-rank test was performed.

*CD27* and *CD70* gene expression obtained from a recent DNA-microarray analysis [145] confirmed this finding (Fig. 20B). The strong correlation between *CD27* and the subunits of the T cell marker *CD*3 indicated that the CD27 stained lymphocytes were T cells (Fig. 14C). To validate the gene expression data on protein level, we investigated CD70 and CD27 expression patterns on large consecutive tissue sections of 41 ccRCC infiltrated by lymphocytes. We observed that 37 ccRCCs (90%) contained also $CD27^+$ lymphocytes (Fig. 20D). Interestingly, correlations between TMA expression data and clinico-pathological data showed that patients with CD70-negative ccRCCs and no lymphocyte infiltration had a better survival compared to those with CD70 strongly positive and lymphocyte infiltrated ccRCCs ($p<0.05$) (Fig. 20E). The latter tumors were significantly associated with a high Fuhrman grade but not with late tumor stage (Table 5).

**Table 5. Correlation analysis between tumor stage, grade and CD70 expression in presence or absence of TILs in ccRCC.**

| | **CD70 strong with TILs n (%)** | **CD70 negative without TILs n (%)** | Pearson $\chi^2$ test |
|---|---|---|---|
| **Fuhrman low grade (1-2)** | 9 (10.8) | 7 (77.8) | p<0.0001 |
| **Fuhrman high grade (3-4)** | 74( 89.2) | 2 (22.2) | |
| **Early tumor stage (pT1/2)** | 29 (34.9) | 6 (66.7) | ns |
| **Late tumor stage (pT3/4)** | 54 (64.1) | 3 (33.3) | |

### 6.1.9 PBMCs trigger the release of sCD27 in a CD70-dependent manner

CD27 is known to be cleaved by a protease into its soluble form sCD27 on activated T cells [115, 155]. It was also shown that CD70-expressing glioma cells enhance the release of sCD27 from PBMCs [149]. To test if CD27 can also be cleaved after interaction with CD70 in RCC, we cocultured RCC cells with freshly isolated PBMCs and measured sCD27 in the supernatant by ELISA (Fig. 21A). Supernatants of PBMC and RCC cell monocultures contained basic levels of sCD27 after two days. The increase of the sCD27 concentrations of 786-O cells cocultured with PBMCs correlated with the PBMC/RCC cells ratio (Fig. 21B). PBMC cocultures with the CD70-expressing cell lines 786-O, A498 and SLR23 significantly increased the sCD27 concentration (2.7-fold, 1.9-fold and 2.3-fold, respectively) (Fig. 21C). Cocultures with CD70 low-expressing cell lines Caki-2, SLR22, SLR24 and SLR25 had only slightly elevated sCD27 concentration levels compared to PBMC monocultures. Both *CD70* silencing and reconstitution of pVHL in 786-O and A498 cells caused a reduction of sCD27 levels.

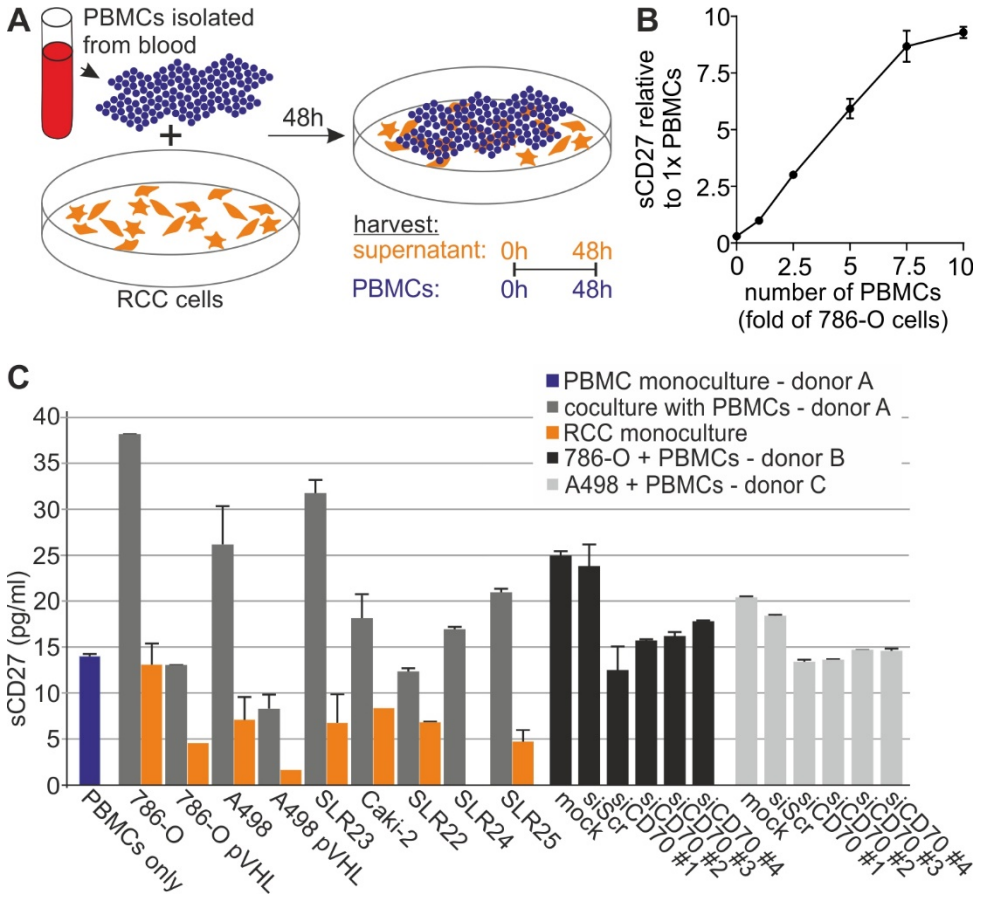


**Figure 21. Release of sCD27 via CD70 *in vitro*.**

A) Schematic illustration of a coculture experiment. PBMCs were isolated from fresh blood by Ficoll density centrifugation and cocultured with 0.1 times RCC cells for 48 hours (h). Supernatent and PBMC samples were harvested before and after coculture. Concentrations of sCD27 in supernatants of PBMC and RCC cell line cocultures or monocultures were determined by ELISA. B) 786-O cocultured with different numbers of PBMCs. C) CD70 expression was silenced in 786-O and A498 by siRNA (siCD70#1-4). siScr: control siRNA. Donor A-C: PBMCs from different healthy individuals.

### 6.1.10 Soluble CD27 levels are elevated in sera of patients with CD70-expressing RCC

After informed consent, we collected serum and heparin of 57 RCC patients within 2.5 years in collaboration with the department of Urology, University Hospital Zurich (Table 7). To investigate if our *in vitro* results were conferrable to patients we measured sCD27 concentration in sera of ccRCC and papillary RCC patients as well as of healthy individuals (Fig. 22A). sCD27 levels were compared with the expression status of CD27 and CD70 on large tissue sections of the corresponding patients (Fig. 22B). sCD27 serum levels of patients with CD70-expressing tumor cells and $CD27^+$ TILs were significantly higher compared to those of healthy individuals and RCCs of patients that either had CD70-positive tumor cells but no $CD27^+$ TILs or had $CD27^+$ TILs and CD70-negative tumor cells or were negative for both. To

investigate if the sCD27 serum concentration is suited to predict the clinical course of RCC patients, we measured serum sCD27 after nephrectomy. The sCD27 levels of patients that either had CD70-positive tumor cells but no $CD27^+$ TILs or had $CD27^+$ TILs and CD70-negative tumor cells or were negative for both remained low, irrespective of the course of their disease. The on average higher sCD27 serum levels of patients with CD70-expressing tumor cells in combination with $CD27^+$ TILs rarely increased after nephrectomy. However, a retrospective prediction for the outcome of the patient could not be made based on the alteration of sCD27 serum levels. Notably, ELISA analysis of CD70 revealed that CD70 protein expression levels in 31 RCCs were not reflected in the sera of these patients as most of the CD70 levels were below the detection limit (data not shown). Taken together this data indicates that CD70 expressed on RCCs triggers the release of lymphocyte-derived CD27, most likely causing the on average higher sCD27 serum levels in patients with CD70-positive RCCs infiltrated by $CD27^+$ lymphocytes.

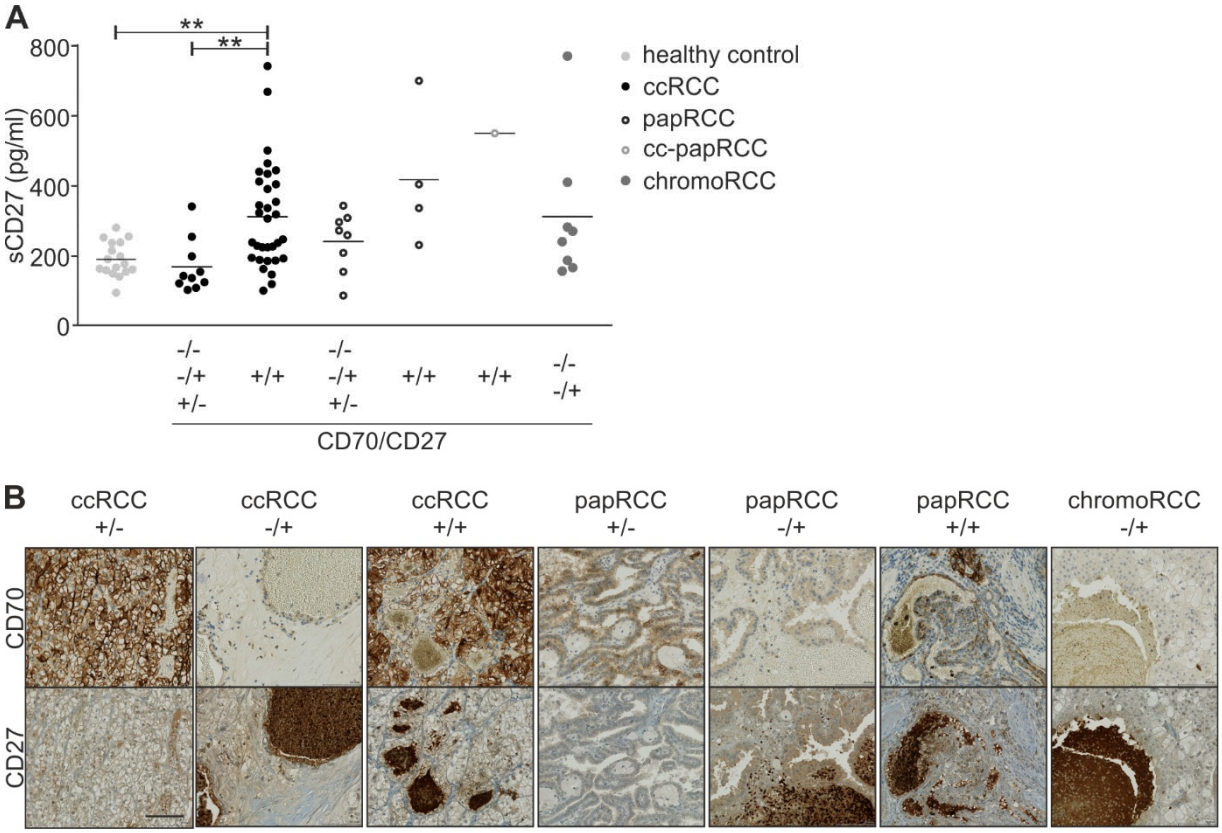


**Figure 22. Correlation of sCD27 serum levels with CD70/CD27 expression state in RCC patients**

A) Serum concentrations of sCD27 of RCC patients and healthy controls. **, $p<0.005$ by *t* test. B) Representative pictures of anti-CD70 and anti-CD27-immunostained ccRCCs of consecutive slides of large sections (40x magnification, bar: 100 µm). The existence of CD70 expression and $CD27^+$ lymphocyte infiltrations (CD70/CD27) of the tumor tissues is indicated as absent (-) or present (+). pap: papillary, chromo: chromophobe, cc-pap: clear cell papillary.

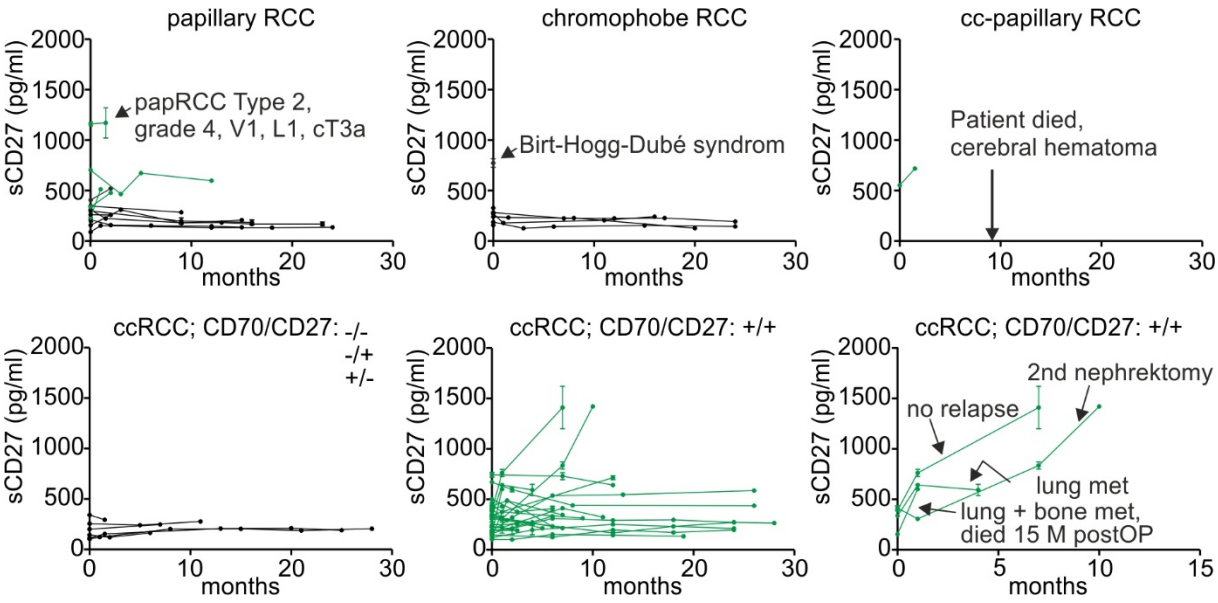


**Figure 23. Serum sCD27 and clinical outcome of RCC patients.**

Serum concentrations of sCD27 of RCC patients at the day of nephrectomy (time point 0) and post surgery. The existence of CD70 expression and CD27⁺ lymphocyte infiltrations (CD70/CD27) of the tumor tissues is indicated as absent (-) or present (+). Serum levels of patients with CD70/CD27-positive tumors are highlighted in green. Error bars, SD (n=2).

### 6.1.11 Chronic CD70 /CD27 interaction in RCC leads to T cell exhaustion

The higher nuclear differentiation grade and a significantly worse survival of patients with ccRCCs strongly expressing CD70 containing TILs compared to patients with CD70-negative tumors that were not infiltrated by lymphocytes lead us to speculate that the interaction of CD70-expressing tumor cells and CD27⁺ TILs may play a role in tumor progression.

Different tumor-promoting mechanisms are possible in this context. Soluble CD27 can induce proliferation in CD70-positive acute lymphoblastic leukemia and nasal natural killer (NK)/T cell lymphoma [156, 157]. Therefore we tested if the interaction of CD27 present on TILs with CD70 present on ccRCC cells have similar effects and accelerate RCC cell proliferation. Recombinant sCD27 rather lead to a decrease than to an increase of the metabolic activity of two RCC cell lines (Fig. 24).

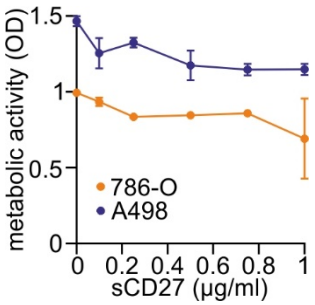


**Figure 24. Recombinant sCD27 reduces the metabolic activity of RCC cells.**

MTT assay after adding 0; 0.1; 0.25; 0.5; 0.75 or 1 µg/ml sCD27 to 786-O and A498 cells for 24 hours.

It was also reported that CD70-expressing ccRCC and glioma cells were able to provoke T cell apoptosis in coculture experiments [129, 149, 158]. However, the immune inhibitory properties of CD70 *in vitro* seem to be clearly overwhelmed by the immune activating properties observed in mouse glioma models *in vivo* [159]. Finally, the chronic ligation of CD27 and CD70 may also lead to T cell exhaustion, a kind of "immune escape", since it was shown that constitutive expression of CD70 on B cells in mice converted naïve T cells into effector memory cells and culminated in the depletion of naïve T cells [160].

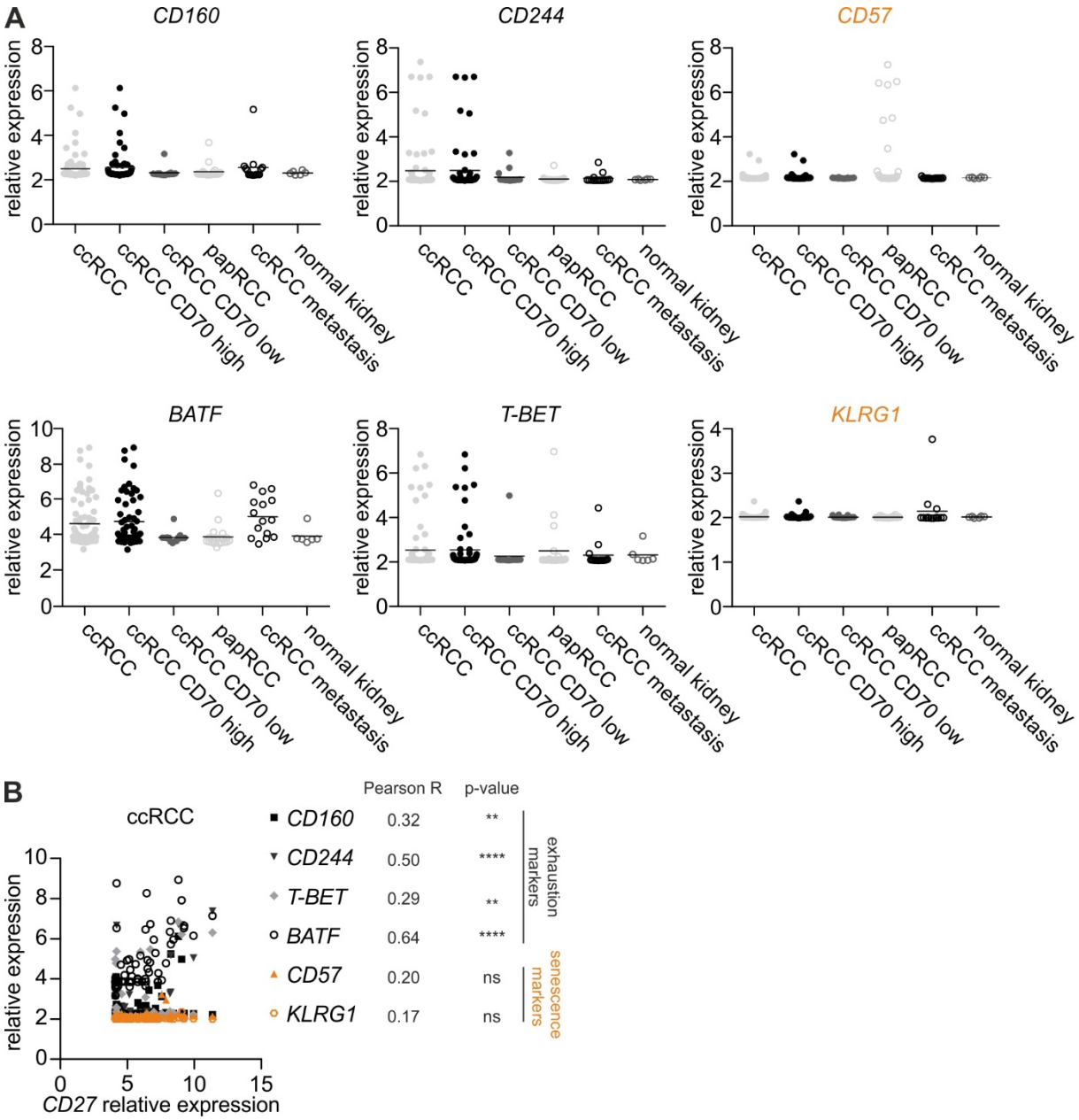


**Figure 25. T cell exhaustion and senescence markers in RCC.**

A) Exhaustion and senescence marker gene expression in RCCs and normal kidney tissue. pap: papillary. B) ) Exhaustion and senescence markers (highlighted in orange) plotted against *CD27* mRNA levels obtained from gene expression data. Pearson R correlation analysis is depicted.

In keeping with this, Wang *et al.* [130] observed less naïve and central memory T cell subpopulations but more effector memory cells in ccRCC in contrast to matched PBMCs. They suggested that this phenotypic conversion of T cell is caused by high CD70 expression in ccRCC. To test if the chronic ligation to CD70 leads to T cell exhaustion in RCC, we compared T cell exhaustion markers (*CD160*, *CD244*, *BATF*, *T-BET* [161, 162]) and senescence markers (*CD57* and *KLRG1* [163]) with *CD70* and *CD27* in RCC subtypes using gene expression data [145]. T cell exhaustion markers were higher expressed in CD70-positive ccRCCs than in CD70-negative ccRCCs and other RCC subtypes (Fig. 25A), whereas senescence markers levels are equally common, except *CD57* in papillary RCC. The exhaustion markers correlated significantly with *CD27* (Fig. 25B), but neither without normalization nor normalized to $CD27^+$ T cells (*CD27*) or T cells in general (*CD*3), they showed any correlation with *CD70*. *CD70* expression significantly correlates with *CD27* in ccRCC (p=0.0003; see fig. 20B). This means that CD70-expressing ccRCCs harbor more exhausted $CD27^+$ T cells than CD70-negative ccRCCs in total, but not that $CD27^+$ T cells are more exhausted in CD70-expressing ccRCCs than in CD70-negative ccRCCs.

To test if CD70 leads to a conversion of T cells to a more exhausted phenotype *in vitro* we cocultured IL2-activated PBMCs with CD70-postive and -negative RCC cell lines as before (see fig. 21). Before and after coculture we measured the IFN-γ release and the expression of exhaustion markers (*CD160*, *LAG3*, *PBRM*1) and the senescence marker *CD57* of the PBMCs.

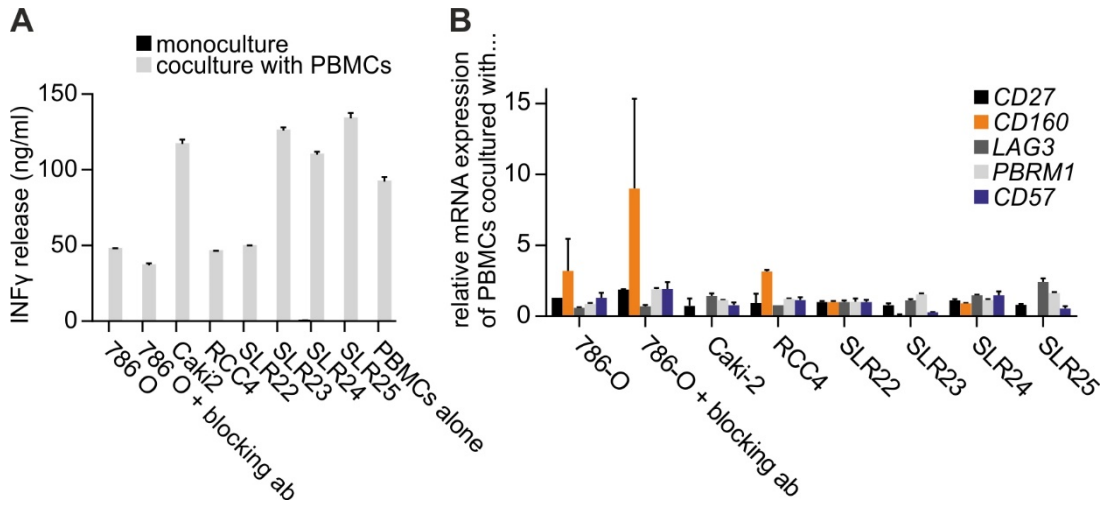


**Figure 26. T cells exhaustion state is not dependent on the CD70 expression of RCC cells *in vitro*.**

Concentrations of INFγ in supernatants of PBMC and RCC cell line cocultures or monocultures were determined by ELISA. B) *CD27, CD160, LAG3, PBRM1 and CD57* mRNA levels obtained by qPCR of PBMCs of one healthy donor, which were cocultured with different RCC cell lines before. Blocking ab = anti-CD70 antibody Ki-24.

Neither from the INFγ release data nor from the expression of T cell exhaustion and senescence markers we can conclude that CD70 on RCC cells provokes a phenotypic conversion of PBMCs to a more exhausted state *in vitro* within the time analyzed (Fig. 20A, B). After coculture with activated PBMCs for 48 hours no RCC cells were left, making the assessment of putative changes in the migration behavior of CD70-positive and CD70-negative RCC cell in response to the interaction with lymphocytes impossible.

However, our gene expression analysis of exhaustion markers *in vivo* accords with the hypothesis that the existence of CD70 in ccRCC fosters immune exhaustion effects by the chronic attraction and stimulation of $CD27^+$ T cells.

## 6.2 PTPRJ is negatively regulated by the pVHL/HIF axis in RCC

A previous PhD thesis project focused on one of the biomarker candidates termed PTPRJ, which was reduced in ccRCC as a consequence of pVHL loss [103]. To validate the findings of PTPRJ's role in RCC, additional experiments were needed to publish the study. First, we validated reduced levels of PTPRJ protein in tumor tissues. By using additional siRNAs we confirmed an experiment showing that *PTPRJ* mRNA is increased to its basic level when HIF2α was silenced. Finally, we proofed that the *PTPRJ* promoter activity was lowered in the presence of HIF2α with a luciferase assay. This study was published in *Journal of Pathology*, 2013 [144].

## 6.3 The tumor progression suppressor TGF-βRIII increases with tumor progression in the sera of RCC patients

In addition to CD70, the presence of six other promising biomarker candidates, which were found to be upregulated in ccRCC in a previous study [103] were analyzed in serum of RCC patients.

A

| | RNA | | | | | protein | |
|---|---|---|---|---|---|---|---|
| | tissue | | | cell lines | | | |
| Gene name | ccRCC/ normal | pRCC/ normal | ccRCC/ pRCC | VHL-/ VHL19+ | VHL-/VHL30+ | VHL-/VHL+ | Full protein name |
| ALCAM | 1.68 | 1.21 | 1.39 | 0.89 | 1.51 | 786-O, -19, -30 | activated leukocyte cell adhesion molecule |
| MME / CD10 | 0.77 | 0.08 | 9.81 | 16.67 | 3.70 | 1.50 | Neprilysin |
| TGFBR3 | 0.48 | 0.21 | 2.26 | 1.39 | 1.37 | 786-O | Transforming growthfactor, beta receptor III |
| KDR | 5.20 | 0.21 | 24.45 | 0.05 | 0.00 | 786-O | kinase insert domain receptor |
| EPHA2 | 0,67 | 0,67 | 1,01 | 0,62 | 0,99 | 786-O, -19, -30 | EPH receptor A2 |
| M6PR / IGF2R | 0,84 | 9,00 | 0,94 | 0,90 | 0,70 | 786-O, -19, -30 | mannose-6-phosphatereceptor |

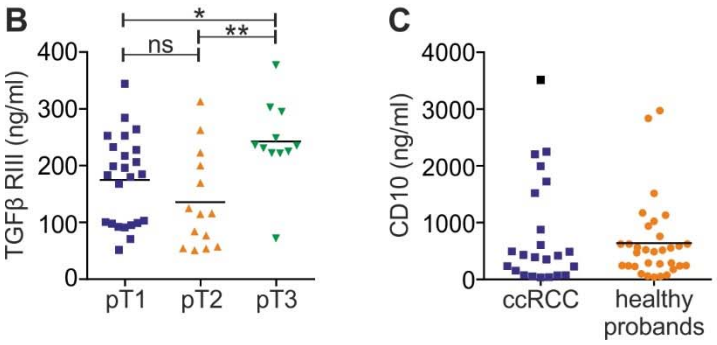


**Figure 27. TGF-βRIII rises with tumor progression in the serum of RCC patients.**

A) Analyzed biomarker candidates. B) TGF-βRIII serum concentrations of RCC patients separated according to tumor stage (pT). **, $p<0.005$; * , $p<0.05$ by *t* test. C) CD70 serum concentrations of RCC patients and healthy probands determined by ELSIA.

The first candidate, transforming growth factor beta receptor 3, TGF-βRIII, a suppressor of cancer progression was shown to be reduced in RCC as well as in multiple cancers [164]. Low density array- and genechip-based experiments revealed a generally lower expression in RCC compared to normal kidney and a pVHL-dependent surface expression in ccRCC [103], (Fig. 27A). Interestingly, in serum of RCC patients we found higher TGF-βRIII concentrations with increasing tumor stage (Fig. 27B). Serum levels of TGF-βRIII were not differing between RCC subtypes and healthy probands (data not shown).

In the previous study it was shown that CD10, another biomarker candidate, which was highly expressed on ccRCC surfaces showed ccRCC-specific serum levels [103]. By using a cohort with more healthy probands we could not confirm this data (Fig. 27C).

The RCC surface expression observed for both the activated leukocyte cell adhesion molecule (ALCAM) and the receptor tyrosine kinase VEGFRII, which is used as a target of angiogenesis

in the treatment of metastatic RCC (sorafenib) [165] was not reflected in the sera of patients. For two other candidates (EPHA2 and IFG2R) the serum concentrations could not reach the detection limit of the ELISAs.

# 7 Discussion

## 7.1 CD70 is regulated by the pVHL/HIF axis in ccRCC

In this study we demonstrated that the high and frequent CD70 expression in ccRCC is driven by HIF as a consequence of pVHL loss of function. We further observed a strong association between CD70-expressing tumor cells and the presence of $CD27^{+}$ T cells in TILs. The ability of CD70 to trigger the release of sCD27 on PBMCs *in vitro* and the increased levels of sCD27 in the sera of patients with CD70-expressing tumors suggest that sCD27 is a putative serum marker for CD70-positive ccRCC patients (Fig. 28).

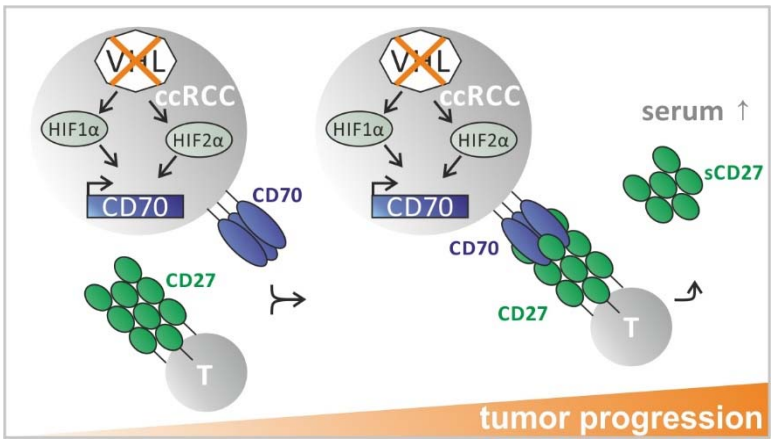


**Figure 28. A model showing the biological and clinical relevance of CD70 and sCD27 in ccRCC.**

### 7.1.1 The high and frequent expression of CD70 in ccRCC is unique among RCC and other solid tumors

In healthy cells CD70 expression is tightly regulated and restricted to a small subset of antigen-stimulated B and T lymphocytes [105, 109]. Within the last years aberrant expression of CD70 has also been described in other solid tumors including RCC.

CD70 expression is dependent on the RCC subtype. IHC staining of TMAs with more than 600 RCCs showed abnormal CD70 expression in 78% of ccRCCs, which was consistent with previously described frequencies [124, 125]. Our comprehensive CD70 analysis of 348 papillary RCCs revealed 11% strongly and 22% moderately expressing tumors, which was lower compared to the frequencies observed in recently published smaller cohorts [123, 125, 126]. In addition, we found CD70 more frequently expressed in low-grade papillary RCCs and in the less aggressive type 1 than in type 2 papillary RCC [148]. Opposite to our finding in a

previous study of a smaller cohort of 46 papillary RCCs there was a trend towards higher CD70 expression in type 2 papillary tumors than in type 1 papillary tumors [126]. Why type 1 of papillary RCC expresses CD70 more often needs to be further elucidated.

No expression was seen in 21 oncocytomas and 13 chromophobe RCCs suggesting a negligible role of CD70 in these tumor subtypes. The absence of CD70 in oncocytoma and chromophobe RCC was described before [123-126].

It is important to see, that the frequencies observed in other solid tumors are low, differ from study to study and also depend on the antibody used for tissue staining. Ryan *et al.* [134] described CD70 expression in 10% (17/172) lung and 2% (5/204) breast cancer. In our cohorts of 111 lung and 20 breast cancers we could not observe any CD70 expression that reached the lowest intensity counted as positive in RCC. Similar persistent high and frequent expression of CD70 as in ccRCC was not reported for any other solid tumor [106].

### 7.1.2 CD70 is linked to the *VHL* mutation state

We show that the abnormal upregulation of CD70 in ccRCC is closely related to the deregulation of the pVHL/HIF axis. CD70 expression patterns in ccRCC tissue were significantly correlated with those seen for HIFα and the HIF targets CA-IX, Glut1 and CD10 [103]. The analysis of the mutation status of *VHL* in 363 ccRCCs and 17 RCC cell lines further supported the association of CD70 expression with *VHL* sequence alterations. High CD70 expression levels were significantly linked to *VHL* mutations that very likely abrogate pVHL's function. Inactivation of *VHL* by hypermethylation of its promoter [166] and missense mutations with no or only minor effects on pVHL's ability to bind HIFα [151] may explain the presence or absence of CD70 in several *VHL* wt and mutated tumors, respectively. In pVHL-affected cell lines the expression pattern of CD70 was comparable with that of HIF1α, HIF2α as well as HIF targets Glut1 and CA-IX. Our results suggest that CD70 is driven by both HIF1α and HIF2α. Some *VHL*-mutated ccRCC cell lines exhibited no CD70 although HIFα was elevated. They may resemble those 20% (34/174) of CD70-negative ccRCCs, which had *VHL* mutations with functional impact on pVHL, presumably causing HIFα stabilization. Epigenetic modification of HREs may also influence the transcriptional response to hypoxia [77]. Aberrant DNA methylation of the two CpG islands (-993 to -323 bp relative to the transcription start site) [142] which overlap the region with the putative HREs in the *CD70* promoter may thus prevent

HIF from binding and may explain why CD70 is not or only weakly expressed in the presence of HIF in those tumors.

### 7.1.3 CD70 is regulated by the pVHL/HIF axis in ccRCC

*In vitro* experiments including pVHL reconstitution, *HIF$\alpha$* silencing and overexpression, hypoxia experiments, ChIP and luciferase assays confirmed that CD70 expression is dependent on pVHL's functional integrity and the transcriptional activation by HIF. Only the reconstitution of the full length pVHL ($pVHL_{30}$) attenuates CD70 expression, whereas the isoform lacking the *N*-terminal 53 amino acids ($pVHL_{19}$) does not. Although both $pVHL_{30}$ and $pVHL_{19}$ act as a substrate recognition subunit in the E3 ubiquitin ligase complex, interaction partners of $pVHL_{30}$ were identified, that do not bind $pVHL_{19}$ [167, 168]. Knockdown of the two HIFα isoforms provided evidence, that CD70 can indeed be sustained by both HIF1α and HIF2α in ccRCC. In the two cell lines with homozygous HIF1α deletions [71], knockdown of HIF2α was sufficient to reduce the expression of CD70. Whereas in SLR22 CD70 attenuation could only be achieved when both endogenous HIFα-forms were silenced. Overexpression of both HIF1α and HIF2α lead to increased CD70. A *HIF2α* mutant construct, which eliminates the ability of HIF2α to bind to DNA and to act as a transcription factor [69], could not upregulate CD70.

Controversial results were obtained when cell lines 786-O and A498 were subjected to hypoxia. In contrast to the first 12 hours, CD70 expression decreased slightly after 12 hours under hypoxic conditions. This attenuation of CD70 protein expression may be caused by oxygen-sensitive pathways that are HIF-independent [169].

A strong relationship between HIF$\alpha$ activation, CD70 upregulation and tumor formation was demonstrated in TRACK mice (transgenic model of cancer of the kidney), which specifically express a mutated, constitutively active form of HIF1α in kidney proximal tubule cells [70]. A recent study showed that activated HIF1α was sufficient to induce phenotypic alterations characteristic of human *VHL* ccRCC, including upregulation of CA-IX, Glut1 and even CD70, whereas a constitutively activated form of HIF2α was neither able to promote ccRCC, nor to enhance the expression of CD70 [170]. Gordon *et al.* [171] showed that HIF2$\alpha$ rather than HIF1$\alpha$ mediates ccRCC progression. Our *in vitro* data indicate that *CD70* can be activated by both HIF$\alpha$ isoforms. However, strong CD70 expression is preferentially seen in RCC cell lines

in which only HIF2α is present suggesting that HIF2α might be the main regulator for CD70 expression in progressing ccRCC.

### 7.1.4 HIF acts as a transcription factor, activating the expression of CD70

We tested the binding of HIF to the eight potential HREs located in the promoter region of *CD70* by ChIP. Interestingly this data showed that both HIF1α and 2α preferentially bind to three HREs located -1203; -860 and +359 bases from the *CD70* gene. Using luciferase assays we could validate that binding of HIF to these HREs induces the transcription of *CD70* in RCC.

### 7.1.5 CD70 expression is not regulated by hypomethylation of its promoter in RCC

It is obvious that in ccRCC the mechanism of CD70's upregulation is different to that reported in several T cell affecting diseases, such as systemic lupus erythematosus and systemic sclerosis [141, 172] in which hypomethylation of the *CD70* promoter contributes to CD70 overexpression. Using the same methylation-specific PCR protocol described by Yu *et al.* [142] no hypomethylation of the *CD70* promoter was seen in ccRCC tissues, which strongly expressed CD70. This suggests that the transcriptional regulation of *CD70* does not depend on promoter hypomethylation and is therefore mainly driven by HIF in this tumor subtype.

### 7.1.6 CD70 posttranslational modification is potentially organ-specific

The multiple banding pattern of CD70 in RCC seen in the Western blot was found and validated before [126, 149]. CD70 is a homotrimer [105, 107]. Protter predicts that they are held together by disulfide bonds [122]. Moreover we could show that some of these bands are *N*-glycosylated forms of CD70, as predicted by the NetNGlyc server [150]. We observed that CD70 is glycosylated in a different way in RCC cells than in lymphpoma cell line Raji. Since the banding pattern in RCC cells is the same as in the embryonic kidney cell line HEK293 transfected with CD70 [134], we concluded that the organ expressing CD70 probably determines how it will be glycosylated what might lead to organ specific signaling characteristics.

## 7.2 CD27$^+$ tumor infiltrating lymphocytes in CD70-expressing ccRCCs

### 7.2.1 CD70 attracts CD27$^+$ tumor infiltrating lymphocytes in RCC

In addition to the molecular mechanisms for abnormal CD70 expression in ccRCC, we were also interested to investigate the role of the interaction with its receptor CD27, which is known to be expressed on the surface of memory B cells, naïve and activated T cells and a subset of NK cells [104]. It was previously reported, that CD27 expression can be induced in kidney cells by renal ischemia-reperfusion injury [154]. This plays most likely a negligible role for RCC, because we only found very weak expression of CD27 in rare cases in the tumor cells of RCC. However, microarray gene expression data of ccRCC revealed a significant correlation between *CD70* and *CD27* expression. A detailed IHC analysis of large ccRCC tissue sections demonstrated that the lymphocyte infiltrates in CD70-expressing tumors contained almost always CD27$^+$ lymphocytes. Since CD27 highly correlated with T cell marker CD3 subunits (ε, γ and δ), we concluded that CD27 is expressed on T cells infiltrating ccRCCs. The significant correlation of *CD70* and *CD27* expression suggested that CD70 expression in ccRCCs attracts CD27$^+$ tumor infiltrating lymphocytes.

### 7.2.2 Continuous CD70/CD27 interaction promotes tumor progression in ccRCC

Neither we nor others have found a strong correlation between CD70 expression alone and tumor grade, stage and patient survival in ccRCC [125, 126]. In contrast, high CD70 was associated with a worse overall survival outcome in diffuse large B cell lymphoma and advanced ovarian carcinomas in previous reports [173, 174]. As the loss of pVHL function is considered an early event in ccRCC [80], the subsequent upregulation of CD70 may also contribute to tumor formation. We observed that the frequency of strong CD70 expression in pVHL-deficient primary ccRCC is retained in metastatic lesions. It is therefore conceivable that the persistent expression of CD70 in tumors leads to an enhanced attraction and infiltration of CD27$^+$ lymphocytes. Interestingly, ccRCC with strong CD70 expression and TILs had a higher nuclear differentiation grade and a significantly worse survival compared to CD70-negative tumors that were not infiltrated by lymphocytes. Based on this finding, we concluded that the interaction of CD70-expressing tumor cells and CD27$^+$ TILs may play a role in tumor progression.

### 7.2.3 CD27 does not induce RCC cell proliferation *in vitro*

Different tumor-promoting mechanisms have been proposed in this context. Soluble CD27 was able to induce proliferation in CD70-positive acute lymphoblastic leukemia and nasal NK/T cell lymphoma [156, 157]. Adding sCD27 to stimulated PBMCs was shown to increase T cell activation and proliferation [175]. T cells proliferation was enhanced in a dose-dependent manner with increasing amounts of recombinant sCD27 when they were treated additionally with a TCR-stimulus (anti-CD3/CD28 and IL-2) [175]. It was therefore tempting to speculate that the interaction of $CD27^+$ TILs with CD70 present on ccRCC cells could have similar effects and accelerate tumor cell growth. However, we could not see any proliferative effects of recombinant sCD27 in response to CD70 in two RCC cell lines. CD70-positive RCC cells most likely cannot proliferate in response to a sCD27 stimulus because these tumor cells are not able to transmit a second TCR-stimulus.

### 7.2.4 CD27 does most likely not mediate apoptosis of TILs of RCC *in vivo*

It was previously reported, that CD70-expressing ccRCC and glioma cells were able to provoke T cell apoptosis in coculture experiments via a protein called Siva [129, 149, 158]. Using mouse glioma models it could be shown subsequently, that the immune inhibitory properties of CD70 *in vitro* seem to be clearly overwhelmed by the immune activating properties observed *in vivo* [159]. *In vivo* CD27 promotes survival of activated T cells throughout successive rounds of division and thereby contributes to the accumulation of effector T cells [176]. For these reasons and because we do see many $CD27^+$ T cells *in situ*, we presume that the chronic CD70/CD27 interaction within ccRCCs rather promotes T cell activation instead of T cell apoptosis *in vivo*.

### 7.2.5 Continuous T cell activation leads to T cell exhaustion

The continuous ligation of CD27 and CD70 may also lead to T cell exhaustion, a kind of “immune escape”. It was shown that constitutive expression of CD70 on B cells in mice converted naïve T cells into effector memory cells. This culminated in the depletion of naïve T cells, which lead to lethal immunodeficiency [160]. In addition, CD70 continuously expressed on dendritic cells also contributed to a rapid CD27-mediated phenotypic conversion of naïve T cells to effector cells and to the development of a concomitant immunopathology [177]. In conformance with this Wang *et al.* [130] recently observed less naïve and central memory T

cell subpopulations but more effector memory cells in ccRCC in contrast to PBMCs of the same patients. They suggested that this phenotypic conversion of T cell is caused by high CD70 expression in ccRCC. By incubating naïve human T cells on a plate coated with recombinant CD70 and anti-CD3 antibodies they showed that naïve human T cells differentiate when they receive both a TCR signal and costimulation by CD70 [130], but not by one of the signals alone. This phenotypic conversion was CD70-dose-dependent. Since neither CD70-negative ccRCCs nor CD70-negative ccRCC-derived cell lines were available in this study, Wang *et al.* [130] could only confirm this CD70-dependency by comparing the TILs of CD70-positive RCCs to the TILs of a CD70-negative tumor of a different type, melanoma [130]. From our coculture experiments with CD70-positve and -negative ccRCC cell lines we cannot clearly conclude that CD70 drives the T cell exhaustion. Analysis of the gene expression data, however, revealed that ccRCC harbors more exhausted T cells than in other CD70-negative RCC subtypes. This suggests that these ccRCCs might be per se more infiltrated than the other RCC subtypes. It is of note, that there were also more exhausted $CD27^+$ T cells in ccRCC which have higher CD70 levels compared to those ccRCCs with low CD70 expression. The heterogeneous distribution of CD70-positive tumor cells and TILs within the tumor could be the reason why the extent of T cell exhaustion does not significantly correlate with CD70. The punches used for the geneChip microarray might therefore not represent the situation of the whole tumor.

Claus and colleagues [131] studied the CD70/CD27 interaction in the immunologic control of different CD70-negative solid tumors in CD27-deficient mice. They found that in tumor-bearing wild-type mice, the CD27 signaling increased the frequency of regulatory T cells, reduced tumor-specific T-cell responses, increased angiogenesis and promoted tumor growth. Other research groups proposed that CD70/CD27 interaction improves antitumor immunity [159, 178]. For example, injection of a CD27-activating antibody improved tumor rejection [178] and B cell- and dendritic cell-specific CD70-transgenic mice were protected against poorly immunogenic tumor cells [177, 179]. Two reviews concluded that the duration and dosing of CD70 expression may be decisive weather CD70/CD27 interaction leads to adaptive immune response or immunopathology (Fig. 29) [117, 180]. In the context of the previous findings by Wang *et al.* [130] our results supports the presumption that the coexistence of CD70 and CD27 in ccRCC fosters immune exhaustion effects by chronic CD70/CD27 costimulation in ccRCC. Since we could also observe a survival disadvantage by the presence

of both CD70 and CD27 within ccRCC, we presume that the persistent CD70 expression in primary tumors and metastatic sites of ccRCC causes immunopathology.

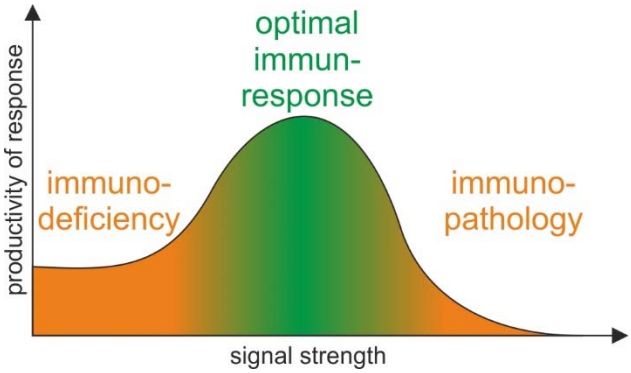


**Figure 29. The strength of costimulatory signals determines the outcome of immune reactions.**

Adapted from Nolte *et al.*, 2009 [117]. Low-level triggering (as in deficient mice or after treatment with blocking antibodies) diminishes immune responses (left-hand side of the figure), whereas continuous and strong activation limits immune reactivity and leads via chronic immune activation to the collapse of the immune system (right-hand side). Optimal responses depend on the proper dosing and timing of costimulatory signals (middle part of the graph).

## 7.3 CD70/CD27 interaction triggers the release of sCD27

As reported for glioma cells [149], coculturing of PBMCs with RCC cells resulted also in a CD70-dependent increase of sCD27 in the supernatant in our study. A similar effect may occur in CD70-expressing ccRCC tissue infiltrated by $CD27^+$ lymphocytes because sCD27-concentrations in sera of those patients were significantly higher than in sera of patients with tumors negative for CD70 and CD27 or healthy probands. Clear cell RCC is the first solid tumor type in which increased serum levels of sCD27 has been observed. Soluble CD27 in plasma has been measures to monitor disease burden in patients with Waldenström's macroglobulinemia [181] and to monitor immune activation during antiretroviral therapy in HIV patients [182]. Huang J. and colleagues [175] showed that the extracellular domain of CD27 can be released after lymphocyte activation by anti-CD3/ anti-CD28 and IL-2 increasingly with time and that $CD4^+$ T cells are its predominant source. They observed that the production of sCD27 correlated linearly with the amount of CD70-expressing $CD8^+$ T cells within the culture and that the sCD27 production can be significantly inhibited by a CD70-blocking antibody. Furthermore they suggest that sCD27 results more likely from shedding from T cells' surface rather than from T cell death, because they found only minimal cell death in the course of *in vitro* activation [175]. Together with this data we concluded that high serum concentration of sCD27 is a result of CD70-mediated shedding thus representing a potential predictive marker for CD70 expression in ccRCC. The on average higher sCD27 serum levels of patients with CD70-expressing tumor cells and $CD27^+$ TILs increased or remained stable after nephrectomy, irrespectively of the progression of the disease. The sometimes observed increase instead of

the expected decrease of serum sCD27 after removal of the CD70-positive tumor could either emerge from metastasized tumors or from tumor-independent immune activation. Soluble CD27 may not be suitable as a marker to monitor the disease' clinical course (longer observation periods and more patients are needed), but it may be applicable to predict the presence of CD70 in ccRCC of patients who may benefit from CD70-targeted therapy.

In conclusion, we demonstrated that in ccRCC CD70 is upregulated via the pVHL/HIF axis. A model illustrating our hypothesis is shown in figure 28. The stable expression of CD70 during tumor progression encourages to use CD70 as a tissue marker to identify metastatic sites derived from primary ccRCC. CD70/CD27 interaction seems to boost the release of sCD27 in sera of ccRCC patients suggesting CD27 a potential diagnostic serum marker which predicts the applicability of CD70-targeted therapies or CD27-targeted immunotherapies [183]. At the moment three novel anti-CD70 antibody-drug-conjugates are under evaluation for metastatic ccRCC in clinical trial phase I [136, 184]. All of them have shown promising anti-tumor activity in CD70-expressing RCC mouse xenografts [135]. One should, however, bear in mind that blocking of CD70/CD27 interaction by CD70-targeting drugs may impede *de novo* T cell priming [177, 185], thus hampering patients' immune response capability.

## 7.4 PTPRJ is negatively regulated by the pVHL/HIF axis in RCC

Our studies provided evidence that PTPRJ expression is downregulated in 85% of ccRCCs. In papillary RCC, however, mRNA and protein levels of PTPRJ were retained to the levels of normal kidney. We showed that stabilized HIF2α in pVHL-deficient ccRCCs activate the transcription of *PTPRJ*. As it was reported for other solid tumors [186-188], we found, that PTPRJ is inhibiting cell proliferation in ccRCC. Therefore downregulation of PTPRJ has tumor-promoting effects, which was reflected by worse survival outcome of patients with PTPRJ-lacking ccRCC. These cell proliferation-inhibitory effect may be caused by reduced dephosphorylation of EGFR in the absence of PTPRJ, as PTPRJ acts as a negative regulator of the EGFR signaling pathway [189]. Taken together, we showed that in ccRCC deregulation of the pVHL/HIF axis leads to the downregulation of PTPRJ which positively influences tumor cell proliferation.

## 7.5 TGF-βRIII, a promising serum marker for tumor progression in RCC

TGF-βRIII is ubiquitously expressed in healthy tissue, but reduced in multiple cancers including ovarian, breast, lung, pancreas and prostate cancer [190-193]. Loss of TGF-βRIII expression with cancer progression has also been described in RCC [194]. TGF-βRIII is a suppressor of cancer progression by reducing cancer cell motility [193, 195]. Besides its regulation by binding of TGF-β1 to its promoter [196] and by epigenetic silencing [191, 192], it was also reported that chronic hypoxia leads to reduced TGF-βRIII expression in rat lungs [197]. We found that its surface expression is lower in ccRCC and papillary RCC than in normal kidney. However, higher expression in pVHL-deficient ccRCCs than in ccRCCs with intact pVHL function was also observed [103], suggesting a pVHL- or HIF-directed regulation of TGF-βRIII. A pVHL-dependency was not observed in sera of patients. Sera levels of TGF-βRIII in ccRCC patients were similar to those seen in healthy probands, although 70-80% of the ccRCC patients harbor a *VHL*-mutation.

Surprisingly, the serum of TGF-βRIII levels increased in RCC with tumor stage. Soluble TGF-βRIII results from proteolytic cleavage and has been shown to correlate with the cell surface expression [198]. Soluble TGF-βRIII can bind and neutralize TGF-β, thereby antagonizing tumor promotion in late stage breast cancers [190]. Maybe there is a mechanism driving TGF-βRIII expression with tumor progression, what results in concomitant increase of the soluble TGF-βRIII serum levels. It might be possible, that soluble TGF-βRIII acts also in ccRCC in tumor-suppressive way, as it does in late stage breast cancer. If TGF-βRIII could serve as a serum marker predicting the tumor stage needs further verification. The underlying mechanism of the increased release of soluble TGF-βRIII in late stage ccRCCs needs to be clarified, too.

# 8 Conclusion

The proteomics-based identification of the pVHL-dependent surfacome enabled us to further validate the functional and clinical relevance of selected biomarker candidates in ccRCC *in vitro* and *in vivo* in more detail (Fig. 30).

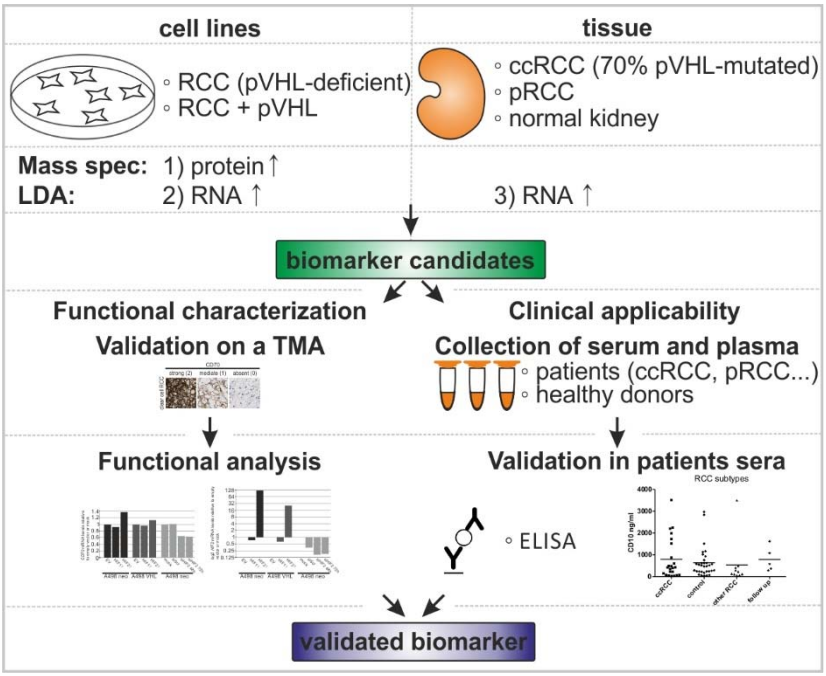


**Figure 30. Schematic illustration of the functional characterization of selected biomarker candidates derived from the earlier defined ccRCC surface proteome.**

We confirmed that the converse expression of the two proteins CD70 and PTPRJ in ccRCC results from differential regulation via pVHL and HIF. The clinical relevance of CD70 was revealed by the close relationship between i) CD70 overexpression and CD70 receptor $(CD27)^{+}$ infiltrating lymphocytes which was linked to a more aggressive biological behavior and ii) by elevated levels of sCD27 in serum of ccRCC patients as a consequence of CD70 overexpression. An additional promising serum marker for ccRCC progression is TGF-βRIII, since its serum levels correlated with the tumor stage.

In conclusion, the large amounts of data generated by high-throughput technologies such as mass spectrometry or microarrays are useful to identify potential tumor biomarkers. However, a thorough investigation of the mechanisms and functions of putative biomarker candidates using appropriate models will remain mandatory to better understand the biology and consequently, treatment options of ccRCC. Detailed investigation of three cell surfaceome

members revealed their common regulatory dependence of the pVHL/HIF axis and their roles in different steps of tumorigenesis of ccRCC (Fig. 31). In addition to *in vitro* models and high-throughput tools the analysis of human tumor tissue and clinical performance is of absolute importance to translate research findings into clinical practice.

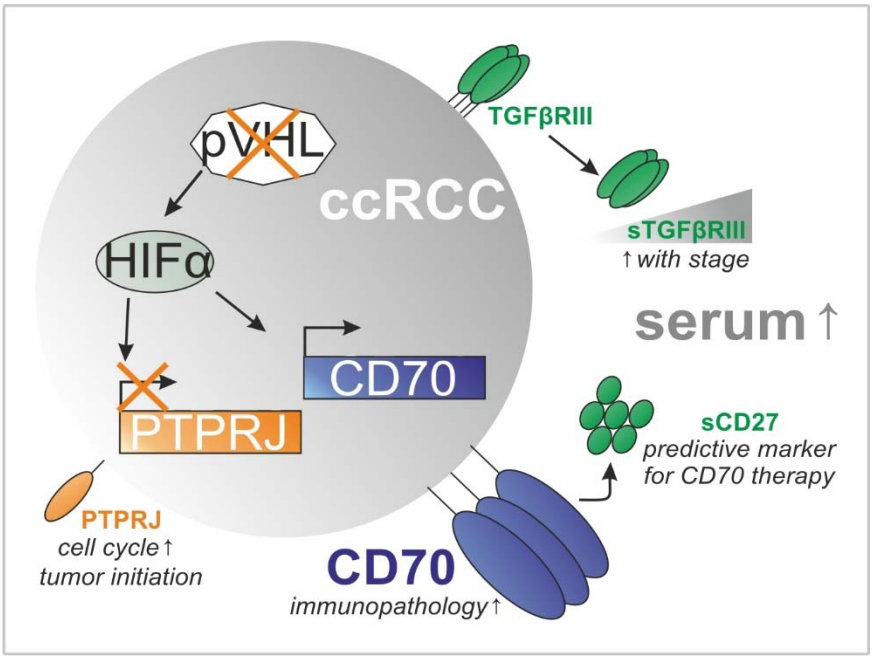


**Figure 31. Schematic illustration of the regulation and potential clinical applicability (in italics) of selected biomarker candidates.**

# 9 Materials and Methods

## 9.1 Patient material

For IHC-analyses TMAs with 252 ccRCCs [103] and 54 ccRCC brain metastases [199, 200] from the Institute of Surgical Pathology, University Hospital of Zurich, Switzerland, and a TMA comprising 300 papillary RCCs [146] from the University of Erlangen, Germany, were used. Each TMA was histologically reviewed by one pathologist (H.M. and A.H., respectively) (Table 6). Clinico-pathological parameters of the TMAs have already been described [146, 201]. This study was approved by the local ethics commission (reference no. StV38-2005). Human blood samples of 20 ml of 74 patients, who underwent full or partial nephrectomy as part of their standard treatment at the Department of Urology, University Hospital Zurich , Switzerland were collected on the day of surgery following informed consent (Table 7). Additional blood samples from the same patients were collected at the time of each follow up investigation, at about one, six and twelve months after surgery. 3-5 ml of serum and heparin-plasma were separated from the blood cells in a standardized manner by centrifugation for 15 minutes at 3500 rpm at 4 °C and stored at -80 °C in two 100 µl and several 1 ml aliquots. Formalin-fixed, paraffin-embedded tissue samples from these patients were also available. Sera and plasma of 17 healthy persons, with prior informed consent, served as control. Serum or plasma concentrations of sCD27 (M1960, Sanquin), CD10 (DY1182, R&D Systems) CD70 (CSB-EL004954HU, Cusabio) TGF-βRII (DY242, R&D Systems), ALCAM (DY656, R&D Systems), EphA2 (DYC3055E, R&D Systems), VEGFRII (DYC1780-5, R&D Systems) and IGF2R (DYC5537-5, R&D Systems) were determined by ELISAs according to the manufacturers‘ instructions. This study was approved by the local ethics commission (KEK-ZH no. 2011-0072/4).

**Table 6. Microarrays.**

| Microarray | Number of cases | Sample origin | Source |
|---|---|---|---|
| RCC | 252 | ccRCC | Institute of Surgical Pathology, University Hospital of Zurich, Switzerland |
| | 48 | papillary RCC | |
| | 13 | chromophobe RCC | |
| | 21 | normal kidney | |
| Papillary RCC | 300 | papillary RCC | Institute of Pathology, University Hospital of Erlangen, Germany |
| | 300 | matched normal kidney | |
| RCC brain metastasis | 54 | RCC brain metastasis | Institute of Surgical Pathology, University Hospital of Zurich, Switzerland |
| | 9 | benign brain tumor | |
| solid tumor | 24 | ccRCC, of which 13 match to the brain metastasis TMA | Institute of Surgical Pathology, University Hospital of Zurich, Switzerland |
| | 112 | pulmonary carcinoma | |
| | 20 | mammary carcinoma | |
| RCC cell line | 23 | cell lines derived from RCC or kidney | Institute of Surgical Pathology, University Hospital of Zurich, Switzerland |
| RCC_2 | 25 | ccRCC | Institute of Surgical Pathology, University Hospital of Zurich, Switzerland |
| | 3 | papillary RCC | |
| | 28 | matched normal kidney | |

**Table 7. Blood biobank**

| number of tumors | Fuhrman grade | | | | tumor stage (pT) | | | | follow up samples (months after surgery) | | | | | met. |
|---|---|---|---|---|---|---|---|---|---|---|---|---|---|---|
| | I | II | III | IV | 1a | 1b | 2 | 3 | 1-3 | 4-6 | 7-12 | 13-23 | 24-28 | |
| 33 ccRCCs | 3 | 18 | 8 | 3 | 11 | 10 | 1 | 8 | 20 | 12 | 17 | 9 | 11 | 2 |
| 1 ccRCC + chromophobe | | 1 | | | 1 | | | | | | | | | |
| 3 ccRCC/ papRCC | | 2 | 1 | | 2 | | | | 2 | 2 | 1 | | | 1 died |
| 8 chromophobe RCC | 2 | 3 | | | 3 | 2 | | 1 | 4 | 1 | 6 | 4 | 2 | |
| 11 papillary RCC | 3 | 4 | 3 | 1 | 8 | | 2 | 1 | 9 | 3 | 5 | 7 | 1 | |
| 1 pap./chromo. RCC | | | | | | | | | 1 | 1 | 1 | | | |
| 3 oncocytoma | | | | | | | | | 1 | | | 1 | | |
| 11 benign tumors | | | | | | | | | 5 | 1 | 2 | | | |
| 2 not classified | | 1 | 1 | | 1 | 1 | | | 1 | 1 | 2 | 1 | 1 | |
| 1 perivascular epithelioid cell tumor | | | | | | | | | | | | | | |

## 9.2 Immunohistochemistry

Tissue microarrays and whole tumor sections (2.5 µm) were IHC-stained according to Ventana automat protocols (Ventana Medical System). The antibodies applied for detection are listed in table 8. The staining intensities were classified as absent, moderate and strong. Lymphocyte infiltration was analyzed using hematoxylin and eosin stained large sections and was scored as absent, sparse to loose and dense infiltrate. For detailed analysis TMAs were scanned using the NanoZoomer Digital Slide Scanner (Hamamatsu Photonics K.K.).

**Table 8. Antibodies used for Western blot analysis, IHC and ChIP.**

| Antibody | Name | Dilution for Western blot | Dilution for IHC | Amount for ChIP | Use for blocking | Supplier |
|---|---|---|---|---|---|---|
| CD70 | MAB2738 | 1:500 | 1:75 | - | | R&D systems |
| CD70 | Ki-24 | - | - | - | 10 µg/ml | PharMingen |
| CD27 | ab70103 | 1:1000 | 1:200 | - | | Abcam |
| HIF1α | NB100-479 | 1:500 | - | - | | Novus Biologicals |
| HIF1α | ab16066 | - | 1:400 | - | | Abcam |
| HIF1α | NB100-105 | - | - | 10 µg | | Novus Biologicals |
| HIF2α | PAB12124 | 1:500 | - | - | | Abnova |

| | | | | | | |
|---|---|---|---|---|---|---|
| HIF2α | NB100-122 | - | 1:150 | 10 ug | | Novus Biologicals |
| CA-IX | M75 | 1:1000 | 1:200 | - | | J. Zavada, Prague, Czech Republic |
| Glut1 | AB1341 | - | 1:1000 | - | | Chemicon |
| Glut1 | 07-1401 | 1:1000 | - | - | | Millipore |
| pVHL | | 1:500 | 1:50 | - | | W. Krek, ETH Zurich |
| CD10 | NCL-CD10-270 | - | 1:30 | - | | Novocastra Laboratories |
| E-Cadherin | ECH-6 | - | 1:10 | - | | Cell Marque |
| β-actin | MAB1501 | 1:2000 | - | - | | Millipore |
| IgG2b | MAB004 | - | - | 10 ug | | R and D systems |
| Rabbit IgG | NB810-56910 | - | - | 10 ug | | Novus Biologicals |
| HRP-conjugated anti-mouse | ab672 | 1:2000 | - | - | | Abcam |
| HRP-conjugated anti-rabbit | 7074 | 1:1000 | - | - | | Cell signaling |

## 9.3 *VHL* mutation analysis

*VHL* mutation analysis of cell lines and tissues was performed as described [151] with primers listed in table 9. Cell line *VHL* mutations are listed in table 4. The program Site Directed Mutator (SDM; http://mordred.bioc.cam.ac.uk/~sdm/sdm.php) was used to predict the association of *VHL* missense mutations and disease as described [151, 152].

**Table 9. *VHL* sequencing primers**

| ***VHL* primer** | **sequence (5'-3')** |
|---|---|
| Exon 1 forward | cgagcgcgcgcgaagactac |
| Exon 1 reverse | gaccgtgctatcgtccctgc |
| Exon 2 forward | accggtgtggctctttaaca |
| Exon 2 reverse | tcctgtacttaccacaacaacctt |
| Exon 3 forward | gagaccctagtctgtcactgag |
| Exon 3 reverse | tcatcagtaccatcaaaagctg |

## 9.4 Gene expression analysis

Gene expression data of 116 RCCs and six normal kidneys were obtained from a recently published microarray study [145], for which HG-U133A High-Thoughput Arrays (Affymetrix) were used. Microarray data are available in GEO under GSE19949. The discrimination between CD70-high and CD70-low expressing ccRCCs was made based on the TMA-IHC-data. The 22% lowest CD70-expressing ccRCCs were defined as CD70-low ccRCCs.

## 9.5 Cell lines

The RCC-derived cell lines ACHN, A704, Caki-1, Caki-2, KC12, 769P, 786-O and the human kidney cell lines HK-2 and HEK-293 were supplied by American Type Culture Collection (ATCC). The ccRCC-derived cell lines SLR21, SLR22, SLR23, SLR24, SLR25 and SLR26 were kindly

provided by W.J. Storkus (University of Pittsburgh, USA). Untransfected and stable transfectants of RCC4, 786-O and A498 reexpressing pVHL and empty vector controls were previously generated [202, 203] and provided by W. Krek (ETH Zurich, Switzerland). The Burkitts's lymphoma cell line Raji was kindly provided by M. Tinguely (Institute of Surgical Pathology, University Hospital Zurich). Cell lines were grown under conditions recommended by ATCC and authenticated by short tandem repeat profiling by Identicell (Aarhus University, Denmark). DMEM, RPMI and K1 culture media were supplemented with 10% FBS (life technologies), 2 mM L-glutamine (life technologies), 100 µg/ml streptomycin (life technologies) and 100 U/ml penicillin (life technologies). Transfected cell lines were cultured in the presence of 4 µg/ml puromycin (Sigma-Aldrich; RCC4) or 500 µg/ml geniticin (life technologies; 786-O and A498). For immune staining cell line pellets were formalin-fixed and paraffin-embedded as recently described [204]. For hypoxia experiments cells were incubated under low-oxygen conditions (0.5%) in a hypoxic workstation (Invivo$_2$ 400; Ruskinn Technology, Leeds, United Kingdom) for up to 24 hours. Cell lysates were harvested inside the chamber. Cell viability was measured by MTT assay (Roche). Metabolites were labeled by a 4-hours-incubation of cells grown in a 96-well with 10 µl MTT and subsequent over-night-incubation with 100 µl solubilization solution. The optical density at 570 nm measured by the infinite F200 microplate reader (Tecan) of untreated cells was compared to cell pretreated with recombinant sCD27 (Abnova).

## 9.6 Immunofluorescence

Cells were fixed in 4% formalin for 20 minutes and washed three times with PBS (life technologies). Subsequently, slides were incubated with 200 µl of 0.2% Triton for 10 minutes and then blocked with 200 µl of 2% BSA for 1 hour. Incubation with the primary antibody was performed for 1 hour and 30 minutes. Then slides were washed with PBS three times. Incubation with secondary antibody was performed for 1 hour in the dark. After three times washing with PBS cells were covered with Vector-Shield containing DAPI.

## 9.7 Immunoblot analysis

Cell lysates were prepared at 4°C with NP40-buffer (10 mM Tris pH 8, 1 mM EDTA pH 8, 400 nM NaCl, 0,1% NP40, 1 mM DTT) or RIPA buffer (Sigma-Aldrich) supplemented with complete protease and phosphatase inhibitor cocktails (Roche). Cell debris was removed by

centrifugation at 4°C and 16,000 rcf for 15 minutes and protein concentration was determined by BCA assay (Thermo Fisher Scientific Inc.). For removal of *N*-glycans PNGase F (New England Biolabs) was used. The NetNGlyc 1.0 server (http://www.cbs.dtu.dk/services/NetNGlyc/) was used to predict *N*-glycsylation sites *in silico* [150]. Western blotting were performed with the NuPAGE System (Life technologies). 50-100 µg protein in NuPAGE LDS sample buffer (life technologies) and a size marker (MagicMark XP and SeeBlue Plus2, life technologies) were loaded on 4-12% gradient Bis-Tris gels from life technologies and gel-electrophoresis was performed at 120 Volt for 2 hours with the NuPAGE MOPS SDS running buffer (life technologies), followed by transfer to a PVDF membrane (BioRad) at 30 Volt for 3 hours with the NuPAGE transfer buffer (life technologies). After incubation in 5% milk (Rapilait, Migros) TBS-T (50 mM Tris, 150 mM NaCl, 0.05% Tween 20, pH 7.6 (HCl)) proteins were incubated with primary antibodies at 4°C over night and with secondary antibody at room temperature for 1 hour. Antibodies used are listed in supplementary table 8. Proteins were visualized with the Gel Doc XR$^+$ system (BioRad) using Clarity TM Western ECL substrate kit (BioRad).

## 9.8 Transient transfections

For RNA interference experiments, cells were transfected with 5 nM siRNA using HighPerfect (Qiagen) or Lipofectamine RNAiMAX (life technologies) transfection reagent (Table 10).

**Table 10. siRNAs.**

| siRNA | targeting | supplier |
|---|---|---|
| AllStar Negative Control (siScramble=siScr) | - | Qiagen |
| Hs_HIF1A_5 | *HIF1α* | Qiagen |
| Hs_EPAS1_5 | *HIF2α* | Qiagen |
| Hs_EPAS1_1 | *HIF2α* | Qiagen |
| Hs_EPAS1 | *HIF2α* | Qiagen |
| Hs_VHL_5 | *VHL* | Qiagen |
| Hs_TNFSF7_1 | *CD70* | Qiagen |
| Hs_TNFSF7_2 | *CD70* | Qiagen |
| Hs_TNFSF7_3 | *CD70* | Qiagen |
| Hs_CD70_1 | *CD70* | Qiagen |
| Hs-TNFRSF7_1 | *CD27* | Qiagen |
| Hs-TNFRSF7_2 | *CD27* | Qiagen |
| Hs-TNFRSF7_3 | *CD27* | Qiagen |
| Hs-TNFRSF7_5 | *CD27* | Qiagen |

To study the effects of HIFα overexpression, RCC cells were transfected with 5 µg *HIF1α*-, *HIF2α* or *HIF2α* DNA binding mutant [69] in pcDNA3.1 (+) (Table 11) using XtremeGene HP (Roche) and grown for 24 hours in a six-well format. The mutant *HIF2α* construct was kindly provided by P. Ratcliffe (University of Oxford, UK).

**Table 11. Plasmids**

| vector | insert | origin |
|---|---|---|
| pcDNA3.1 (+) | - | Life technologies |
| HA-HIF1α-pcDNA3.1 (+) | *HIF1α*, HA-tagged | Institute of Surgical Pathology, University Hospital Zurich, Switzerland |
| HA-HIF2α-pcDNA3.1 (+) | *HIF2α*, HA-tagged | Institute of Surgical Pathology, University Hospital Zurich, Switzerland |
| HIF2α-bHLH-mutant-pcDNA3.1 (+) | *HIF2α* DNA binding mutant | kindly provided by P. Ratcliffe (University of Oxford, UK) |
| CD70 promoter-pUC57 | *CD70 promoter* (-2000 to +700 bp of Gene-ID: 970) | Genscript |
| CD70 promoter-pGL4.10 | *CD70 promoter* (-2000 to +700 bp of Gene-ID: 970) | cloned |
| CD70 HRE1-3-pGL4.10 | *CD70 promoter* (-1887 to -1596 bp of Gene-ID: 970) | cloned |
| CD70 HRE4-7-pGL4.10 | *CD70 promoter* (-1221 to -828 bp of Gene-ID: 970) | cloned |
| CD70 HRE8.9-pGL4.10 | *CD70 promoter* (+266 to +623 bp of Gene-ID: 970) | cloned |
| pGL4.10 | - | Promega |
| P2P-pGL4.10 | *PHD2 promoter* | kindly provided by R. Wenger (University of Zurich, Switzerland) |
| pGL4.74 (Renilla) | | Promega |
| pGEM®-T Easy | To insert *CD70* promoter fragments containing CpG islands | Promega |
| pmaxGFP | *GFP* | AMAXA Biosystems |

## 9.9 Quantitative real time-PCR

RNA was isolated with the RNeasy Mini Kit (Qiagen) and quantified with a Nanodrop spectrometer. Complementary DNA was synthesized with the High Capacity cDNA Reverse Transcription Kit (Applied Biosystems) and real time-PCR was performed with ViiaTM7 Real-Time PCR System (Applied Biosystems). TaqMan Gene Assays (Applied Biosystems) for *CA-IX* (Hs00154208_m1), *CD70* (Hs00174297_m1), *CD27* (Hs00386811_m1), *GLUT1* (Hs00197884_m1), *HIF1α* (Hs00936376_m1), *HIF2*α (Hs01026146_m1), *OCT4* (Hs04260367_gH), *PDK1* (Hs01561850_m1), *PHD3* (Hs00222966_m1), *PPIA* (Hs99999904_m1) and *VHL* (Hs00184451_m1) were used. For quantification of the immunoprecipitated DNA fragments SYBR Green PCR Master Mix with primers for the different HREs (Table 13) was used.

## 9.10 Chromatin immunoprecipitation

Chromatin immunoprecipitation was performed according the protocol (version 10.0) of mammalian ChiP-on-chip (Agilent Technologies). Briefly, $5x10^7$-$1x10^8$ cells were fixed in 1% formaldehyde, washed, harvested and lysed. The cell lysates were sonicated to fragment cellular DNA into fragments of 100-600 bp in size and incubated with a HIFα-antibody/magnetic bead (Dynabeads Potein G; Invitrogen) mixture over night at 4°C. After

washing to deplete unbound DNA, DNA-antibody complexes were eluted from the beads at 65°C. Beads were separated from the eluent by centrifugation (16.000xg; 1 min). Cross-linking of DNA and antibody was reversed by incubating the supernatant at 65°C overnight. Cellular protein and RNA were digested by proteinase K and RNase A. DNA was extracted with phenol:chloroform:isoamyl alcohol in Phase Lock Gel tubes (Eppendorf). DNA concentrations were measured using a nanodrop. SYBR Green real-time PCR was performed to quantify the differential binding of HIFα to the HREs of *CD70*. The antibody and primers used for the ChIP experiments are listed in tables 8 and 12.

**Table 12. Primers used for ChIP analysis.**

| Primer name | sequence |
|---|---|
| CD70 HRE1 forward | 5'-GTGCCCACCACCACACCCAG-3' |
| CD70 HRE1 reverse | 5'-CACGCCACTGAACTCCAGCCT-3' |
| CD70 HRE2 forward | 5'-GCTCACTGCAAGCTCCACCTC-3' |
| CD70 HRE2 reverse | 5'-GAGTAGCTGGGACTACAGGCGC-3' |
| CD70 HRE3 forward | 5'-AGCCAGGAGGGTCTCAAAC-3' |
| CD70 HRE3 reverse | 5'-CAAGAAACACCAAGAAGGAGCC-3' |
| CD70 HRE4 forward | 5'-CCCAGATGTTTGAGACCAGC-3' |
| CD70 HRE4 reverse | 5'-GCATAGTTGGGTCTACCAGC-3' |
| CD70 HRE5 forward | 5'-GGCTGCTGTGAGCTGTGTGG-3' |
| CD70 HRE5 reverse | 5'-CAAAGTGCTGGGATTACAGGCG-3' |
| CD70 HRE6 forward | 5'-GGAGACCATCCTCGCTAAC-3' |
| CD70 HRE6 reverse | 5'-CATTCTCCTGCCTCAGCCTCTCA-3' |
| CD70 HRE7 forward | 5'-GCTACTTGAGAGGCTGAGG-3' |
| CD70 HRE7 reverse | 5'-GTCTCGCTCTGTCGCCCAG-3' |
| CD70 HRE8 forward | 5'-GTGATCTGCCTCGTGGTGTG-3' |
| CD70 HRE8 reverse | 5'-GTCACGCGCCTCTCTATGTT-3' |
| KCNJ5 forward (negative control) | 5'-ACC TTA AGC TGT TAC TGG GTC TGG C-3' |
| KCNJ5 reverse (negative control) | 5'-GCC AGA CCC AGT ATC AGC TTA AGG T-3' |
| CD10 HRE2 forward (positive control) | 5'-AAT TAG CTC GGT GTG GTG GT-3' |
| CD10 HRE2 reverse (positive control) | 5'-CTG GAG TGC AGT GGT GTG AT-3' |

## 9.11 Luciferase gene reporter assay

The nucleotides between −2000 and +700 were defined as the putative promoter region of CD70 (Chromosome 19p13; Gene-ID: 970). The promoter region was synthesized from GenScript and cloned into firefly luciferase reporter plasmid pGL4.10 (Promega). Fragmented *CD70* promoter constructs were cloned with primers from table 13 are listed in table 11. The positive control *P2P* contains the *P2P* HREs of the human *PHD2* promoter [205] and was provided by R. Wenger (University of Zurich, Switzerland). Luciferase activity was measured 24 hours after transfection of A498 empty vector, A498 reexpressing pVHL and 786-O with 1 µg of reporter plasmids along with 200 ng of pGL4.74 renilla luciferase reporter plasmid in

24-well plates. HIFα overexpression was performed 48 hours before measurement. Relative luciferase units were determined according to the manufacturer's instructions (Dual luciferase reporter assay system, Promega).

**Table 13. Primers for *CD70* promoter subcloning**

| primer name | sequence (5'-3') |
|---|---|
| **KpnI**-HRE1-3-forward | cgg**GGTACC**GTCTCACTCTGTCACCCAGG |
| HRE1-3-reverse-**HindIII** | ccc**AAGCTT**GAAACACCAAGAAGGAGCCA |
| **KpnI**-HRE4-7-forward | cgg**GGTACC**AATTAGCCGGGCATGGTAGC |
| HRE-4-7-reverse-**HindIII** | ccc**AAGCTT**CTCACTGCAAGCTCCGC |
| **KpnI**-HRE8,9-forward | cgg**GGTACC**GCGCTTCGCACAGGCTC |
| HRE8,9-reverse-**HindIII** | ccc**AAGCTT**CCACGCCCAGCCTTGTG |
| T7 | TAATACGACTCACTATAGGG |
| SP6 | ATTTAGGTGACACTATAG |
| RV3 | CTAGCAAAATAGGCTGTCC |
| RV4 | GACGATAGTCATGCCCCGC |

## 9.12 Molecular cloning

To clone recombinant DNA, specific fragments were amplified with the AmpliTaq Gold DNA Polymerase (Thermo Fisher Scientific), separated by size in an 1% agarose in TAE buffer (40 mM Tris, 20 mM acetic acid, 1 mM EDTA) gel containing gel red and made visible with UV light in an Gel Doc XR$^+$ system (BioRad). The DNA was extracted from the gel (illustra GFX PCR DNA and Gel Band Purification Kit) and digested with restriction enzymes (New England Biolabs) and ligated into a vector with the T4 ligase (Promega).

At an optical density 0.4 at 600 nm of a culture of the *Escherichia coli* (*E. coli*) strain XL1-Blue (Stratagene), which was grown in LB medium (Becton, Dickinson and Company) at 37°C, was incubated on ice for 15 minutes. Cell pellets were generated by 10 minutes centrifugation at 2700 rcf at 4°C, resuspended in TFB1 buffer (100 mM rubidium chloride, 50 mM manganese (II) chloride, 30 mM potassium acetate, 10 mM calcium chloride, 15 % glycerol, pH 5.8) and incubated for 15 minutes on ice. Thereafter, centrifugation generated cell pellets were resuspended in TFB2 buffer (10 mM MOPS, 75 mM calcium chloride, 10 mM rubidium chloride, 15 % glycerol, pH 6.8) and incubated on ice for 15 minutes. Aliquots of the competent bacteria were stored at -80°C.

To multiply plasmids or ligation products, they were added to 100 µl thawed competent bacteria, incubated on ice for 30 minutes and heat-shocked for 90 seconds at 42°C. Afterwards, bacteria were incubated at 37°C for one hour under constant shaking, pelleted

and plated on a LB agar plate containing the selection antibiotic (ampicillin or kanamycin) to grow bacterial colonies over night at 37°C.

Bacterial plasmid DNA from *E. coli* was isolated using the QIAamp DNA Mini kit or High Speed Plasmid Midi kit (Qiagen), DNA concentrations were measured with a Nanodrop spectrometer and DNA was sequenced in collaboration with D. Zimmermann (Molecular pathology diagnostics, University Hospital Zurich).

## 9.13 Bisulfite sequencing

Genomic DNA from five cell lines and fresh frozen tumor and matched normal tissue of six ccRCCs was isolated using the DNeasy Blood & Tissue Kit (Qiagen, Hilden, Germany) and the cytosine bases of genomic DNA (500 ng) were converted to uracil according to the protocol EZ DNA MethylationKit™ (Zymo Research Corporation). The previously established primers [142] forward, 5'-GGGTGGATTATTTAAGGTTAGG-3'; reverse, 5'-ATACCCCTCTCCTACATTTTTTTA-3' were used to amplify a CD70 promoter region containing CpG from the bisulfite-modified DNA with AmpliTaq Gold DNA Polymerase (Thermo Fisher Scientific) at 95°C for 15 minutes, 35 cycles of 94°C for 30 seconds, 60 °C for 30 seconds, and 72°C for 1 minute and a final extension at 72°C for 10 minutes. The PCR products were cloned into pGEM®-T Easy (Promega). After transformation of E. coli seven subclones were selected and sequenced using T7 primers. For bisulfite sequencing of drug-treated cells, 786-O cells were incubated with 5-azacytidine (Sigma-Aldrich) for 24 h. Afterwards, the medium was exchanged and cells were harvested three days later.

## 9.14 Determination of sCD27 in cocultures and sera of RCC patients

The RCC cells were seeded into six-wells that the number of cells reached $2.7x10^5$/well 48 hours later. For siRNA experiments cell transfection was performed 24 hours after seeding. PBMCs of a healthy individual were isolated by Ficoll (GE Healthcare) density centrifugation. Forty-eight hours after seeding and repeated washing, $2.7x10^6$ PBMCs were added in 2 ml RPMI-1640 containing 10% FCS. The cells were cocultured for two additional days. PBMCs and RCC cells were maintained in monoculture in parallel. After two days supernatants were used to analyze sCD27 concentration by sandwich ELISA (M1960, Sanquin) according to the manufacturer's instructions. The different experimental approaches were performed using

PBMCs of different healthy individuals (donor A-C). The sCD27 ELISA was also used for testing sera of RCC patients and healthy individuals.

## 9.15 Statistical and computational analyses

Pearson $\chi^2$ test, Fisher's exact test, student's *t* test and survival analysis were performed using SPSS Statistics 21 (IBM). Correlation analysis (Pearson R) was performed using GraphPad Prism 5 (GraphPad Software).

# 10 Annex

Manuscripts which were published in the course of this PhD project:

pVHL/HIF-regulated CD70 expression is associated with infiltration of $CD27^+$ lymphocytes and increased serum levels of soluble CD27 in clear cell renal cell carcinoma. **Ruf M**, Mittmann C, Nowicka AM, Hartmann A, Hermanns T, Poyet C, van den Broek M, Sulser T, Moch H, Schraml P. Clin Cancer Research, 2014 Dec, accepted.

The protein tyrosine phosphatase receptor type J is regulated by the pVHL/HIF axis in clear cell renal cell carcinoma. Casagrande S, **Ruf M**, Rechsteiner M, Morra L, Brun-Schmid S, von Teichman A, Krek W, Schraml P, Moch H. J Pathol. 2013 Mar;229(4):525-34.

Clinical Cancer Research

# pVHL/HIF-Regulated CD70 Expression Is Associated with Infiltration of CD27$^+$ Lymphocytes and Increased Serum Levels of Soluble CD27 in Clear Cell Renal Cell Carcinoma

Melanie Ruf[1], Christiane Mittmann[1], Anna M. Nowicka[1], Arndt Hartmann[2], Thomas Hermanns[3], Cédric Poyet[3], Maries van den Broek[4], Tullio Sulser[3], Holger Moch[1], and Peter Schraml[1]

## Abstract

**Purpose:** CD70, a member of the TNF ligand superfamily, has been shown frequently overexpressed in clear cell renal cell carcinoma (ccRCC). The mechanisms of CD70's upregulation and its role in ccRCC are unknown.

**Experimental Design:** CD70 expression was immunohistochemically analyzed in 667 RCCs and RCC metastases. Von Hippel–Lindau gene (*VHL*) mutations, expression patterns of *VHL* protein (pVHL), hypoxia-inducible factor (HIF) α, and several HIF targets were studied in tissues and cell lines and correlated with CD70 overexpression. Gene promoter analysis was performed to confirm CD70 as HIF target gene. Consecutive tissue sections were immunostained to reveal the relation between CD70-expressing RCCs and tumor-infiltrating lymphocytes positive for the CD70 receptor (CD27). CD70-mediated release of soluble CD27 in RCC was assessed by coculture experiments and sera analysis of patients with RCC.

**Results:** Elevated CD70 expression was seen in 80% of primary tumors and metastases of ccRCC and correlated with dysregulation of the pVHL/HIF pathway. *In vitro* analyses demonstrated that CD70 upregulation is driven by HIF. Furthermore, CD27$^+$ lymphocytes preferentially infiltrate CD70-expressing ccRCCs. CD70-dependent release of soluble CD27 in cocultures may explain the high CD27 levels observed in sera of patients with CD70-expressing ccRCC. The combination of lymphocyte infiltration and CD70 expression in RCC was associated with worse patient outcome.

**Conclusion:** Our findings demonstrate that in ccRCC, CD70 expression is regulated by HIF as a consequence of pVHL inactivation. Increased serum levels of CD27 suggest the existence of CD70-expressing ccRCC, thus representing a potential serum marker for patients suffering from this disease. *Clin Cancer Res; 21(4); 889–98. ©2015 AACR.*

## Introduction

About 70% of clear cell renal cell carcinoma RCC (ccRCC), the most common RCC subtype, harbor mutations in the von Hippel–Lindau gene (*VHL*; ref. 1). Its gene product, pVHL, acts as an adaptor protein for transcriptional regulation, the extracellular matrix, and the microtubule cytoskeleton (2). The most prominent function of pVHL is its role to target hypoxia-inducible factor (HIF) α for ubiquitin-mediated proteolysis. The loss of function of pVHL stabilizes HIFα and leads to the activation of a series of genes, which encode proteins involved in angiogenesis, metabolism, and cell-cycle regulation. Among them are cell surface proteins, including vascular endothelial growth factor and platelet-derived growth factor, which represent important therapy targets for patients with ccRCC (3). However, these treatments have significant toxic side effects and response is only seen in a subgroup of patients. To improve diagnosis, prognosis, and treatment of patients with RCC, additional biomarkers, in particular cell surface proteins, would be of utmost importance.

CD70 is a member of the TNF ligand superfamily and caught our interest because it was one of the ccRCC surface proteins we previously identified by cell surface capturing technology (4). Under normal conditions, CD70 expression is tightly regulated and restricted to a small subset of antigen-stimulated B and T lymphocytes and mature dendritic cells (5, 6). The interaction of CD70 with its receptor CD27 promotes expansion and differentiation of memory and effector T cells as well as B-cell expansion and plasma cell differentiation (7, 8). Altered CD70 expression was found in hematologic malignancies and also in solid tumors, such as nasopharyngeal carcinoma, thymic carcinoma, and brain tumors (9). The most frequent expression was reported in RCC (10–13), but the mechanism that leads to the upregulation of CD70 in this tumor type is still unclear. Interestingly, CD70

[1]Institute of Surgical Pathology, University Hospital Zurich, Zurich, Switzerland. [2]Institute of Pathology, University Hospital Erlangen, Erlangen, Germany. [3]Department of Urology, University Hospital Zurich, Zurich, Switzerland. [4]Institute of Experimental Immunology, University of Zurich, Zurich, Switzerland.

**Note:** Supplementary data for this article are available at Clinical Cancer Research Online (http://clincancerres.aacrjournals.org/).

H. Moch and P. Schraml share last authorship.

**Corresponding Authors:** Melanie Ruf, Institute of Surgical Pathology, University Hospital Zurich, Schmelzbergstrasse 12, 8091 Zurich, Switzerland. Phone: 41-44-2552537; Fax: 41-44-2554416; E-mail: melanie.ruf@usz.ch; and Peter Schraml, E-mail: peter.schraml@usz.ch

**doi:** 10.1158/1078-0432.CCR-14-1425

## Translational Relevance

The deregulation of the von Hippel–Lindau protein (pVHL)/hypoxia-inducible factor (HIF) axis is a hallmark of clear cell renal cell carcinoma (ccRCC). Consequently, protein products of HIF-regulated genes are considered potential therapeutic targets of this tumor type. We have found that in ccRCC, abundant and frequent CD70 expression is directly driven by HIF. Furthermore, we observed a close relationship between CD70 overexpression and CD70 receptor $(CD27)^+$ infiltrating lymphocytes, which seems to be linked to a more aggressive biologic behavior. Coculturing of pVHL-negative and pVHL-reexpressing RCC cell lines with peripheral blood mononuclear cells demonstrated significant increase of soluble CD27 levels in the presence of CD70. This may be the cause for the high soluble CD27 levels observed in the sera of patients with CD70-expressing ccRCC infiltrated by $CD27^+$ lymphocytes, thus suggesting soluble CD27 as a diagnostic tool for ccRCC patient monitoring.

expression is less prevalent in *VHL* unrelated RCC subtypes. Studies elucidating the consequences of the constitutive expression of CD70 and its interaction with CD27 in ccRCC are rare and controversial. Although some authors hypothesized that CD70 is involved in an immune escape mechanism of RCC by mediating apoptosis in lymphocytes (14), others suggested that CD70 rather triggers a phenotypic conversion of $CD27^+$ tumor-infiltrating lymphocytes (TIL) into a more differentiated state (15).

Here, we studied the impact of pVHL and HIFα on CD70 expression as well as the role of CD27-expressing TILs in ccRCC by (i) analyzing CD70 expression patterns in a large cohort of RCC tissues, (ii) investigating the interrelation of CD70 expression and the pVHL-HIFα axis by *VHL* mutation analysis and *in vitro* experiments, (iii) determining CD27 mRNA and protein expression in TILs and its correlation with the CD70 expression status, and (iv) examining the concentration of soluble CD27 (sCD27) in cocultures and sera of patients with CD70-positive and -negative tumors.

## Materials and Methods

### Patient material

For immunohistochemical (IHC) analyses, tissue microarrays (TMA) with 252 ccRCCs (4) and 54 ccRCC brain metastases (16, 17) from the Institute of Surgical Pathology, University Hospital of Zurich, Switzerland, and a TMA comprising 348 papillary RCCs (18) from the University of Erlangen, Erlangen, Germany, were used. Each TMA was histologically reviewed by one pathologist (H. Moch and A. Hartmann, respectively). Clinicopathological parameters of the first TMA have already been described (19). This study was approved by the local ethics commission (reference no. StV38-2005). Human blood samples of 54 patients, who underwent full or partial nephrectomy as part of their standard treatment at the Department of Urology, University Hospital Zurich (Zurich, Switzerland), were collected on the day of surgery following informed consent. Serum was processed according to a standardized protocol. Sera of 17 healthy persons served as control. Formalin-fixed, paraffin-embedded tissue samples from these patients were also available. This study was approved by the local ethics commission (KEK-ZH no. 2011-0072/4).

### IHC

TMA and whole tumor sections (2.5 μm) were IHC-stained according to Ventana automat protocols (Ventana Medical System). The antibodies applied for detection are listed in Supplementary Table S1. The staining intensities were classified as absent, moderate, and strong. Lymphocyte infiltration was analyzed using hematoxylin and eosin-stained large sections and was scored as absent, sparse to loose and dense infiltrate. For detailed analysis, TMAs were scanned using the NanoZoomer Digital Slide Scanner (Hamamatsu Photonics K.K.).

### *VHL* mutation analysis

*VHL* mutation analysis of cell lines and tissues was performed as described (1). Cell line *VHL* mutations are listed in Supplementary Table S2. The program Site Directed Mutator (SDM) was used to predict the association of *VHL* missense mutations and disease as described (1).

### Gene expression analysis

Gene expression data of 116 RCCs and six normal kidneys were obtained from a recently published microarray study (20). Microarray data are available in Gene Expression Omnibus under GSE19949.

### Cell lines

The RCC-derived cell lines ACHN, A498, A704, Caki-1, Caki-2, HK-2, KC12, 769P, 786-O and the human embryonic kidney cell line HEK-293 were supplied by ATCC. RCC4, SLR21 to SLR26 were kindly provided by W. Krek (ETH Zurich, Switzerland) and W.J. Storkus (University of Pittsburgh, Pittsburgh, PA), respectively. Stable transfectants of 786-O and A498 reexpressing pVHL and empty vector controls were previously generated (21, 22). Cell lines were grown under conditions recommended by ATCC and authenticated by short tandem repeat profiling by Identicell (Aarhus University, Aarhus, Denmark). For immune staining, cell line pellets were formalin fixed and paraffin embedded as recently described (23). For hypoxia experiments, cells were incubated under low-oxygen conditions (0.5%) in a hypoxic workstation ($Invivo_2$ 400; Ruskinn Technology) for up to 24 hours.

### Immunoblot analysis

Preparation of cell lysates, determination of protein concentration, and Western blotting were performed as described (4). Antibodies used are listed in Supplementary Table S1. For removal of *N*-glycans, PNGase F (New England Biolabs) was used.

### Transient transfections

For RNAi experiments, cells were transfected with 5 nmol/L siRNA (HIF1α, HIF2α, and scrambled) as described (24). For silencing of CD70, Hs_TNFSF7_1;_2;_3, and Hs_CD70_1 (00748699, SI00748706, SI00748713, SI04277182, Qiagen) were used.

To study the effects of HIFα overexpression, RCC cells were transfected with 5 μg *HIF1α*, *HIF2α*, or *HIF2α* DNA-binding mutant (25) in pcDNA3.1 using XtremeGene HP (Roche) and grown for 24 hours in a six-well format. The mutant *HIF2α* construct was kindly provided by P. Ratcliffe (University of Oxford, Oxford, United Kingdom).

### Quantitative reverse transcription-PCR

RNA isolation, cDNA synthesis, and quantitative reverse transcription-PCR (qPCR) were performed as described (4). TaqMan Gene Assays (Applied Biosystems) for *CA-IX* (Hs00154208_m1), *CD70* (Hs00174297_m1), *CD27* (Hs00386811_m1), *GLUT1* (Hs00197884_m1), *HIF1α* (Hs00936376_m1), *HIF2α* (Hs01026146_m1), *OCT4* (Hs04260367_gH), *PDK1* (Hs01561850_m1), *PHD3* (Hs00222966_m1), *PPIA* (Hs99999904_m1), and *VHL* (Hs00184451_m1) were used.

### Chromatin immunoprecipitation

Chromatin immunoprecipitation (ChIP) was performed as described (5). Fragments of 100-600 bp of cellular DNA were incubated with a HIFα-antibody/magnetic bead (Dynabeads Protein G; Invitrogen) mixture. SYBR Green real-time PCR was performed to quantify the differential binding of HIFα to the hypoxia-responsive elements (HRE) of *CD70*. The antibody and primers used for the ChIP experiments are listed in Supplementary Tables S1 and S3.

### Luciferase gene reporter assay

The nucleotides between −2,000 and +700 were defined as the putative promoter region of *CD70* (Chr 19p13; Gene-ID: 970). The promoter region was synthesized from GenScript and cloned into firefly luciferase reporter plasmid pGL4.10 (Promega). The positive control P2P contains the *P2P* HREs of the human *PHD2* promoter (26) and were provided by R. Wenger (University of Zurich). Luciferase activity was measured 24 hours after transfection of A498 empty vector and A498 reexpressing pVHL with 1 μg of reporter plasmids along with 200 ng of pGL4.74 *Renilla* luciferase reporter plasmid in 24-well plates. HIFα overexpression was performed 48 hours before measurement. Relative luciferase units were determined according to the manufacturer's instructions (Dual luciferase reporter assay system, Promega).

### Determination of sCD27 in cocultures and sera of patients with RCC

The RCC cells were seeded into six wells that the number of cells reached $2.7 \times 10^5$/well 48 hours later. For siRNA experiments, cell transfection was performed 24 hours after seeding. Peripheral blood mononuclear cells (PBMC) of a healthy individual were isolated by Ficoll (GE Healthcare) density centrifugation. Forty-eight hours after seeding and repeated washing, $2.7 \times 10^6$ PBMCs were added in 2 mL RPMI-1640 containing 10% FCS. The cells were cocultured for 2 additional days. PBMCs and RCC cells were maintained in monoculture in parallel. After 2 days, supernatants were used to analyze sCD27 concentration by sandwich ELISA (M1960, Sanquin) according to the manufacturer's instructions. The different experimental approaches were performed using PBMCs of different healthy individuals (donor A-C). The sCD27 ELISA was also used for testing sera of patients with RCC and healthy individuals.

### Statistical and computational analyses

The Pearson $\chi^2$ test, Fisher exact test, Student *t* test, and survival analysis were performed using SPSS Statistics 21 (IBM). Correlation analysis (Pearson R) was performed using GraphPad Prism 5 (GraphPad Software).

## Results

### CD70 is frequently expressed in ccRCC and ccRCC metastasis

Gene expression analysis of 116 RCC tissues (20) revealed that *CD70* was upregulated in primary and metastatic ccRCC (Fig. 1A). Using TMAs containing a total of 667 RCCs, we observed high

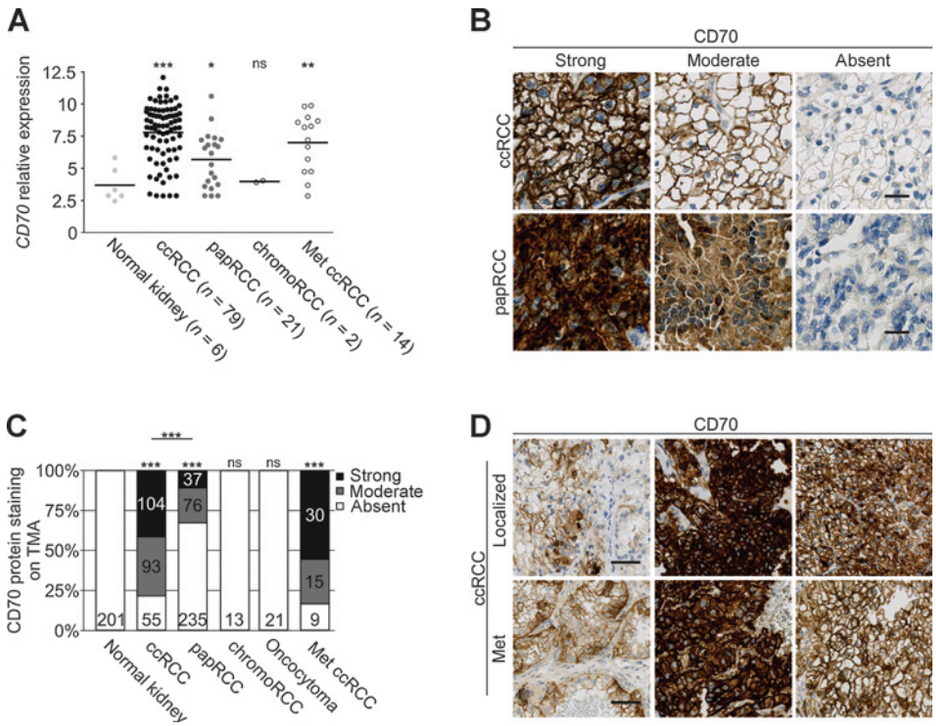


**Figure 1.**
CD70 expression pattern in RCC. A, *CD70* gene expression in 116 RCCs and six normal kidney tissues. *T* tests were performed. B, representative pictures of anti–CD70-immunostained ccRCCs and papillary RCCs (×40 magnification, bars: 20 μm). C, histogram representing CD70 expression intensities in RCC and normal kidney tissue. The Pearson $\chi^2$ test or Fisher exact test was performed. D, representative pictures of anti–CD70-immunostained localized ccRCC and corresponding brain metastasis ($n = 8$, ×20 magnification, bars, 50 μm). pap, papillary; chromo, chromophobe; met, metastasis; ***, $P < 0.0001$; **, $P < 0.005$; *, $P < 0.05$; ns, not significant.

CD70 protein expression in 78% of ccRCCs, but in only 32% of papillary RCC. Oncocytomas, chromophobe RCCs, and normal kidneys were negative (Fig. 1B and C). Furthermore, 54 ccRCC brain metastases showed a similar CD70 expression frequency as observed in primary tumors. Notably, the strong CD70 expression seen in nine primary ccRCC remained constant in their corresponding brain metastasis (Fig. 1D).

### CD70 expression and *VHL* mutation status in ccRCC tissues and cell lines

Many *VHL* mutations are thought to inactivate pVHL's functional integrity in ccRCC. To test whether *VHL* mutations affect CD70 expression, we correlated the mRNA and protein expression patterns of CD70 with *VHL* mutation data in a series of ccRCCs, which were recently published by our group (1). Although *VHL* wild-type (wt) ccRCC may also have lost pVHL activity due to hypermethylation of its gene promoter, we found an association of CD70 expression and mutated *VHL* (Fig. 2A and B). CD70 expression was even more frequent in tumors with *VHL* mutations, which predict impaired function of pVHL compared with tumors with *VHL* wt and *VHL* mutations not affecting the protein function (Fig. 2C). We confirmed these findings in RCC cell lines with different *VHL* and *HIF1α* mutation states (ref. 27; Supplementary table S2). *CD70* mRNA and protein levels were generally higher in RCC cell lines harboring *VHL* loss-of-function mutations (Caki-2, SLR22, SLR23, A498, 786-O, and KC12) and *VHL* missense mutations predicted to affect the pVHL function (RCC4, SLR24, and SLR26). RCC cell lines with *VHL* missense mutations having no functional impact on the protein (SLR25, 769P, and A704) and those with wt *VHL* (SLR21, ACHN, Caki-1, HK-2, and HEK293) showed no or only weak CD70 expression (Fig. 2D–F). CD70 expression was mainly observed in cell lines that either were HIF1α-, HIF2α- or HIF1α- and HIF2α-positive. In most of the cell lines that express CD70, Glut1 and CA-IX were also present (Fig. 2E). This was also true on mRNA level, the *CD70* expression correlated with *GLUT1* and *CA-IX*, but was not associated with other HIF target genes (*PDK1*, *OCT4*, and *PHD3*; Fig. 2D). The multiple banding pattern of CD70 in RCC seen on Western blot analyses was also previously described (13, 28) and results largely from N-linked glycosylation (Supplementary Fig. S1).

### CD70 expression is dependent of the pVHL/HIFα axis in RCC tissue and cell lines

To evaluate the impact of pVHL and HIF on *CD70* expression in RCC, we first performed qPCR (Fig. 3A) and Western blot analyses (Fig. 3B) of pVHL-deficient RCC cell lines 786-O and A498 and

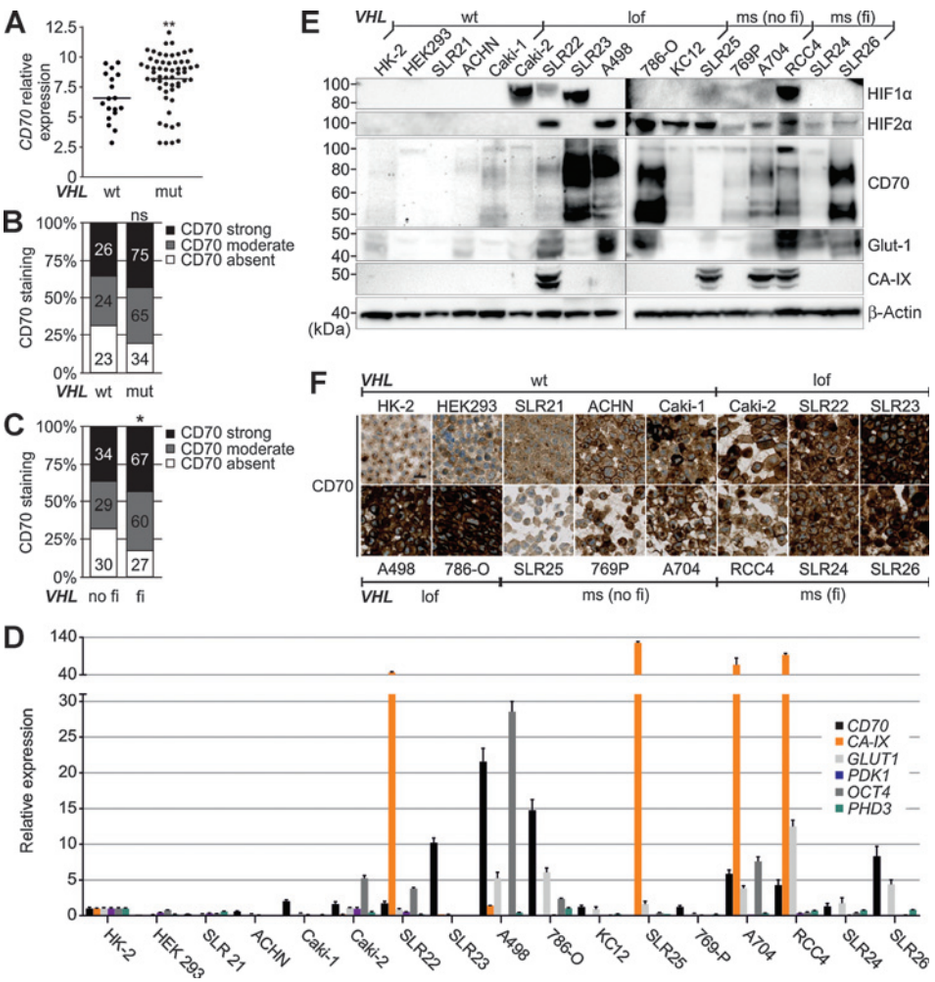


**Figure 2.**
Association of CD70 with the *VHL* mutation status. A, *CD70* gene expression in ccRCC tissue with mutated or wt *VHL*. **, $P < 0.001$ by *t* test. B, histogram representing CD70 expression intensities in ccRCCs with mutated or wt *VHL*. ns, not significant by Pearson $\chi^2$ test. C, CD70 expression intensities assigned to ccRCC tissue with function of pVHL predicted to be impaired or not impaired. *In silico* analysis was done with SDM. *, $P < 0.05$ by Pearson $\chi^2$ test. D, mRNA levels of *CD70*, the HIF1α-dependent genes *CA-IX* and *PDK1*, the HIF2α-dependent genes *GLUT1*, *OCT4*, and *PHD3*; (E) Western blot analysis of HIF1α, HIF2α, CD70, CA-IX, and Glut1; and (F) cell microarray stained for CD70 in different RCC cell lines (×20 magnification; bar, 20 μm). The *VHL* mutation status is indicated as wt, loss of function (lof), missense (ms) with (fi) and without (no fi) functional impact on pVHL.

their stable transfectants reexpressing pVHL. Reconstituted pVHL lead to a decrease of the *CD70* expression and the HIF targets *CA-IX*, *GLUT*1, *OCT4*, and *PHD3*. TMA analyses demonstrated a significant association of CD70 expression and pVHL/HIF deregulation. CD70 expression was directly correlated with the expression of HIF1α ($P = 0.0136$, Pearson $R = 0.1359$) and HIF2α ($P < 0.0001$, Pearson $R = 0.2833$) as well as with the HIF targets CA-IX ($P < 0.0001$, Pearson $R = 0.4267$), Glut1 ($P < 0.0001$, Pearson $R = 0.4093$), and CD10 (ref. 4; $P < 0.0001$, Pearson R = 0.3901). An inverse correlation was seen with pVHL ($P = 0.0144$, Pearson $R = -0.1398$) and E-Cadherin ($P = 0.0485$, Pearson $R = -0.1121$). CD70 expression alone was not associated with grade, stage, and survival in ccRCC (data not shown). Silencing of *HIF2α* in 786-O and A498 exclusively expressing HIF2α (but not HIF1α) lead to a decrease of *CD70* mRNA and protein expression (Fig. 3C–F). In SLR22, CD70 downregulation was achieved only when both *HIF1α* and *HIF2α* were silenced (Supplementary Fig. S2A). Following transient overexpression of *HIF1α* and *HIF2α* in 786-O and A498, an increase of *CD70* mRNA and protein levels was observed (Fig. 3G and H). Even in the pVHL-defective RCC cell lines SLR22 and SLR24 with low endogenous CD70 levels, upregulation of the latter could be induced by overexpression of *HIF2α* (Supplementary Fig. S2B and S2C). In pVHL-negative and -positive 786-O and A498 cells, CD70 expression was continuously increasing under hypoxia within the first 12 hours (Fig. 3H and I).

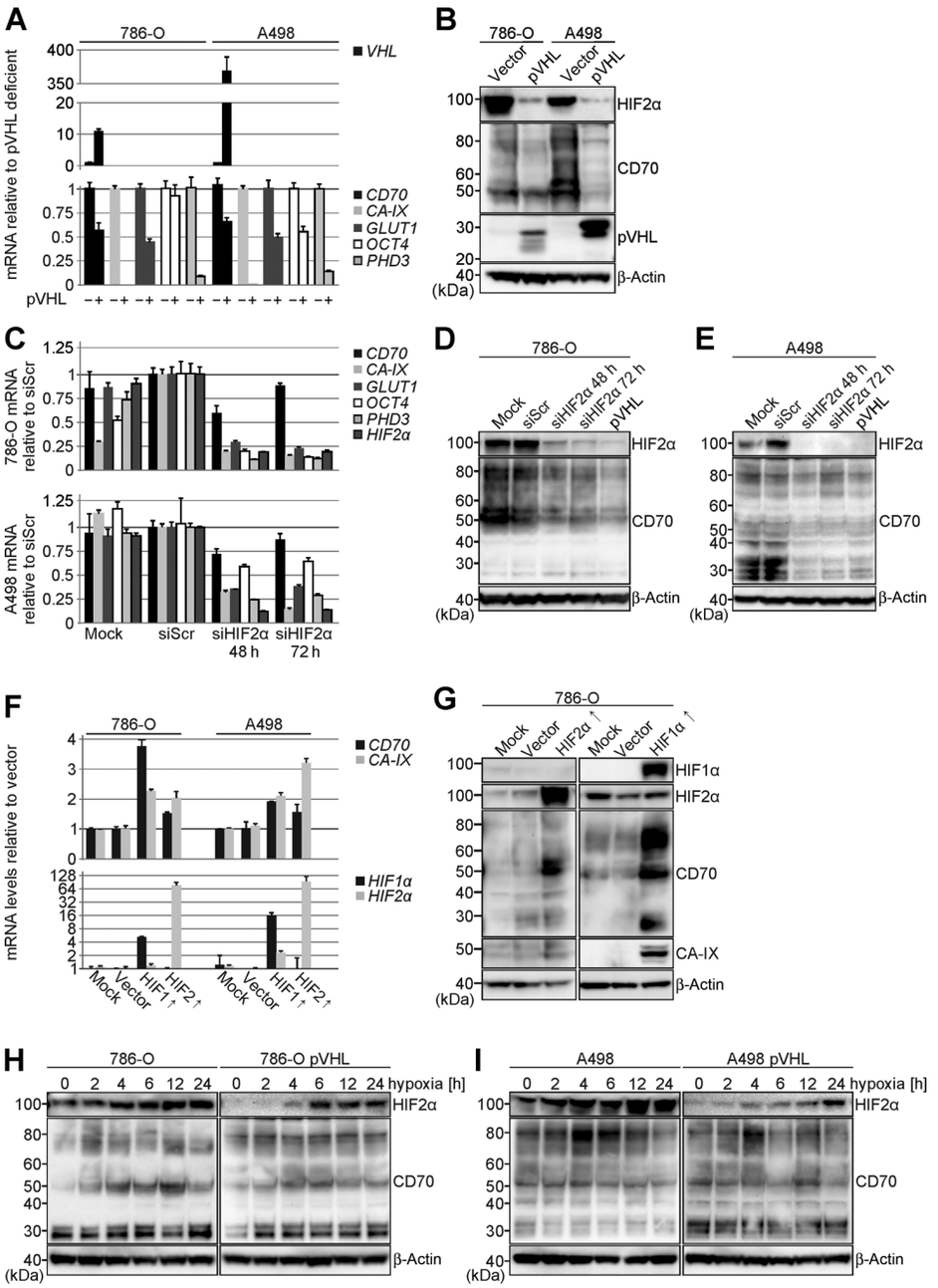


**Figure 3.**
CD70 expression is dependent on the pVHL/HIF axis. A, mRNA levels of *VHL, CD70*, *CA-IX, GLUT1, OCT4*, and *PHD3* in 786-O and A498 with reconstituted pVHL relative to empty vector obtained by qPCR. B, Western blot analysis of HIF2α, CD70, and pVHL in 786-O and A498 with reconstituted pVHL or empty vector. C, mRNA levels of *CD70*, *CA-IX*, *GLUT1, OCT4*, *PHD3*, and *HIF2α* relative to control siRNA (siScr) obtained by qPCR and (D) Western blot analysis of HIF2α and CD70 in 786-O, and (E) A498 after silencing of *HIF2α* for 48 and 72 hours. F, mRNA levels of *CD70*, *CA-IX*, *HIF1α*, and *HIF2α* relative to empty vector control obtained by qPCR and (G) Western blot analysis of HIF1α, HIF2α, CA-IX, and CD70 in 786-O after transient overexpression of *HIF1α* and *HIF2α*. H, Western blot analysis of HIF2α and CD70 in 786-O and (I) A498 with and without reconstituted pVHL incubated at 0.5% oxygen for 0, 2, 4, 6, 12, and 24 hours (h). Error bars, SD ($n = 3$).

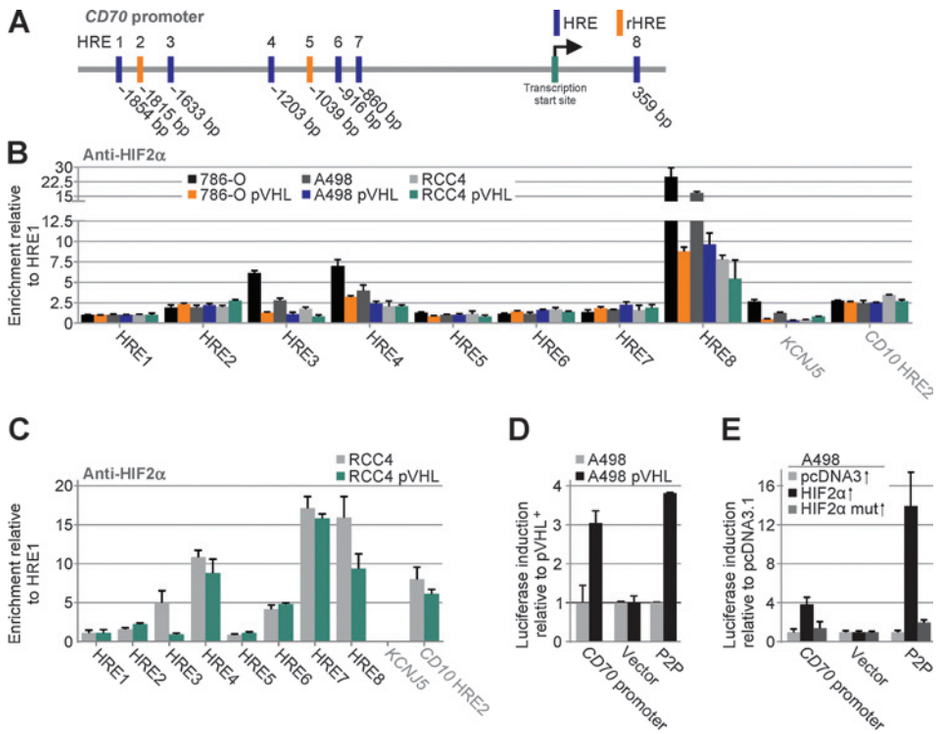


**Figure 4.**
CD70 promoter binding and gene expression by HIFα. A, schematic representation of the 2.7 kb *CD70* promoter with the location of six HREs and two reverse HREs (rHRE). B, binding of HIF2α and (C) HIF1α at the *CD70* promoter relative to its isotype controls analyzed by ChIP. HRE1-8 indicates *in silico* identified HREs in the *CD70* promoter; *KCNJ5* served as negative and *CD10* HRE2 as positive control for HIF1α. Results are shown as ratios of the amplicons detected in 786-O, A498, or RCC4 pVHL-positive and negative relative to HRE1. D, luciferase induction of the 2.7 kb promoter region of *CD70* in A498 empty vector relative to A498 reconstituted with pVHL and (E) after overexpression of HIF2α or a DNA binding mutant of HIF2α in A498 relative to pcDNA3.1-transfected cells. P2P served as a positive control for the HIF activity. (vector = empty luciferase reporter plasmid pGL4.10). Error bars, SD ($n = 3$).

### CD70 expression is directly regulated by HIF

To elucidate whether CD70 represents a potential HIF target, we investigated HIF's ability to bind to the eight potential HREs residing in 2.7 kb of the putative promoter of *CD70* (Fig. 4A) by ChIP using HIF2α-, HIF1α-, and the corresponding isotype control- antibodies (Fig. 4B and C). The reconstitution of pVHL in 786-O, A498, and RCC4 leads to a reduction of the direct binding of HIF2α and HIF1α to HRE3, 4, and 8 in the *CD70* promoter. No binding was observed for the negative control gene *KCNJ5*. CD10 HRE2 served as positive control for HIF1α binding (4).

To confirm this finding, we performed luciferase reporter gene assays. For this purpose, the DNA fragment containing the 5′-region of *CD70* (−2000/+700) was inserted upstream of the luciferase gene. Compared with pVHL reexpressing A498 cells, the luciferase activity of the *CD70* reporter gene construct was increased in A498 empty vector cells to the same extent as for the HIF target gene *PHD2* promoter construct (P2P; Fig. 4D).The same effect was seen by overexpression of HIF2α in A498, but not by overexpression of its DNA-binding mutant (ref. 25; Fig. 4E), which is unable to induce the expression of the CD70 protein product (Supplementary Fig. S2D and S2E).

### Preferential infiltration of CD27$^+$ lymphocytes in CD70-expressing tumors

As the role of CD70–CD27 interaction in ccRCC is unknown, we next asked whether there was an association between CD70-expressing tumor cells and CD27$^+$ TILs. qPCR analysis of 47 ccRCCs selected from the TMA, which was immunostained against CD70, showed higher *CD27* mRNA expression in tumors with strong CD70 staining compared with tumors with lower CD70 expression (Fig. 5A). *CD27* and *CD70* gene expression obtained from a recent DNA-microarray analysis (20) confirmed this finding (Fig. 5B). To validate the gene expression data on protein level, we investigated CD70 and CD27 expression patterns on large consecutive tissue sections of 41 ccRCC infiltrated by lymphocytes. We observed that 37 ccRCCs (90%) contained also CD27$^+$ lymphocytes (Fig. 5C). Interestingly, correlations between TMA expression data and clinicopathological data showed that patients with CD70-negative ccRCCs and no lymphocyte infiltration had a better survival compared with those with CD70 strongly positive and lymphocyte-infiltrated ccRCCs ($P < 0.05$; Fig. 5D). The latter tumors were significantly associated with a high Fuhrman grade ($P < 0.0001$) but not with late tumor stage (Supplementary table S4). The strong correlation between CD27 and the subunits of the T-cell marker CD3 indicates that the CD27-stained lymphocytes were T cells (Supplementary Fig. S3).

### PBMCs trigger the release of sCD27 in a CD70-dependent manner

CD27 is known to be cleaved by a protease into its soluble form sCD27 on activated T cells (29, 30). It was also shown that CD70-expressing glioma cells enhance the release of sCD27 from PBMCs (28). To test whether CD27 can also be cleaved after interaction with CD70 in RCC, we cocultured RCC cells with freshly isolated PBMCs and measured sCD27 in the supernatant by ELISA (Fig. 6A). Supernatants of PBMC and RCC cell monocultures contained basic levels of sCD27 after 2 days. PBMC cocultures with the CD70-expressing cell lines 786-O, A498, and SLR23 significantly increased the sCD27 concentration (2.7-fold, 1.9-fold, and 2.3-fold, respectively). This increase correlated with the PBMC/RCC cells ratio (Supplementary Fig. S4A). Cocultures with CD70 low-expressing cell lines Caki-2, SLR22, SLR24, and SLR25 had only slightly elevated sCD27 concentration levels compared with PBMC monocultures. Both *CD70* silencing (Supplementary

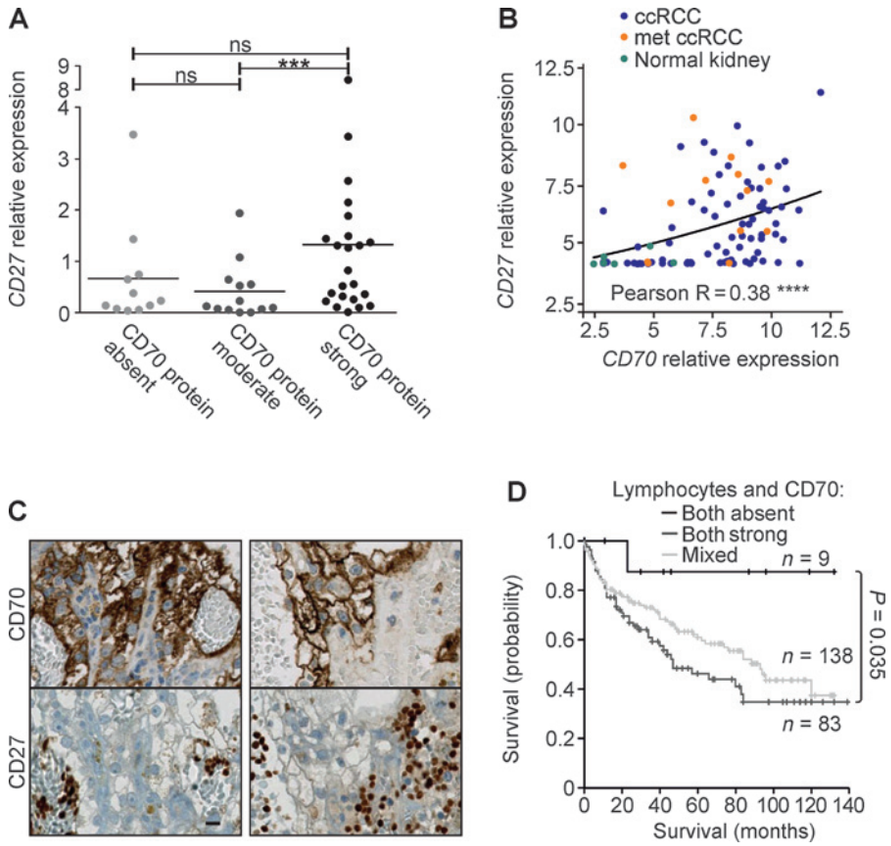


**Figure 5.**
Correlation between CD70 expression and CD27$^+$ TILs. A, *CD27* mRNA levels obtained by qPCR separated into ccRCCs showing no, moderate, or strong CD70 tumor staining on TMA. B, *CD70* plotted against *CD27* mRNA levels of the gene expression data. Pearson R correlation analyses are depicted. (met, metastasis). C, representative pictures of anti-CD70 and anti–CD27-immunostained ccRCCs of consecutive slides (×40 magnification; bar, 100 μm). D, Kaplan–Meier plot of the overall survival of ccRCC patients defined by the CD70 expression accompanied by lymphocyte infiltration. A log-rank test was performed.

Fig. S4B and S4C) and reconstitution of pVHL in 786-O and A498 cells caused a reduction of sCD27 levels (Fig. 6A).

**Elevated sCD27 levels are detectable in sera of patients with CD70-expressing RCC**

To investigate whether our *in vitro* results were conferrable to patients, we measured sCD27 concentration in sera of ccRCC and papillary RCC patients and healthy individuals (Fig. 6B). sCD27 levels were compared with the expression status of CD27 and CD70 on large tissue sections of the corresponding patients (Fig. 6C). sCD27 serum levels of patients with CD70-expressing tumor cells and CD27$^+$ TILs were significantly higher compared with those of healthy individuals and RCCs of patients that either had CD70-positive tumor cells but no CD27$^+$ TILs or had CD27$^+$ TILs and CD70-negative tumor cells or were negative for both.

Notably, ELISA analysis of CD70 revealed that CD70 protein expression levels in 31 RCCs were not reflected in the sera of these patients as most of the CD70 levels were below the detection limit (data not shown).

## Discussion

In this study, we demonstrated that the high and frequent CD70 expression in ccRCC is driven by HIF as a consequence of pVHL loss of function. We further observed a strong association between CD70-expressing tumor cells and the presence of CD27$^+$ T cells in TILs. The ability of CD70 to trigger the release of sCD27 on PBMCs *in vitro* and the increased levels of sCD27 in the sera of patients with CD70-expressing tumors suggest that sCD27 is a putative serum marker for CD70-positive ccRCC patients.

CD70 expression is dependent on the RCC subtype. IHC TMA staining of more than 600 RCCs showed abnormal CD70 expression in 78% of ccRCCs, which was consistent with previously described frequencies (11, 12). Our comprehensive CD70 analysis of 348 papillary RCCs revealed 11% strongly and 22% moderately expressing tumors, which was lower compared with the frequencies observed in recently published smaller cohorts (10, 12, 13). No expression was seen in 21 oncocytomas and 13 chromophobe RCCs suggesting a negligible role of CD70 in these tumor subtypes.

We show that the abnormal upregulation of CD70 in ccRCC is closely related to the deregulation of the pVHL/HIF axis. CD70 expression patterns in RCC tissue were significantly correlated with those seen for HIFα and the HIF targets CA-IX, Glut1, and CD10. The analysis of the mutation status of *VHL* in 363 ccRCCs and 17 RCC cell lines further supported the association of CD70 expression with *VHL* sequence alterations. High CD70 expression levels were significantly linked to *VHL* mutations that very likely abrogate pVHL's function. Inactivation of *VHL* by hypermethylation of its promoter (31) and missense mutations with no or only minor effects on pVHL's ability to bind HIFα (1) may explain the presence or absence of CD70 in several *VHL* wt and mutated tumors, respectively. In pVHL-affected cell lines, the expression pattern of CD70 was comparable with that of HIF1α, HIF2α as well as HIF targets Glut1 and CA-IX. Our results suggest that CD70 is driven by both HIF1α and HIF2α. Some pVHL-deficient ccRCC

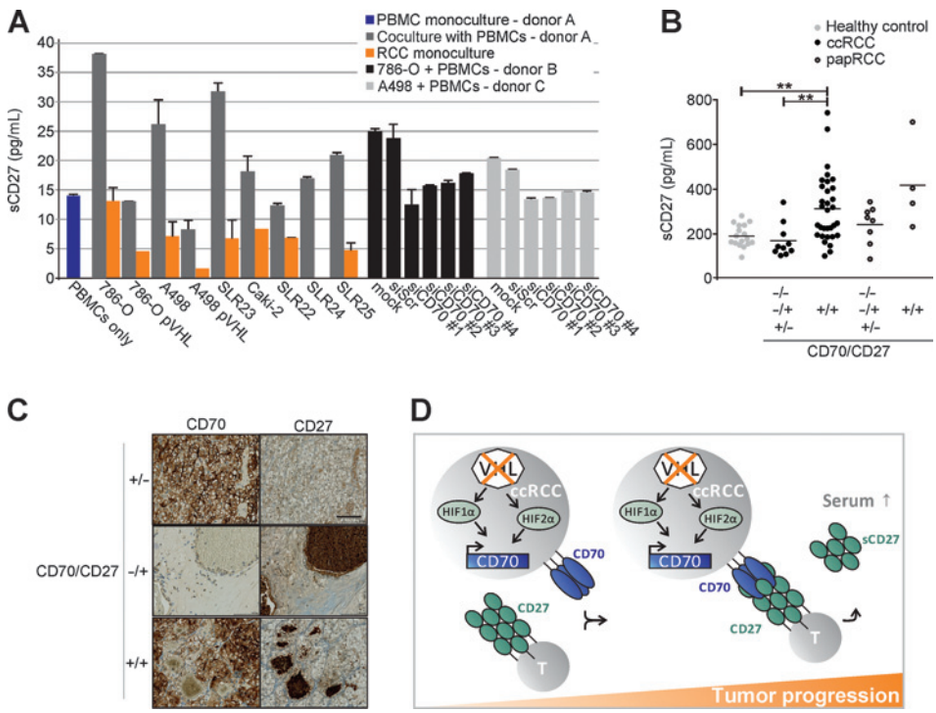


**Figure 6.**
Release of sCD27 via CD70 *in vitro* and high serum levels of sCD27 in CD70-expressing RCC patients. A, concentrations of sCD27 in supernatants of PBMC and RCC cell line cocultures or monocultures were determined by ELISA. In 786-O and A498, CD70 expression was silenced by siRNA (siCD70#1–4). siScr, control siRNA. Donor A–C, PBMCs from different healthy individuals. B, sCD27 serum concentrations of patients with RCC and healthy controls. **, $P < 0.005$ by the *t* test. C, representative pictures of anti-CD70 and anti–CD27-immunostained ccRCCs of consecutive slides of large sections (×40 magnification; bar, 100 μm). The existence of CD70 expression and $CD27^+$ infiltrations (CD70/CD27) of the tumor tissues was indicated as absent (−) or present (+). D, a model showing the biologic and clinical relevance of CD70 and CD27 in ccRCC.

cell lines exhibited elevated HIFα although CD70 was absent. They may resemble those 20% (34/174) of CD70-negative ccRCCs, which had *VHL* mutations with functional impact on pVHL, presumably causing HIFα stabilization. Epigenetic regulation of HIF-binding sites can probably influence the transcriptional response to hypoxia (32). Aberrant DNA methylation of the two CpG islands (−993 to −323 bp relative to transcription start site; ref. 33), which overlap the region with the putative HREs in the *CD70* promoter, may thus prevent HIF from binding and may explain why CD70 is not or only weakly expressed in the presence of HIF in those tumors.

*In vitro* experiments, which included pVHL reconstitution, *HIFα* silencing and overexpression, hypoxia experiments, ChIP and luciferase assays confirmed that CD70 expression is dependent on pVHL's functional integrity and the transcriptional activation by HIF. The attenuation of CD70 protein expression after 12 hours under hypoxic conditions may be caused by oxygen-sensitive pathways that are HIF-independent (34).

It is obvious that in ccRCC, the mechanism of CD70's upregulation is different to that reported in several T-cell affecting diseases, such as systemic lupus erythematosus and systemic sclerosis (35, 36) in which hypomethylation of the *CD70* promoter contributes to CD70 overexpression. Using the same methylation-specific PCR protocol described by Yu and colleagues (33), no hypomethylation of the *CD70* promoter was seen in ccRCC tissues, which strongly expressed CD70 (data not shown). This suggests that the transcriptional regulation of *CD70* is rather driven by HIF and does not depend on promoter hypomethylation in this tumor subtype.

A strong relationship between HIFα activation, CD70 upregulation, and tumor formation was demonstrated in TRACK mice (transgenic model of cancer of the kidney), which specifically express a mutated, constitutively active form of HIF1α in kidney proximal tubule cells (37). Activated HIF1α was sufficient to promote phenotypic alterations characteristic of human *VHL* ccRCC, including upregulation of CA-IX, Glut1, and CD70, whereas a constitutively activated form of HIF2α was neither able to promote ccRCC nor to enhance the expression of CD70 (38). This stands in contrast with the findings of Gordan and colleagues (39) who showed that HIF2α rather than HIF1α mediates ccRCC progression. Our *in vitro* data indicate that *CD70* can be activated by both HIFα isoforms. However, strong CD70 expression is preferentially seen in RCC cell lines in which only HIF2α is present suggesting that HIF2α is a key regulator for CD70 expression in progressing ccRCC.

In addition to the mechanisms for abnormal CD70 expression in ccRCC, we were also interested to investigate the role of the interaction with its receptor CD27, which is known to be expressed on the surface of memory B cells, naïve, and activated T cells and a subset of natural killer (NK) cells (7). Microarray gene expression data of ccRCC revealed a significant correlation between *CD70* and *CD27* expression. A detailed IHC analysis of large ccRCC tissue sections demonstrated that the lymphocyte infiltrates in CD70-expressing tumors were almost always accompanied by $CD27^+$ TILs.

Neither we nor others have found a strong correlation between CD70 expression alone and tumor grade, stage, and patient survival (12, 13). As the loss of pVHL function is considered an early event in ccRCC (3), the subsequent upregulation of CD70 may also contribute to tumor formation. We observed that the frequency of strong CD70 expression in pVHL-deficient primary ccRCC is retained in metastatic lesions. It is therefore conceivable that the persistent expression of CD70 in tumors leads to an enhanced attraction and infiltration of $CD27^+$ lymphocytes. Interestingly, ccRCC with strong CD70 expression and TILs had a higher nuclear differentiation grade and a significantly worse

survival compared with CD70-negative tumors that were not infiltrated by lymphocytes. On the basis of this finding, we conclude that the interaction of CD70-expressing tumor cells and $CD27^+$ TILs may play a role in tumor progression.

Different tumor-promoting mechanisms have been proposed in this context. sCD27 can induce proliferation in CD70-positive acute lymphoblastic leukemia and nasal NK/T-cell lymphoma (40, 41). It was therefore tempting to speculate that the interaction of $CD27^+$ TILs with CD70 present on ccRCC cells has similar effects and accelerate tumor growth. Both sCD27 (42) and CD70 (8) contribute to T-cell activation and proliferation. However, we could not see any proliferative effects of recombinant sCD27 in response to CD70 in two RCC cell lines (data not shown). Second, although CD70-expressing ccRCC and glioma cells were able to provoke T-cell apoptosis in coculture experiments (14, 28, 43), the immune inhibitory properties of CD70 *in vitro* seem to be clearly overwhelmed by the immune activating properties observed in mouse glioma models *in vivo* (44). Finally, the chronic ligation of CD27 and CD70 may also lead to T-cell exhaustion, a kind of "immune escape." It was shown that constitutive expression of CD70 on B cells in mice converted naïve T cells into effector memory cells. This culminated in the depletion of naïve T cells, which lead to lethal immunodeficiency (45). In keeping with this, Wang and colleagues observed less naïve and central memory T-cell subpopulations but more effector memory cells in ccRCC in contrast with peripheral blood lymphocytes and melanoma (15). They suggested that this phenotypic conversion of T cell is caused by high CD70 expression in ccRCC. These results together with our findings suggest that the coexistence of CD70 and CD27 in ccRCC fosters immune exhaustion effects by chronic costimulation.

As it was shown with glioma cells (28), coculturing of PBMCs with RCC cells resulted in a CD70-dependent increase of sCD27 in the supernatant. A similar effect may occur in CD70-expressing ccRCC tissue with $CD27^+$ TILs because the levels of sCD27 in sera of those patients were significantly higher compared with patients with CD70- and CD27-negative tumors and healthy persons. Besides lymphoid malignancies (40, 41), ccRCC is the first solid tumor type in which increased serum levels of sCD27 have been observed. High serum concentration of sCD27 may thus represent a potential predictive marker in patients with ccRCC, which indirectly indicates the presence of CD70-expressing tumors.

In conclusion, we demonstrated that in pVHL-deficient ccRCC, CD70 is upregulated via HIF. A model illustrating our hypothesis is shown in Fig. 6D. CD70 and CD27 interaction seems to boost the release of sCD27 in sera of patients with ccRCC suggesting CD27 a potential prognostic and diagnostic marker that may also be used to predict the applicability of CD70-targeted therapies or CD27-targeted immunotherapies (46). At the moment, three novel anti-CD70 antibody–drug conjugates are under evaluation for metastatic ccRCC in clinical trial phase I (47), which have shown promising antitumor activity in CD70-expressing RCC mouse xenografts (48). One should, however, bear in mind that blocking of CD70–CD27 interaction by CD70-targeting drugs may impede *de novo* T-cell priming (49, 50), thus hampering patients' immune response capability.

## Disclosure of Potential Conflicts of Interest

No potential conflicts of interest were disclosed.

## Authors' Contributions

**Conception and design:** M. Ruf, H. Moch, P. Schraml
**Development of methodology:** M. Ruf, C. Mittmann, A.M. Nowicka, H. Moch
**Acquisition of data (provided animals, acquired and managed patients, provided facilities, etc.):** M. Ruf, C. Mittmann, A.M. Nowicka, A. Hartmann, T. Hermanns, C. Poyet, T. Sulser
**Analysis and interpretation of data (e.g., statistical analysis, biostatistics, computational analysis):** M. Ruf, M. van den Broek, T. Sulser, H. Moch, P. Schraml
**Writing, review, and/or revision of the manuscript:** M. Ruf, A. Hartmann, T. Hermanns, M. van den Broek, T. Sulser, H. Moch, P. Schraml
**Administrative, technical, or material support (i.e., reporting or organizing data, constructing databases):** M. Ruf, A. Hartmann, T. Hermanns, H. Moch
**Study supervision:** H. Moch, P. Schraml

## Acknowledgments

The authors thank Susanne Dettwiler, Martina Storz, Adriana von Teichman, Sonja Brun-Schmid and André Fitsche (Institute of Surgical Pathology, University Hospital Zurich) for their excellent technical support; Alexandra Veloudios (Department of Urology, University Hospital Zurich) for collecting RCC patients sera; Markus Rechsteiner (Institute of Surgical Pathology, University Hospital Zurich) for supporting experimental setups; and Jannie Borst (Netherlands Cancer Institute, Amsterdam, the Netherlands) for valuable suggestions and for critically reading the manuscript.

## Grant Support

This work was supported by the Swiss National Cancer Foundation (to H. Moch; 3238BO-10314) and the Zurich Cancer League (to H. Moch).

The costs of publication of this article were defrayed in part by the payment of page charges. This article must therefore be hereby marked *advertisement* in accordance with 18 U.S.C. Section 1734 solely to indicate this fact.

Received June 4, 2014; revised November 12, 2014; accepted November 14, 2014; published online February 17, 2015.

## References

1. Rechsteiner MP, von Teichman A, Nowicka A, Sulser T, Schraml P, Moch H. VHL gene mutations and their effects on hypoxia inducible factor HIFalpha: identification of potential driver and passenger mutations. Cancer Res 2011;71:5500–11.
2. Frew IJ, Krek W. pVHL: a multipurpose adaptor protein. Sci Signal 2008;1:pe30.
3. Shen C, Kaelin WG Jr. The VHL/HIF axis in clear cell renal carcinoma. Semin Cancer Biol 2013;23:18–25.
4. Boysen G, Bausch-Fluck D, Thoma CR, Nowicka AM, Stiehl DP, Cima I, et al. Identification and functional characterization of pVHL-dependent cell surface proteins in renal cell carcinoma. Neoplasia 2012;14:535–46.
5. Goodwin RG, Alderson MR, Smith CA, Armitage RJ, VandenBos T, Jerzy R, et al. Molecular and biological characterization of a ligand for CD27 defines a new family of cytokines with homology to tumor necrosis factor. Cell 1993;73:447–56.
6. Watts TH. TNF/TNFR family members in costimulation of T cell responses. Annu Rev Immunol 2005;23:23–68.
7. Croft M. The role of TNF superfamily members in T-cell function and diseases. Nat Rev Immunol 2009;9:271–85.
8. Nolte MA, van Olffen RW, van Gisbergen KP, van Lier RA. Timing and tuning of CD27-CD70 interactions: the impact of signal strength in setting the balance between adaptive responses and immunopathology. Immunol Rev 2009;229:216–31.
9. Grewal IS. CD70 as a therapeutic target in human malignancies. Expert Opin Ther Targets 2008;12:341–51.
10. Junker K, Hindermann W, von Eggeling F, Diegmann J, Haessler K, Schubert J. CD70: a new tumor specific biomarker for renal cell carcinoma. J Urol 2005;173:2150–3.
11. Adam PJ, Terrett JA, Steers G, Stockwin L, Loader JA, Fletcher GC, et al. CD70 (TNFSF7) is expressed at high prevalence in renal cell carcinomas

and is rapidly internalised on antibody binding. Br J Cancer 2006;95: 298–306.
12. Law CL, Gordon KA, Toki BE, Yamane AK, Hering MA, Cerveny CG, et al. Lymphocyte activation antigen CD70 expressed by renal cell carcinoma is a potential therapeutic target for anti-CD70 antibody-drug conjugates. Cancer Res 2006;66:2328–37.
13. Jilaveanu LB, Sznol J, Aziz SA, Duchen D, Kluger HM, Camp RL. CD70 expression patterns in renal cell carcinoma. Hum Pathol 2012;43:1394–9.
14. Diegmann J, Junker K, Loncarevic IF, Michel S, Schimmel B, von Eggeling F. Immune escape for renal cell carcinoma: CD70 mediates apoptosis in lymphocytes. Neoplasia 2006;8:933–8.
15. Wang QJ, Hanada K, Robbins PF, Li YF, Yang JC. Distinctive features of the differentiated phenotype and infiltration of tumor-reactive lymphocytes in clear cell renal cell carcinoma. Cancer Res 2012;72:6119–29.
16. Ingold B, Wild PJ, Nocito A, Amin MB, Storz M, Heppner FL, et al. Renal cell carcinoma marker reliably discriminates central nervous system haemangioblastoma from brain metastases of renal cell carcinoma. Histopathology 2008;52:674–81.
17. Wyler L, Napoli CU, Ingold B, Sulser T, Heikenwalder M, Schraml P, et al. Brain metastasis in renal cancer patients: metastatic pattern, tumour-associated macrophages and chemokine/chemoreceptor expression. Br J Cancer 2014;110:686–94.
18. Herrmann E, Trojan L, Becker F, Wulfing C, Schrader AJ, Barth P, et al. Prognostic factors of papillary renal cell carcinoma: results from a multi-institutional series after pathological review. J Urol 2010;183:460–6.
19. Dahinden C, Ingold B, Wild P, Boysen G, Luu VD, Montani M, et al. Mining tissue microarray data to uncover combinations of biomarker expression patterns that improve intermediate staging and grading of clear cell renal cell cancer. Clin Cancer Res 2010;16:88–98.
20. Beleut M, Zimmermann P, Baudis M, Bruni N, Buhlmann P, Laule O, et al. Integrative genome-wide expression profiling identifies three distinct molecular subgroups of renal cell carcinoma with different patient outcome. BMC Cancer 2012;12:310.
21. Staller P, Sulitkova J, Lisztwan J, Moch H, Oakeley EJ, Krek W. Chemokine receptor CXCR4 downregulated by von Hippel-Lindau tumour suppressor pVHL. Nature 2003;425:307–11.
22. Hergovich A, Lisztwan J, Thoma CR, Wirbelauer C, Barry RE, Krek W. Priming-dependent phosphorylation and regulation of the tumor suppressor pVHL by glycogen synthase kinase 3. Mol Cell Biol 2006;26: 5784–96.
23. Pawlowski R, Muhl SM, Sulser T, Krek W, Moch H, Schraml P. Loss of PBRM1 expression is associated with renal cell carcinoma progression. Int J Cancer 2013;132:E11–7.
24. Casagrande S, Ruf M, Rechsteiner M, Morra L, Brun-Schmid S, von Teichman A, et al. The protein tyrosine phosphatase receptor type J is regulated by the pVHL-HIF axis in clear cell renal cell carcinoma. J Pathol 2013;229:525–34.
25. Raval RR, Lau KW, Tran MG, Sowter HM, Mandriota SJ, Li JL, et al. Contrasting properties of hypoxia-inducible factor 1 (HIF-1) and HIF-2 in von Hippel-Lindau-associated renal cell carcinoma. Mol Cell Biol 2005;25:5675–86.
26. Metzen E, Stiehl DP, Doege K, Marxsen JH, Hellwig-Burgel T, Jelkmann W. Regulation of the prolyl hydroxylase domain protein 2 (phd2/egln-1) gene: identification of a functional hypoxia-responsive element. Biochem J 2005;387:711–7.
27. Shen C, Beroukhim R, Schumacher SE, Zhou J, Chang M, Signoretti S, et al. Genetic and functional studies implicate HIF1alpha as a 14q kidney cancer suppressor gene. Cancer Discov 2011;1:222–35.
28. Wischhusen J, Jung G, Radovanovic I, Beier C, Steinbach JP, Rimner A, et al. Identification of CD70-mediated apoptosis of immune effector cells as a novel immune escape pathway of human glioblastoma. Cancer Res 2002;62:2592–9.
29. Hintzen RQ, de Jong R, Hack CE, Chamuleau M, de Vries EF, tenBerge IJ, et al. A soluble form of the human T cell differentiation antigen CD27 is released after triggering of the TCR/CD3 complex. J Immunol 1991;147: 29–35.
30. Loenen WA, De Vries E, Gravestein LA, Hintzen RQ, Van Lier RA, Borst J. The CD27 membrane receptor, a lymphocyte-specific member of the nerve growth factor receptor family, gives rise to a soluble form by protein processing that does not involve receptor endocytosis. Eur J Immunol 1992;22:447–55.
31. Herman JG, Latif F, Weng Y, Lerman MI, Zbar B, Liu S, et al. Silencing of the VHL tumor-suppressor gene by DNA methylation in renal carcinoma. Proc Natl Acad Sci U S A 1994;91:9700–4.
32. Schodel J, Oikonomopoulos S, Ragoussis J, Pugh CW, Ratcliffe PJ, Mole DR. High-resolution genome-wide mapping of HIF-binding sites by ChIP-seq. Blood 2011;117:e207–17.
33. Yu SE, Park SH, Jang YK. Epigenetic silencing of TNFSF7 (CD70) by DNA methylation during progression to breast cancer. Mol Cells 2010;29: 217–21.
34. Wouters BG, Koritzinsky M. Hypoxia signalling through mTOR and the unfolded protein response in cancer. Nat Rev Cancer 2008;8:851–64.
35. Hedrich CM, Rauen T. Epigenetic patterns in systemic sclerosis and their contribution to attenuated CD70 signaling cascades. Clin Immunol 2012;143:1–3.
36. Zhao M, Sun Y, Gao F, Wu X, Tang J, Yin H, et al. Epigenetics and SLE: RFX1 downregulation causes CD11a and CD70 overexpression by altering epigenetic modifications in lupus $CD4^+$ T cells. J Autoimmun 2010;35: 58–69.
37. Fu L, Wang G, Shevchuk MM, Nanus DM, Gudas LJ. Generation of a mouse model of Von Hippel-Lindau kidney disease leading to renal cancers by expression of a constitutively active mutant of HIF1alpha. Cancer Res 2011;71:6848–56.
38. Fu L, Wang G, Shevchuk MM, Nanus DM, Gudas LJ. Activation of HIF2alpha in kidney proximal tubule cells causes abnormal glycogen deposition but not tumorigenesis. Cancer Res 2013;73:2916–25.
39. Gordan JD, Lal P, Dondeti VR, Letrero R, Parekh KN, Oquendo CE, et al. HIF-alpha effects on c-Myc distinguish two subtypes of sporadic VHL-deficient clear cell renal carcinoma. Cancer Cell 2008;14:435–46.
40. Nilsson A, de Milito A, Mowafi F, Winberg G, Bjork O, Wolpert EZ, et al. Expression of CD27-CD70 on early B cell progenitors in the bone marrow: implication for diagnosis and therapy of childhood ALL. Exp Hematol 2005;33:1500–7.
41. Yoshino K, Kishibe K, Nagato T, Ueda S, Komabayashi Y, Takahara M, et al. Expression of CD70 in nasal natural killer/T cell lymphoma cell lines and patients; its role for cell proliferation through binding to soluble CD27. Br J Haematol 2013;160:331–42.
42. Huang J, Jochems C, Anderson AM, Talaie T, Jales A, Madan RA, et al. Soluble CD27-pool in humans may contribute to T cell activation and tumor immunity. J Immunol 2013;190:6250–8.
43. Chahlavi A, Rayman P, Richmond AL, Biswas K, Zhang R, Vogelbaum M, et al. Glioblastomas induce T-lymphocyte death by two distinct pathways involving gangliosides and CD70. Cancer Res 2005;65:5428–38.
44. Aulwurm S, Wischhusen J, Friese M, Borst J, Weller M. Immune stimulatory effects of CD70 override CD70-mediated immune cell apoptosis in rodent glioma models and confer long-lasting antiglioma immunity *in vivo*. Int J Cancer 2006;118:1728–35.
45. Tesselaar K, Arens R, van Schijndel GM, Baars PA, van der Valk MA, Borst J, et al. Lethal T cell immunodeficiency induced by chronic costimulation via CD27-CD70 interactions. Nat Immunol 2003;4:49–54.
46. Thomas LJ, He LZ, Marsh H, Keler T. Targeting human CD27 with an agonist antibody stimulates T-cell activation and antitumor immunity. Oncoimmunology 2014;3:e27255.
47. Conti A, Santoni M, Amantini C, Burattini L, Berardi R, Santoni G, et al. Progress of Molecular Targeted Therapies for Advanced Renal Cell Carcinoma. Biomed Res Int 2013;2013:419176.
48. Jeffrey SC, Burke PJ, Lyon RP, Meyer DW, Sussman D, Anderson M, et al. A potent anti-CD70 antibody-drug conjugate combining a dimeric pyrrolobenzodiazepine drug with site-specific conjugation technology. Bioconjug Chem 2013;24:1256–63.
49. Keller AM, Schildknecht A, Xiao Y, van den Broek M, Borst J. Expression of costimulatory ligand CD70 on steady-state dendritic cells breaks $CD8^+$ T cell tolerance and permits effective immunity. Immunity 2008;29:934–46.
50. Schildknecht A, Miescher I, Yagita H, van den Broek M. Priming of $CD8^+$ T cell responses by pathogens typically depends on CD70-mediated interactions with dendritic cells. Eur J Immunol 2007;37:716–28.

**Journal of Pathology**
*J Pathol* 2013; **229:** 525–534
Published online 21 January 2013 in Wiley Online Library (wileyonlinelibrary.com) DOI: 10.1002/path.4107

**ORIGINAL PAPER**

# The protein tyrosine phosphatase receptor type J is regulated by the pVHL–HIF axis in clear cell renal cell carcinoma

Silvia Casagrande,[1] Melanie Ruf,[1] Markus Rechsteiner,[1] Laura Morra,[1] Sonja Brun-Schmid,[1] Adriana von Teichman,[1] Wilhelm Krek,[2] Peter Schraml[1†*] and Holger Moch[1†]

[1] *Institute of Surgical Pathology, University Hospital Zurich, Schmelzbergstrasse 12, 8091, Zurich, Switzerland*
[2] *Institute of Molecular Health Sciences, Swiss Federal Institute of Technology (ETH) Zurich, 8093, Zurich, Switzerland*

**Correspondence to: Peter Schraml, PhD, Institute of Surgical Pathology, University Hospital Zurich, Schmelzbergstrasse 12, 8091 Zurich, Switzerland. e-mail: Peter.Schraml@usz.ch*

†These authors shared last co-authorship.

## Abstract

**Mass spectrometry analysis of renal cancer cell lines recently suggested that the protein-tyrosine phosphatase receptor type J (PTPRJ), an important regulator of tyrosine kinase receptors, is tightly linked to the von Hippel–Lindau protein (pVHL). Therefore, we aimed to characterize the biological relevance of PTPRJ for clear cell renal cell carcinoma (ccRCC). In pVHL-negative ccRCC cell lines, both RNA and protein expression levels of PTPRJ were lower than those in the corresponding pVHL reconstituted cells. Quantitative RT-PCR and western blot analysis of ccRCC with known *VHL* mutation status and normal matched tissues as well as RNA *in situ* hybridization on a tissue microarray (TMA) confirmed a decrease of *PTPRJ* expression in more than 80% of ccRCCs, but in only 12% of papillary RCCs. ccRCC patients with no or reduced *PTPRJ* mRNA expression had a less favourable outcome than those with a normal expression status ($p = 0.05$). Sequence analysis of 32 *PTPRJ* mRNA-negative ccRCC samples showed five known polymorphisms but no mutations, implying other mechanisms leading to PTPRJ's down-regulation. Selective silencing of HIF-α by siRNA and reporter gene assays demonstrated that pVHL inactivation reduces *PTPRJ* expression through a HIF-dependent mechanism, which is mainly driven by HIF-2α stabilization. Our results suggest *PTPRJ* as a member of a pVHL-controlled pathway whose suppression by HIF is critical for ccRCC development.**



**Keywords:** RCC; VHL/HIF pathway; PTPRJ

Received 20 June 2012; Revised 20 August 2012; Accepted 12 September 2012

*No conflicts of interest were declared.*

## Introduction

Most clear cell renal cell carcinomas (ccRCCs) are characterized by a bi-allelic somatic inactivation of the von Hippel–Lindau (*VHL*) tumour suppressor gene [1]. The VHL protein (pVHL) is an important regulator of the hypoxia inducible factor-α (HIF-α), microtubule stabilization, maintenance of the primary cilium, mitotic regulation, and cell mobility [2]. Loss of function of pVHL leads to HIF-α stabilization and up-regulation of HIF target genes which are involved in cell growth and proliferation, angiogenesis, invasion, and metastasis. Examples of up-regulated HIF-target genes are *VEGF-A*, *EPO*, *EGFR*, and *CAIX* [3], which also represent potential anti-cancer drug targets. Data about genes and proteins down-regulated due to pVHL functional deficiency are rare. Examples include important genes/proteins such as fibronectin [4], E-cadherin [5], PAX2 [6], and p53 [7].

Recent mass spectrometry experiments with ccRCC cell lines [8] showed that the expression of the protein tyrosine phosphatase receptor type J (PTPRJ) is associated with the presence of pVHL. PTPRJ is composed of an extracellular domain that contains eight fibronectin type III repeats, a transmembrane domain, and a cytoplasmic end comprising a single catalytic domain [9]. *In vitro*, the receptor is involved in the regulation of cellular differentiation, proliferation, growth, and migration [10–14], which supports its potential relevance for cancer development. In colon, lung, and breast cancer, *PTPRJ* is affected by allelic imbalances and missense mutations [15,16]. Furthermore, several membrane-associated tyrosine kinase receptors are controlled by PTPRJ; among them there are established or potential molecular anti-cancer drug targets, eg EGFR [17], PDGFR-β [18], VEGFR2 [19], and HGFR (also termed c-MET) [20].

To date, the molecular mechanisms leading to down-regulation of *PTPRJ* expression in ccRCC are

unknown. Consequently, here we have investigated the influence of the pVHL–HIF axis on *PTPRJ* expression in human ccRCC.

## Materials and methods

### Tissue specimens and tissue microarray

For quantitative RT-PCR analysis of *PTPRJ* mRNA levels, frozen tissue samples of 17 ccRCCs and matched non-tumorous tissue were used. The pathological parameters of the ccRCCs are presented together with the *VHL* mutations in Supplementary Table 1. A previously described tissue microarray (TMA) was used [21] to determine *PTPRJ* mRNA expression in ccRCCs, pRCCs, and normal kidney samples. This study was approved by the Local Ethics Commission (reference number StV. 38-2005). All tissue specimens were supplied by the Tissue Biobank of the University Hospital Zurich.

### mRNA quantification

Quantitative analysis of *PTPRJ* mRNA expression was performed by qRT-PCR using 17 ccRCCs with known *VHL* mutation status. Normal matched tissue was available for each tumour and used as a control. Total RNA was isolated using the RNeasy Mini Kit (Qiagen, Hilden, Germany) and quantified using the Nanodrop spectrometer. Total RNA (0.2–1 μg) was reverse-transcribed using the High Capacity cDNA Reverse Transcription Kit (Applied Biosystems, Foster City, CA, USA). The expression of the mRNAs of *PTPRJ*, *HIF-1*α, *HIF-2*α, and *GLUT-1* was quantified using the following TaqMan gene expression assays: Hs00174561_m1 (*PTPRJ*), Hs00936376_m1 (*HIF-1*α), Hs01026146_m1 (*HIF-2*α), and Hs00197884_m1 (*GLUT-1*). The expression assays were designed by Applied Biosystems and analysed using the 7900 Fast Real-Time PCR System (Applied Biosystems). The data were quantified with the comparative $C_t$ method for relative gene expression and normalized using *PPIA* (expression assay Hs99999904_m1) [22].

### RNA *in situ* hybridization (RISH)

*PTPRJ* mRNA expression was analysed on a TMA by non-radioactive *in situ* hybridization adapted from a previously published protocol [23]. Briefly, total mRNA was extracted from HeLa cells and the following primers containing the T7 polymerase binding site (5'-TAATACGACTCACTATAGGGAGAG-3') were chosen to amplify two parts of the *PTPRJ* mRNA: 5'-GTGAAAGCTCTGGAGCCAAC-3' and 5'-ACTCCTCATGGCTTCCAATG-3' spanning exons 3–5 and 5'-GAGATCGGCTTAGCATGGAG-3' and 5'-TATAAGGTGCCCGGAATCAG-3' spanning exons 8 and 9. Digoxigenin (DIG)-labelled antisense and sense riboprobes were transcribed *in vitro* with T7 RNA polymerase in the presence of digoxigenin-UTP (Roche Diagnostics, Rotkreuz, Switzerland). For the hybridization procedure, 1–2 μl of DIG-labelled sense and antisense probes (about 100–200 ng) was added to the hybridization mix and denatured at 85°C for 5 min. Two-micrometre-thick TMA sections were incubated at 60°C overnight. Detection of probe-target hybrids was performed with NBT/BCIP substrate (Roche Applied Science). The intensity of the staining for *PTPRJ* mRNA expression was classified as follows: 0 = negative staining; + = 1 reduced staining; and +2 = strong staining. The intensity of staining detected in normal proximal tubules was considered as a reference for strong staining.

### Mutation analysis of *PTPRJ* and *VHL*

For the mutation analysis of *PTPRJ*, genomic DNA was extracted from 32 formalin-fixed and paraffin-embedded ccRCCs which were also on the large TMA. Five normal matched tissues were included in the analysis. The mutation analysis of *PTPRJ* and *VHL* was performed as previously described [16,24]. Mutations were confirmed with at least one separate PCR and sequence analysis.

### Cell lines

The ccRCC cell lines 786-O and RCC4 (transfected with empty vector), 786-O VHL and RCC4 VHL (stably expressing pVHL), RCC4 Y98H and RCC4 Y98N (stably expressing the type 2A and type 2B pVHL mutants Y98H and Y98N, respectively) and the human renal proximal tubular epithelial cell line HK2 were used in this study. All cell lines were grown under conditions recommended by ATCC and authenticated by short tandem repeat profiling by Identicell (Department of Molecular Medicine, Aarhus University, Hospital Skejby, Aarhus, Denmark).

### Western blotting and antibodies

Total cell lysates were prepared with RIPA buffer (Sigma-Aldrich Corp, St Louis, MO, USA) supplemented with protease inhibitors (Complete Protease Inhibitor Cocktail; Roche, Basel, Switzerland). For cell and tissue fractioning, a Nuclear Extraction Kit (Active Motif, Carlsbad, CA, USA) and the TissueLyser (Qiagen, Hilden, Germany) were used, respectively. Western blot was performed as previously described [6]. The primary antibodies used were anti-pVHL (diluted 1 : 500; provided by Wilhelm Krek, ETH Zurich, Switzerland), anti-HIF-1α (1 : 1000; Cell Signalling, Danvers, MA, USA), anti-HIF-2α (1 : 200; NB 100-122; Novus Biologicals, Littleton, CO, USA), anti-β-actin (1 : 1000; Chemicon International, Temecula, CA, USA); anti-PTPRJ (cell line extracts) (1 : 200; H300 sc-22749; Santa Cruz Biotechnology, Santa Cruz, CA, USA), and anti-PTPRJ (cell line and tissue extracts) (1 : 500; Proteintech, Chicago, IL, USA). Secondary antibodies were HRP-conjugated anti-mouse (1 : 2000; ab672;

Abcam Plc, Cambridge, UK) and HRP-conjugated anti-rabbit (1 : 2000; Millipore, Billerica, MA, USA). The protein–antibody complexes were detected by using ECL (Amersham, Little Chalfont, Buckinghamshire, UK). Band intensities of PTPRJ and β-actin from western blots were measured using ImageJ software.

### Transient transfections

For RNA interference experiments, RCC4, 786-O, and HK2 cells were transfected with 5 nM siRNA oligonucleotides using HiPerfect transfection reagent (Qiagen). The siRNA sequences (Qiagen; Life Technologies, Carlsbad, CA, USA) are listed in Supplementary Table 2. AllStars negative controls (Qiagen) were used as negative controls. To study the effects of *PTPRJ* overexpression in RCC4 cells, the pQE-TriSystem-6 vector (Qiagen) containing the ORF of the *PTPRJ* gene (Entrez Gene: 5795; Ensembl: ENSG00000149177; UniProtKB: Q12913) was used. The pQE-TriSystem-6 served as a control (empty vector). Cells were grown for 24 h in a six-well format and then transiently transfected with the expression vector. Cells were harvested after 96 h to evaluate PTPRJ expression levels by qRT-PCR and western blot.

### Luciferase gene reporter assay

Luciferase gene expression assays were performed as previously described [6]. The nucleotides between −2682 and +515 were defined as the putative promoter region of *PTPRJ* (Chr 11p11.2; 47,971,665:48,222,839, positive strand, NCBI) considering the A(TG) translation site as +1 reference. The promoter region was synthesized from GenScript (Piscataway, NJ, USA) and cloned into firefly luciferase reporter plasmid pGL4.10 (Promega, Madison, WI, USA). pGL4.10P2P vector containing wild-type *P2P* hypoxia response elements (HREs) of the human *PHD2* promoter were provided by Roland Wenger (University of Zurich, Switzerland) and was used as a positive control as previously described [6,25].

For transcriptional transactivation experiments, 786-O cells were transfected with siRNA (HIF-2α #1 or siScr) and grown in a 24-well format. After 48 h, the cells were transfected with 1 μg of luciferase reporter plasmid and 200 ng of pGL4.74 renilla luciferase reporter plasmid (Promega) using FuGene 6 reagent (Roche Diagnostics). Luciferase activity was measured 24 h later after cell lysis using the Dual-Luciferase Reporter Assay System (Promega). Relative luciferase units were determined according to the manufacturer's instructions (Promega) to generate the ratio of the values obtained from siHIF-2α and siSc treatments.

### MTT proliferation assay

RCC4 cells were grown in a six-well format for 24 h and transfected with the expression or control vector. MTT proliferation assay (Cell Proliferation Kit I MTT, Roche Diagnostics) was performed according to the manufacturer's protocol. Briefly, transfected cells were plated in a 96-well plate. After the incubation period, 10 μl of the MTT labelling reagent (final concentration 0.5 mg/ml) was added to each well and cells were incubated for 4 h. Subsequently, 100 μl of the solubilization solution was added to the wells and cells were incubated overnight at 37°C. The solubilized formazan product was quantified using an ELISA reader (Infinite F200 PRO, Tecan Group Ltd., Männedorf, Switzerland) at wavelength 570 nm. The analysis of cell proliferation was performed after 96, 120, 144, and 168 h.

### Statistical analysis

Analysis between groups was carried out with two-way ANOVA and *post-hoc* Bonferroni multiple comparison (GraphPad Prism 5). Contingency table analysis and Pearson's chi-squared tests were calculated using the SPSS 17.0 statistical software package. Survival curves were estimated with the Kaplan–Meier method and the log-rank test. $p$ values $\leq 0.05$ were considered statistically significant.

## Results

### Direct correlation of PTPRJ and pVHL expression in RCC cell lines

Previous mass spectrometry experiments performed with pVHL-deficient and pVHL-re-expressing RCC cell lines identified PTPRJ positively linked to pVHL expression [8]. To confirm that *PTPRJ* is influenced by the VHL–HIF axis, we used the pVHL-deficient renal cancer cell lines 786-O and RCC4 and their corresponding stable pVHL transfectants. Compared with the corresponding pVHL-negative cell lines, both *PTPRJ* mRNA (Figure 1A) and protein levels (Figures 1B and 1C) were increased in the presence of pVHL.

### *PTPRJ* mRNA expression is decreased in ccRCC tissue

To quantitatively evaluate *PTPRJ* mRNA expression in human RCC samples, we performed qRT-PCR with 17 ccRCCs and normal matched tissues. *PTPRJ* expression was reduced in 15 of 17 ccRCCs (88%) (Figure 1D) compared with normal renal tissues. Strong *PTPRJ* expression was seen in one *VHL* wild-type tumour and in one ccRCC with a missense mutation that causes an amino acid exchange at codon 88 (Figure 1D and Supplementary Table 1). Western blot analysis with three matched normal/tumour pairs demonstrated a direct correlation between mRNA and protein expression of PTPRJ (Figure 1E).

As commercially available PTPRJ antibodies were not specific in formalin-fixed and paraffin-embedded tissues, the expression of *PTPRJ* was analysed by

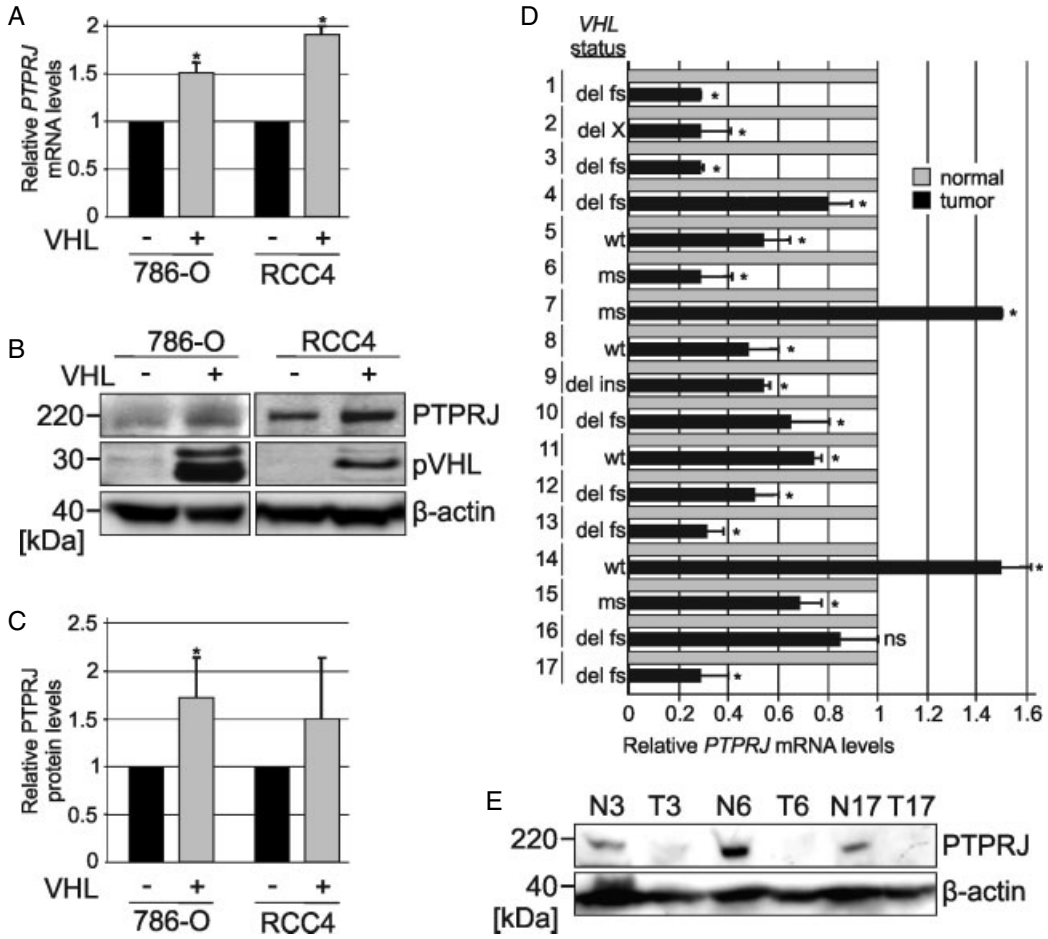


**Figure 1.** Positive correlation between PTPRJ and pVHL expression. (A) *PTPRJ* mRNA levels measured by qRT-PCR (three replicas ± SD) in pVHL-negative RCC cell lines and their stable *VHL* transfectants (increase 1.5- to 1.9-fold). (B) Western blot showing PTPRJ protein expression in pVHL-negative ccRCC cells and their stable *VHL* transfectants (loading control: β-actin). (C) Elevated PTPRJ expression in pVHL expressing 786-O (normalized mean 1.73 ± 0.42 SD, $n = 5$, $p = 0.026$) and RCC4 cells (1.51 ± 0.64, $n = 4$, $p$ = ns.). (D) Normalized *PTPRJ* mRNA levels measured by qRT-PCR in 17 ccRCCs and their normal matched tissues (three replicas ± SD). The *VHL* mutation status in the tumours is indicated (wt = wild type; ms = missense; del fs = deletion leading to frameshift; del ins = deletion and insertion; del X = deletion leading to a stop codon). (E) Western blot showing PTPRJ protein expression in three ccRCC tissues and matched normal tissues (loading control: β-actin). Significant differences ($p < 0.05$) are indicated by asterisks.

RNA *in situ* hybridization (RISH). The specificity of DIG-labelled RNA probes for *PTPRJ* was confirmed by northern blot analysis using total RNA from HeLa cells (positive control). The antisense probes bound a 7.8 kb band corresponding to the *PTPRJ* transcript (data not shown).

*PTPRJ* RISH analysis on a TMA showed strong positivity in the proximal tubular cells of all analysed normal kidney tissue samples (Figure 2), whereas in 198 of 232 (85%) analysable ccRCCs, but in only 5 of 41 (12%) pRCCs, *PTPRJ* expression was reduced ($p < 0.001$). ccRCC patients with no or low *PTPRJ* mRNA expression showed a worse prognosis than those with a normal expression status ($p = 0.05$) (Figure 3). No associations were seen between *PTPRJ* expression and tumour stage and grade. The highly significant difference between the survival curves of patients with organ-confined and locally advanced tumours confirmed the validity of the clinical data (Supplementary Figure 2).

## Mutation analysis of *PTPRJ* in ccRCC

Twenty-two *PTPRJ*-negative and ten weakly expressing ccRCC samples included in the TMA were selected for mutation analysis of exons 5, 6, 7, and 13 of *PTPRJ*. So far, all cancer-related amino acid substitutions have been identified in these four exons, which code the extracellular portion responsible for interactions with ligands or other proteins [16]. Five normal matched tissues were also included in this analysis. We found two conservative (E206E and T233T) and three non-conservative (Q276P, R326Q, and E872D) polymorphisms which have been previously reported [UniprotKB/Swiss-Prot, Q12913 (PTPRJ_HUMAN)]. There were no mutations affecting the reading frame of *PTPRJ*.

## *PTPRJ* expression is HIF-2α-dependent

To determine the influence of the pVHL–HIF axis on *PTPRJ* expression, we used different pVHL-expressing and non-expressing RCC cell lines. In

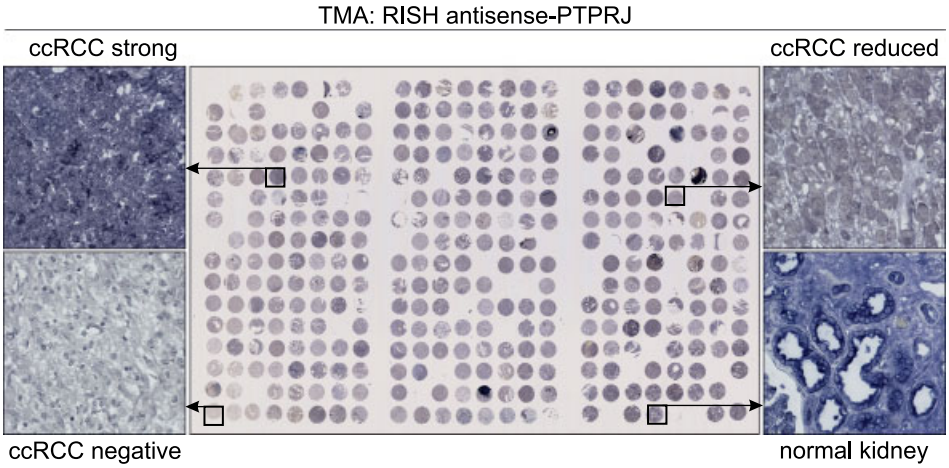


Figure 2. *PTPRJ* RISH on a TMA with examples of negative, reduced, and strong *PTPRJ* mRNA expression in ccRCC and normal kidney.

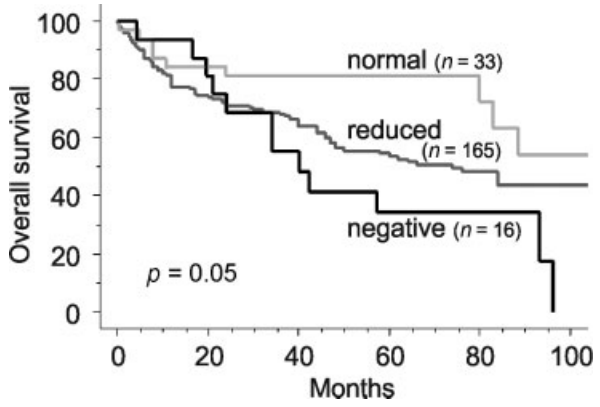


Figure 3. Kaplan–Meier plot of the overall survival of ccRCC patients defined by *PTPRJ* mRNA expression. Survival data were not available from 18 patients. *PTPRJ* expression was defined as reduced if the mRNA staining in a tumour was unequivocally weaker than that seen in normal kidney.

RCC4 cells expressing the pVHL mutant Y98N, which fail to degrade HIF-α [26], *PTPRJ* mRNA expression was comparable to pVHL-deficient RCC4. In contrast, in RCC4 cells expressing the pVHL mutant Y98H, which has only a slight defect in ubiquitination of HIF-α [26], the *PTPRJ* mRNA level was increased and similar to the RCC4 VHL cell line (Figure 4A). An opposite effect was observed with *GLUT1* mRNA, whose expression increased in the presence of HIF-α (Figure 4B).

Next, we silenced *HIF-1*α and *HIF-2*α by siRNA in the pVHL-deficient RCC4 cell line to determine whether the two HIF-α isoforms were able to down-regulate *PTPRJ* mRNA expression. Efficient knockdown of HIF-1α and HIF-2α was confirmed by qRT-PCR and western blot analysis (Figures 4C–4G). In RCC4, silencing of *HIF-1*α had positive effects on *PTPRJ* mRNA expression after 48 h (Figure 5A). In contrast, silencing of *HIF-2*α produced an increase of *PTPRJ* mRNA expression after just 24 h and reached a two-fold up-regulation after 48 h (Figure 5B). We also silenced *HIF-2*α by siRNA in the pVHL and HIF-1α-null 786-O cell line. After 48 h, we obtained an increase of *PTPRJ* mRNA expression which was comparable to that observed in 786-O VHL (Figure 5D). Efficient knockdown of *HIF-2*α was confirmed by analysing the level of *GLUT-1* mRNA (Figure 5F). Western blot analysis confirmed a strong increase of PTPRJ protein expression in both HIF-2α silenced ccRCC cell lines (Figures 5C and 5E). Similar results were obtained with two additional HIF-2α siRNAs excluding possible off target effects (Supplementary Figures 1A–1C).

## Hypoxia response elements in the promoter region influence *PTPRJ* expression

The putative promoter region of *PTPRJ* contains five HREs and three reverse HREs (Supplementary Table 3 and Figure 6A). To study the influence of the HREs on *PTPRJ* expression, a luciferase reporter plasmid pGL4.10 construct containing 3.2 kb of the *PTPRJ* promoter was generated (Figure 6A). By silencing *HIF-2*α in 786-O cells (Figure 6B), the reporter activity of the vector increased significantly compared with those of the empty plasmid and the *P2P* promoter construct (Figure 6C). These results show that HIF-2α negatively regulates *PTPRJ* via the identified putative HREs in its promoter region.

## PTPRJ regulates cell proliferation

RCC4 cells transfected with the Qiagen expression vector pQE-TriSystem 6 containing the *PTPRJ* gene showed increased mRNA and protein expression of PTPRJ (Figure 6D and 6E). RCC4 cells transfected with the *PTPRJ* vector showed a significantly reduced proliferation rate compared with the control group (Figure 6F).

We also silenced *PTPRJ* by siRNA in wild-type pVHL expressing HK2 to see if PTPRJ down-regulation leads to increased cell proliferation in the presence of pVHL. Reduced expression negatively influenced cell proliferation after 72 h (Supplementary

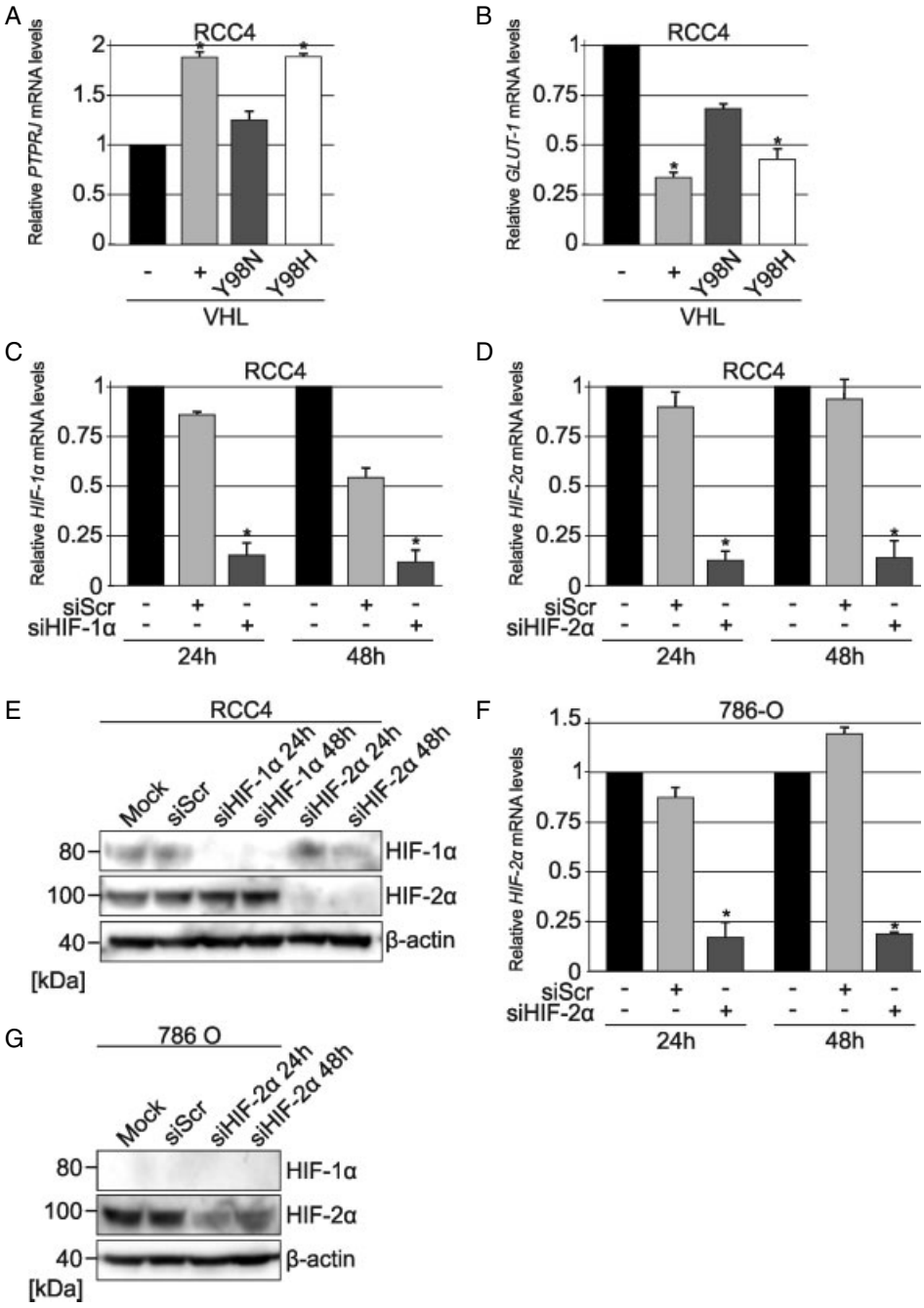


**Figure 4.** (A) *PTPRJ* mRNA transcription in RCC4 VHL, RCC4 Y98H (HIF-α destabilizing *VHL* mutation), and RCC4 Y98N (HIF-α non-destabilizing *VHL* mutation) cells. (B) *GLUT-1* mRNA expression in the same RCC4 cells. (C, D) Knockdown efficiency of siHIF-1α and siHIF-2α on *HIF-1α* (C) and *HIF-2α* (D) mRNA expression after 24 and 48 h in RCC4 cells. (E) Western blot showing down-regulated HIF-1α and HIF-2α protein expression in RCC4 cells. (F) *HIF-2α* mRNA expression in siHIF-2α transfected 786-O cells after 24 and 48 h. (G) Western blot showing down-regulated HIF-2α protein expression (loading control: β-actin). Significant differences ($p < 0.05$) of *PTPRJ*, *GLUT-1*, *HIF-1α*, and *HIF-2α* expression compared with wild-type cell lines are indicated by asterisks.

Figures 3A and 3B) and suggests that loss of PTPRJ is biologically relevant to promote growth of ccRCC, independently of the pVHL expression status.

## Discussion

We have demonstrated that decreased *PTPRJ* expression is characteristic for the vast majority of ccRCCs. *In vitro* experiments showed that higher *PTPRJ* mRNA and protein expression levels are closely linked to the presence of functional pVHL. Down-regulation of *PTPRJ* is mainly dependent on HIF-2α stabilization following pVHL loss.

Our TMA analysis showed no or low *PTPRJ* mRNA expression in 85% of ccRCCs, whereas in most of the pRCCs, *PTPRJ* mRNA levels were comparable to those in normal tissues. The fact that *VHL* is mutationally affected in about 70–80% of ccRCCs [1,27,28] suggests a close relationship between *PTPRJ* mRNA

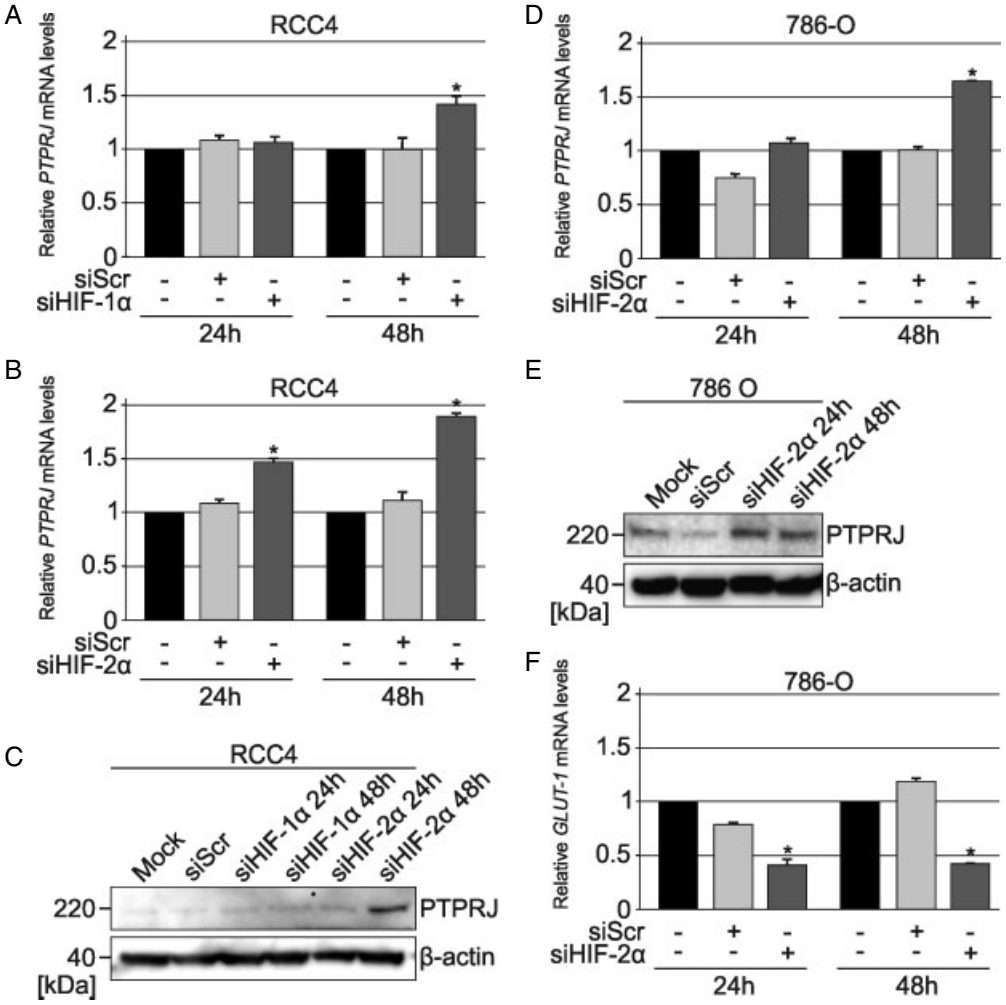


**Figure 5.** PTPRJ expression depends mainly on HIF-2α. (A) Increase of *PTPRJ* mRNA expression in RCC4 cells after silencing of HIF-1α and (B) after silencing of HIF-2α. (C) Western blot showing PTPRJ protein expression in RCC4 cells after silencing of HIF-1α and HIF-2α. (D) Increase of *PTPRJ* mRNA levels in 786-O cells after silencing of HIF-2α. (E) PTPRJ protein expression after silencing of HIF-2α. (F) *GLUT-1* mRNA expression in HIF-2α silenced 786-O cells. Data represent the mean of two experiments carried out in triplicate ± SD. Significant differences ($p < 0.05$) of *PTPRJ* and *GLUT-1* expression compared with wild-type cell lines are indicated by asterisks.

expression and pVHL functional integrity. This is supported by the observation that *PTPRJ* expression was normal in almost 90% of the analysed pRCCs in which *VHL* is hardly mutated [29]. This result confirms our recent proteomics finding of a relationship between *PTPRJ* expression and pVHL in human tissue [8]. In our test set of 17 ccRCCs, reduced *PTPRJ* mRNA expression was also seen in two of four tumours with wild-type *VHL*. Other mechanisms of *VHL* inactivation, such as tumour hypoxia or hypermethylation of the *VHL* promoter, which occurs in about half of *VHL* wild-type ccRCCs [1,28,30], may explain this observation.

Here, we identified *PTPRJ* as a potential target of HIF-2α. HIF-1α and HIF-2α share high similarity in their DNA binding and dimerization domains, but they differ in their transactivation domains [31]. As a consequence, there are common gene targets, but also genes that are preferentially regulated by one of the two isoforms. HIF-1α seems to preferentially drive the transcription of genes encoding glycolytic enzymes and pro-apoptotic factors, such as BCL2/adenovirus E1B-interacting protein 1, NIP3 (BNIP3). In contrast, HIF-2α induces the expression of pro-survival factors such as VEGF, TGF-α, and CCND1 [32]. Studies demonstrated that HIF-α can also down-regulate genes either by inducing repressors of transcription or by directly binding to HREs and to reverse HREs. The latter are present in the antisense strand of the promoter of HIF target genes. Examples of genes directly down-regulated by HIF-1α are *AFP* [33], *PPARA* [34], and *RECK* [35], whereas genes directly or indirectly down-regulated by HIF-2α have not been described to date.

The analysis of the putative *PTPRJ* promoter showed the presence of five putative HREs and three putative reverse HREs. Since we observed *PTPRJ* down-regulation in the presence of HIF-2α, we asked whether HIF could directly act as a suppressor of *PTPRJ* transcription. Using 786-O cells, significant effects were seen with our luciferase gene reporter assays, suggesting that the HREs and reverse HREs identified in the putative *PTPRJ* promoter region

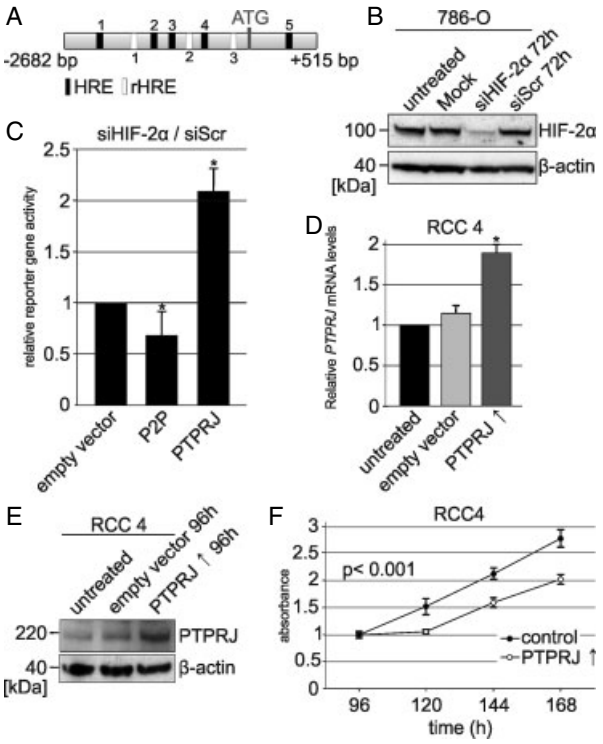


Figure 6. *PTPRJ* promoter activity is HIF-2α-dependent. (A) Schematic representation of the 3.2 kb *PTPRJ* promoter with the location of the five HREs and three reverse HREs. (B) Western blot showing efficient knockdown of *HIF*-2α in 786-O cells after 72 h (loading control: β-actin). (C) Luciferase reporter gene assay with *P2P* (HIF target) and *PTPRJ* vector constructs after transient transfection of siScrambled and siHIF-2α using 786-O cells. Decrease of *P2P* and increase of *PTPRJ* promoter activity after *HIF*-2α silencing. (D) *PTPRJ* mRNA levels measured by qRT-PCR in RCC4 cells untreated, transfected with scrambled control, and with *PTPRJ* expression vector 96 h after transfection. Data represent the mean of three replicas ± SD. (E) Immunoblot of PTPRJ expression in RCC4 cells untreated, transfected with scrambled control, and with *PTPRJ* expression vector 96 h after transfection. RQ = relative quantification. (F) Proliferation of RCC4 cells 96, 120, 144, and 168 h after transfection with empty vector (control) or *PTPRJ* expression vector (PTPRJ).

are important for suppressing *PTPRJ* expression by HIF-2α. It is of note that only two-fold overexpression of *PTPRJ* in RCC4 cells was sufficient to produce a significant inhibitory effect on cell proliferation. Our result expands the findings of previous studies that describe anti-proliferative properties of *PTPRJ* in non-RCC tumour cell lines [10,12,14].

To evaluate the presence of mutations of the *PTPRJ* gene, we performed a sequence analysis of exons 5, 6, 7, and 13 of *PTPRJ* in 32 ccRCCs. We found two conservative and three non-conservative polymorphisms, but no mutation predicting severe consequences on PTPRJ function. Similar frequencies of these polymorphisms were found in studies which analysed the *PTPRJ* genotype in other tumour types and in other populations [36–38]. The real influence of these polymorphisms on *PTPRJ* expression and function is still not fully understood. Our results suggest that in ccRCC the down-regulation of *PTPRJ* expression is obviously

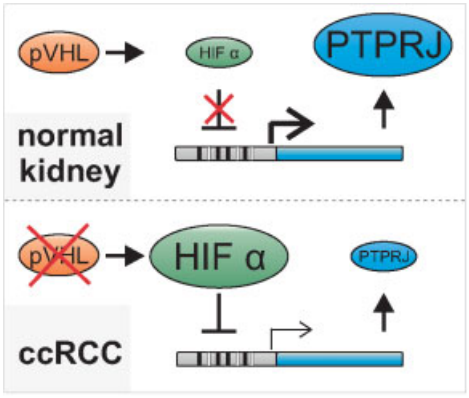


Figure 7. Schematic representation of the HIF-α-dependent regulation of *PTPRJ* expression in normal kidney and ccRCC.

not caused by mutations but is mainly due to the deregulation of the pVHL/HIF pathway (Figure 7).

PTPRJ's inhibitory effect on cell proliferation in ccRCC, as shown by us, and in other tumour types [14,39,40], as well as its ability to regulate EGFR phosphorylation [17], suggests its important influence on the activity of EGFR. Although EGFR overexpression occurs in the majority of ccRCCs and is correlated with rapid tumour cell proliferation and worse patient outcome [41,42], anti-EGFR targeted therapies have shown only low response rates [43,44]. As demonstrated in non-small cell lung cancer, the success of such therapies is obviously dependent on EGFR activating mutations [45], which have not been found in ccRCC [41]. Antibodies against phosphorylated and activated EGFR are available but their use for reliably determining its tyrosine kinase activity status on formalin-fixed, paraffin-embedded tissue in routine diagnostics is challenging [46]. Despite the low number of tumours analysed, our western blot data indicate reduced PTPRJ expression also at the protein level in a subset of ccRCCs. It is conceivable that EGFR-positive tumours with strongly reduced PTPRJ may respond better to inhibitors against EGFR and its downstream targets, such as PI3K, AKT, and mTOR, than those showing normal PTPRJ expression. However, additional experiments using optimized antibodies as well as appropriate mouse models are needed to characterize the biological relevance of PTPRJ down-regulation by the pVHL–HIF axis and its clinical applicability for this tumour subtype.

In summary, we have shown that down-regulation of *PTPRJ* is a characteristic feature in ccRCC that is closely linked to the loss of pVHL function and the activation of HIF. Molecular studies of low abundance genes, such as *PTPRJ*, are a big challenge in cancer research as they are more sophisticated compared to investigations of those genes that become clearly up- or down-regulated in tumours. They are, nevertheless, necessary to better understand the complex genetic network of cancer.

## Acknowledgments

We thank Roger Santimaria and Martina Storz for excellent technical assistance. We thank Claudio Thoma (ETH Zurich, Switzerland) and Rudolf Wüthrich (University Hospital of Zurich, Switzerland) for the cell lines and Daniel Stiehl (University of Zurich, Switzerland) for the luciferase vectors. This study was supported by the Swiss National Science Foundation (3238BO-103145; to HM) and the Zurich Cancer League (to HM).

## Author contribution statement

SC and MRu conceived and carried out experiments and generated the figures. MRe conceived experiments and interpreted data. LM, SB-S, and AvT carried out experiments. WK designed the study. PS and HM designed the study, analysed data, and wrote the manuscript. HM reviewed the tumours. All authors had final approval of the submitted and published versions.

## References

1. Banks RE, Tirukonda P, Taylor C, *et al*. Genetic and epigenetic analysis of von Hippel–Lindau (VHL) gene alterations and relationship with clinical variables in sporadic renal cancer. *Cancer Res* 2006; **66:** 2000–2011.
2. Frew IJ, Krek W. Multitasking by pVHL in tumour suppression. *Curr Opin Cell Biol* 2007; **19:** 685–690.
3. Gossage L, Eisen T. Alterations in VHL as potential biomarkers in renal-cell carcinoma. *Nature Rev Clin Oncol* 2010; **7:** 277–288.
4. Bluyssen HA, Lolkema MP, van Beest M, *et al*. Fibronectin is a hypoxia-independent target of the tumor suppressor VHL. *FEBS Lett* 2004; **556:** 137–142.
5. Esteban MA, Tran MG, Harten SK, *et al*. Regulation of E-cadherin expression by VHL and hypoxia-inducible factor. *Cancer Res* 2006; **66:** 3567–3575.
6. Luu VD, Boysen G, Struckmann K, *et al*. Loss of VHL and hypoxia provokes PAX2 up-regulation in clear cell renal cell carcinoma. *Clin Cancer Res* 2009; **15:** 3297–3304.
7. Roe JS, Kim H, Lee SM, *et al*. p53 stabilization and transactivation by a von Hippel–Lindau protein. *Mol Cell* 2006; **22:** 395–405.
8. Boysen G, Bausch-Fluck D, Thoma CR, *et al*. Identification and functional characterization of pVHL-dependent cell surface proteins in renal cell carcinoma. *Neoplasia* 2012; **14:** 535–546.
9. Honda H, Inazawa J, Nishida J, *et al*. Molecular cloning, characterization, and chromosomal localization of a novel protein-tyrosine phosphatase, HPTP eta. *Blood* 1994; **84:** 4186–4194.
10. Balavenkatraman KK, Jandt E, Friedrich K, *et al*. DEP-1 protein tyrosine phosphatase inhibits proliferation and migration of colon carcinoma cells and is upregulated by protective nutrients. *Oncogene* 2006; **25:** 6319–6324.
11. Jandt E, Denner K, Kovalenko M, *et al*. The protein-tyrosine phosphatase DEP-1 modulates growth factor-stimulated cell migration and cell–matrix adhesion. *Oncogene* 2003; **22:** 4175–4185.
12. Kellie S, Craggs G, Bird IN, *et al*. The tyrosine phosphatase DEP-1 induces cytoskeletal rearrangements, aberrant cell–substratum interactions and a reduction in cell proliferation. *J Cell Sci* 2004; **117:** 609–618.
13. Trapasso F, Iuliano R, Boccia A, *et al*. Rat protein tyrosine phosphatase eta suppresses the neoplastic phenotype of retrovirally transformed thyroid cells through the stabilization of p27(Kip1). *Mol Cell Biol* 2000; **20:** 9236–9246.
14. Trapasso F, Yendamuri S, Dumon KR, *et al*. Restoration of receptor-type protein tyrosine phosphatase eta function inhibits human pancreatic carcinoma cell growth *in vitro* and *in vivo*. *Carcinogenesis* 2004; **25:** 2107–2114.
15. Ruivenkamp C, Hermsen M, Postma C, *et al*. LOH of PTPRJ occurs early in colorectal cancer and is associated with chromosomal loss of 18q12–21. *Oncogene* 2003; **22:** 3472–3474.
16. Ruivenkamp CA, van Wezel T, Zanon C, *et al*. *Ptprj* is a candidate for the mouse colon-cancer susceptibility locus *Scc1* and is frequently deleted in human cancers. *Nature Genet* 2002; **31:** 295–300.
17. Tarcic G, Boguslavsky SK, Wakim J, *et al*. An unbiased screen identifies DEP-1 tumor suppressor as a phosphatase controlling EGFR endocytosis. *Curr Biol* 2009; **19:** 1788–1798.
18. Kovalenko M, Denner K, Sandstrom J, *et al*. Site-selective dephosphorylation of the platelet-derived growth factor beta-receptor by the receptor-like protein-tyrosine phosphatase DEP-1. *J Biol Chem* 2000; **275:** 16219–16226.
19. Grazia Lampugnani M, Zanetti A, Corada M, *et al*. Contact inhibition of VEGF-induced proliferation requires vascular endothelial cadherin, beta-catenin, and the phosphatase DEP-1/CD148. *J Cell Biol* 2003; **161:** 793–804.
20. Palka HL, Park M, Tonks NK. Hepatocyte growth factor receptor tyrosine kinase met is a substrate of the receptor protein-tyrosine phosphatase DEP-1. *J Biol Chem* 2003; **278:** 5728–5735.
21. Mertz KD, Demichelis F, Kim R, *et al*. Automated immunofluorescence analysis defines microvessel area as a prognostic parameter in clear cell renal cell cancer. *Hum Pathol* 2007; **38:** 1454–1462.
22. Jung M, Ramankulov A, Roigas J, *et al*. In search of suitable reference genes for gene expression studies of human renal cell carcinoma by real-time PCR. *BMC Mol Biol* 2007; **8:** 47.
23. Theurillat JP, Zurrer-Hardi U, Varga Z, *et al*. Distinct expression patterns of the immunogenic differentiation antigen NY-BR-1 in normal breast, testis and their malignant counterparts. *Int J Cancer* 2008; **122:** 1585–1591.
24. Schraml P, Frew IJ, Thoma CR, *et al*. Sporadic clear cell renal cell carcinoma but not the papillary type is characterized by severely reduced frequency of primary cilia. *Mod Pathol* 2009; **22:** 31–36.
25. Metzen E, Stiehl DP, Doege K, *et al*. Regulation of the prolyl hydroxylase domain protein 2 (*phd2/egln-1*) gene: identification of a functional hypoxia-responsive element. *Biochem J* 2005; **387:** 711–717.
26. Thoma CR, Frew IJ, Hoerner CR, *et al*. pVHL and GSK3beta are components of a primary cilium-maintenance signalling network. *Nature Cell Biol* 2007; **9:** 588–595.
27. Rechsteiner MP, von Teichman A, Nowicka A, *et al*. *VHL* gene mutations and their effects on hypoxia inducible factor HIFα: identification of potential driver and passenger mutations. *Cancer Res* 2011; **71:** 5500–5511.
28. Nickerson ML, Jaeger E, Shi Y, *et al*. Improved identification of von Hippel–Lindau gene alterations in clear cell renal tumors. *Clin Cancer Res* 2008; **14:** 4726–4734.
29. Brauch H, Weirich G, Brieger J, *et al*. *VHL* alterations in human clear cell renal cell carcinoma: association with advanced tumor stage and a novel hot spot mutation. *Cancer Res* 2000; **60:** 1942–1948.
30. Herman JG, Latif F, Weng Y, *et al*. Silencing of the *VHL* tumor-suppressor gene by DNA methylation in renal carcinoma. *Proc Natl Acad Sci U S A* 1994; **91:** 9700–9704.

31. Hu CJ, Wang LY, Chodosh LA, *et al*. Differential roles of hypoxia-inducible factor 1α (HIF-1α) and HIF-2α in hypoxic gene regulation. *Mol Cell Biol* 2003; **23:** 9361–9374.
32. Raval RR, Lau KW, Tran MG, *et al*. Contrasting properties of hypoxia-inducible factor 1 (HIF-1) and HIF-2 in von Hippel–Lindau-associated renal cell carcinoma. *Mol Cell Biol* 2005; **25:** 5675–5686.
33. Mazure NM, Chauvet C, Bois-Joyeux B, *et al*. Repression of α-fetoprotein gene expression under hypoxic conditions in human hepatoma cells: characterization of a negative hypoxia response element that mediates opposite effects of hypoxia inducible factor-1 and c-Myc. *Cancer Res* 2002; **62:** 1158–1165.
34. Narravula S, Colgan SP. Hypoxia-inducible factor 1-mediated inhibition of peroxisome proliferator-activated receptor alpha expression during hypoxia. *J Immunol* 2001; **166:** 7543–7548.
35. Lee KJ, Lee KY, Lee YM. Downregulation of a tumor suppressor RECK by hypoxia through recruitment of HDAC1 and HIF-1α to reverse HRE site in the promoter. *Biochim Biophys Acta* 2010; **1803:** 608–616.
36. Iuliano R, Le Pera I, Cristofaro C, *et al*. The tyrosine phosphatase PTPRJ/DEP-1 genotype affects thyroid carcinogenesis. *Oncogene* 2004; **23:** 8432–8438.
37. Iuliano R, Palmieri D, He H, *et al*. Role of PTPRJ genotype in papillary thyroid carcinoma risk. *Endocr Relat Cancer* 2010; **17:** 1001–1006.
38. Mita Y, Yasuda Y, Sakai A, *et al*. Missense polymorphisms of *PTPRJ* and *PTPN13* genes affect susceptibility to a variety of human cancers. *J Cancer Res Clin Oncol* 2010; **136:** 249–259.
39. Iuliano R, Trapasso F, Le Pera I, *et al*. An adenovirus carrying the rat protein tyrosine phosphatase eta suppresses the growth of human thyroid carcinoma cell lines *in vitro* and *in vivo*. *Cancer Res* 2003; **63:** 882–886.
40. Keane MM, Lowrey GA, Ettenberg SA, *et al*. The protein tyrosine phosphatase DEP-1 is induced during differentiation and inhibits growth of breast cancer cells. *Cancer Res* 1996; **56:** 4236–4243.
41. Minner S, Rump D, Tennstedt P, *et al*. Epidermal growth factor receptor protein expression and genomic alterations in renal cell carcinoma. *Cancer* 2012; **118:** 1268–1275.
42. Moch H, Sauter G, Buchholz N, *et al*. Epidermal growth factor receptor expression is associated with rapid tumor cell proliferation in renal cell carcinoma. *Hum Pathol* 1997; **28:** 1255–1259.
43. Drucker B, Bacik J, Ginsberg M, *et al*. Phase II trial of ZD1839 (IRESSA) in patients with advanced renal cell carcinoma. *Invest New Drugs* 2003; **21:** 341–345.
44. Rowinsky EK, Schwartz GH, Gollob JA, *et al*. Safety, pharmacokinetics, and activity of ABX-EGF, a fully human anti-epidermal growth factor receptor monoclonal antibody in patients with metastatic renal cell cancer. *J Clin Oncol* 2004; **22:** 3003–3015.
45. Lynch TJ, Bell DW, Sordella R, *et al*. Activating mutations in the epidermal growth factor receptor underlying responsiveness of non-small-cell lung cancer to gefitinib. *N Engl J Med* 2004; **350:** 2129–2139.
46. Becker KF, Mack H, Schott C, *et al*. Extraction of phosphorylated proteins from formalin-fixed cancer cells and tissues. *Open Pathol J* 2008; **2:** 46–52.

# 11 References


1. Bedke, J. and A. Stenzl, *[Renal cell carcinoma: recent developments in diagnostics and therapy].* Urologe A, 2010. **49 Suppl 1**: p. 178-84.

2. Jemal, A., et al., *Global cancer statistics.* CA Cancer J Clin, 2011. **61**(2): p. 69-90.

3. Bhatt, J.R. and A. Finelli, *Landmarks in the diagnosis and treatment of renal cell carcinoma.* Nat Rev Urol, 2014. **11**(9): p. 517-25.

4. Znaor, A., et al., *International Variations and Trends in Renal Cell Carcinoma Incidence and Mortality.* Eur Urol, 2014.

5. Chow, W.H. and S.S. Devesa, *Contemporary epidemiology of renal cell cancer.* Cancer J, 2008. **14**(5): p. 288-301.

6. Jemal, A., et al., *Cancer statistics, 2010.* CA Cancer J Clin, 2010. **60**(5): p. 277-300.

7. Siegel, R., D. Naishadham, and A. Jemal, *Cancer statistics, 2013.* CA Cancer J Clin, 2013. **63**(1): p. 11-30.

8. Levi, F., et al., *The changing pattern of kidney cancer incidence and mortality in Europe.* BJU Int, 2008. **101**(8): p. 949-58.

9. Ferlay, J., et al., *Cancer incidence and mortality worldwide: Sources, methods and major patterns in GLOBOCAN 2012.* Int J Cancer, 2014.

10. Ljungberg, B., et al., *The epidemiology of renal cell carcinoma.* Eur Urol, 2011. **60**(4): p. 615-21.

11. Hunt, J.D., et al., *Renal cell carcinoma in relation to cigarette smoking: meta-analysis of 24 studies.* Int J Cancer, 2005. **114**(1): p. 101-8.

12. Renehan, A.G., et al., *Body-mass index and incidence of cancer: a systematic review and meta-analysis of prospective observational studies.* Lancet, 2008. **371**(9612): p. 569-78.

13. Cancer Genome Atlas Research, N., *Comprehensive molecular characterization of clear cell renal cell carcinoma.* Nature, 2013. **499**(7456): p. 43-9.

14. Lee, J.E., et al., *Intakes of fruit, vegetables, and carotenoids and renal cell cancer risk: a pooled analysis of 13 prospective studies.* Cancer Epidemiol Biomarkers Prev, 2009. **18**(6): p. 1730-9.

15. Gupta, K., et al., *Epidemiologic and socioeconomic burden of metastatic renal cell carcinoma (mRCC): a literature review.* Cancer Treat Rev, 2008. **34**(3): p. 193-205.

16. Athar, U. and T.C. Gentile, *Treatment options for metastatic renal cell carcinoma: a review.* Can J Urol, 2008. **15**(2): p. 3954-66.

17. Lopez-Beltran, A., et al., *2009 update on the classification of renal epithelial tumors in adults.* Int J Urol, 2009. **16**(5): p. 432-43.

18. Algaba, F., et al., *Current pathology keys of renal cell carcinoma.* Eur Urol, 2011. **60**(4): p. 634-43.

19. Cohen, H.T. and F.J. McGovern, *Renal-cell carcinoma.* N Engl J Med, 2005. **353**(23): p. 2477-90.

20. Linehan, W.M., M.M. Walther, and B. Zbar, *The genetic basis of cancer of the kidney.* J Urol, 2003. **170**(6 Pt 1): p. 2163-72.

21. Linehan, W.M., R. Srinivasan, and L.S. Schmidt, *The genetic basis of kidney cancer: a metabolic disease.* Nat Rev Urol, 2010. **7**(5): p. 277-85.

22. Moch, H., *An overview of renal cell cancer: pathology and genetics.* Semin Cancer Biol, 2013. **23**(1): p. 3-9.

23. Eble J, S.G., Epstein J, Sesterhenn I, *Tumors of the kidney. Tumors of the urinary system and male genital organs.* IARC press. WHO classification of tumors, 2004.

24. Grignon, D.J. and M. Che, *Clear cell renal cell carcinoma.* Clin Lab Med, 2005. **25**(2): p. 305-16.

25. Frew, I.J. and H. Moch, *A Clearer View of the Molecular Complexity of Clear Cell Renal Cell Carcinoma.* Annu Rev Pathol, 2014.

26. Sato, Y., et al., *Integrated molecular analysis of clear-cell renal cell carcinoma.* Nat Genet, 2013. **45**(8): p. 860-7.

27. Patard, J.J., et al., *Targeted therapy in renal cell carcinoma.* World J Urol, 2008. **26**(2): p. 135-40.

28. Linehan, W.M., et al., *Molecular diagnosis and therapy of kidney cancer.* Annu Rev Med, 2010. **61**: p. 329-43.

29. Grignon, D.J. and J.N. Eble, *Papillary and metanephric adenomas of the kidney.* Semin Diagn Pathol, 1998. **15**(1): p. 41-53.

30. Delahunt, B. and J.N. Eble, *Papillary renal cell carcinoma: a clinicopathologic and immunohistochemical study of 105 tumors.* Mod Pathol, 1997. **10**(6): p. 537-44.

31. Schmidt, L., et al., *Germline and somatic mutations in the tyrosine kinase domain of the MET proto-oncogene in papillary renal carcinomas.* Nat Genet, 1997. **16**(1): p. 68-73.

32. Jiang, F., et al., *Chromosomal imbalances in papillary renal cell carcinoma: genetic differences between histological subtypes.* Am J Pathol, 1998. **153**(5): p. 1467-73.

33. Brunelli, M., et al., *Gains of chromosomes 7, 17, 12, 16, and 20 and loss of Y occur early in the evolution of papillary renal cell neoplasia: a fluorescent in situ hybridization study.* Mod Pathol, 2003. **16**(10): p. 1053-9.

34. Speicher, M.R., et al., *Specific loss of chromosomes 1, 2, 6, 10, 13, 17, and 21 in chromophobe renal cell carcinomas revealed by comparative genomic hybridization.* Am J Pathol, 1994. **145**(2): p. 356-64.

35. Presti, J.C., Jr., et al., *Comparative genomic hybridization for genetic analysis of renal oncocytomas.* Genes Chromosomes Cancer, 1996. **17**(4): p. 199-204.

36. Gill, I.S., et al., *Clinical practice. Small renal mass.* N Engl J Med, 2010. **362**(7): p. 624-34.

37. Leveridge, M.J., et al., *Outcomes of small renal mass needle core biopsy, nondiagnostic percutaneous biopsy, and the role of repeat biopsy.* Eur Urol, 2011. **60**(3): p. 578-84.

38. Moch, H., et al., *Reassessing the current UICC/AJCC TNM staging for renal cell carcinoma.* Eur Urol, 2009. **56**(4): p. 636-43.

39. Lee, L.S. and M.H. Tan, *Predictive models for the practical management of renal cell carcinoma.* Nat Rev Urol, 2012. **9**(2): p. 73-84.

40. Koul, H., et al., *Molecular aspects of renal cell carcinoma: a review.* Am J Cancer Res, 2011. **1**(2): p. 240-254.

41. Eichelberg, C., et al., *Diagnostic and prognostic molecular markers for renal cell carcinoma: a critical appraisal of the current state of research and clinical applicability.* Eur Urol, 2009. **55**(4): p. 851-63.

42. Delahunt, B., et al., *Grading of clear cell renal cell carcinoma should be based on nucleolar prominence.* Am J Surg Pathol, 2011. **35**(8): p. 1134-9.

43. Bonsib, S.M., *Renal veins and venous extension in clear cell renal cell carcinoma.* Mod Pathol, 2007. **20**(1): p. 44-53.

44. Tang, P.A., M.M. Vickers, and D.Y. Heng, *Clinical and molecular prognostic factors in renal cell carcinoma: what we know so far.* Hematol Oncol Clin North Am, 2011. **25**(4): p. 871-91.

45. Huang, W.C., et al., *Partial nephrectomy versus radical nephrectomy in patients with small renal tumors--is there a difference in mortality and cardiovascular outcomes?* J Urol, 2009. **181**(1): p. 55-61; discussion 61-2.

46. Haferkamp, A., et al., *Renal cell carcinoma with tumor thrombus extension into the vena cava: prospective long-term followup.* J Urol, 2007. **177**(5): p. 1703-8.

47. Bensalah, K. and J.J. Patard, *Kidney cancer in 2010: drugs, surgery and survival in RCC.* Nat Rev Urol, 2011. **8**(2): p. 66-8.

48. Margulis, V., et al., *Renal cell carcinoma clinically involving adjacent organs: experience with aggressive surgical management.* Cancer, 2007. **109**(10): p. 2025-30.

49. Sciarra, A., et al., *The emerging role of targeted therapy in renal cell carcinoma (RCC): is it time for a neoadjuvant or an adjuvant approach?* Crit Rev Oncol Hematol, 2012. **81**(2): p. 151-62.

50. Rini, B.I., S.C. Campbell, and B. Escudier, *Renal cell carcinoma.* Lancet, 2009. **373**(9669): p. 1119-32.

51. Larkin, J., et al., *Second-line treatments for the management of advanced renal cell carcinoma: systematic review and meta-analysis.* Expert Opin Pharmacother, 2013. **14**(1): p. 27-39.

52. Breau, R.H. and B.C. Leibovich, *Therapy for metastatic RCC--questions remain.* Nat Rev Urol, 2009. **6**(11): p. 580-1.

53. Gnarra, J.R., et al., *Mutations of the VHL tumour suppressor gene in renal carcinoma.* Nat Genet, 1994. **7**(1): p. 85-90.

54. Maxwell, P.H., et al., *The tumour suppressor protein VHL targets hypoxia-inducible factors for oxygen-dependent proteolysis.* Nature, 1999. **399**(6733): p. 271-5.

55. Hergovich, A., et al., *Regulation of microtubule stability by the von Hippel-Lindau tumour suppressor protein pVHL.* Nat Cell Biol, 2003. **5**(1): p. 64-70.

56. Thoma, C.R., et al., *pVHL and GSK3beta are components of a primary cilium-maintenance signalling network.* Nat Cell Biol, 2007. **9**(5): p. 588-95.

57. Roe, J.S., et al., *p53 stabilization and transactivation by a von Hippel-Lindau protein.* Mol Cell, 2006. **22**(3): p. 395-405.

58. Lee, S., et al., *Neuronal apoptosis linked to EglN3 prolyl hydroxylase and familial pheochromocytoma genes: developmental culling and cancer.* Cancer Cell, 2005. **8**(2): p. 155-67.

59. Pantuck, A.J., et al., *NF-kappaB-dependent plasticity of the epithelial to mesenchymal transition induced by Von Hippel-Lindau inactivation in renal cell carcinomas.* Cancer Res, 2010. **70**(2): p. 752-61.

60. Welford, S.M., et al., *Renal oxygenation suppresses VHL loss-induced senescence that is caused by increased sensitivity to oxidative stress.* Mol Cell Biol, 2010. **30**(19): p. 4595-603.

61. Thoma, C.R., et al., *VHL loss causes spindle misorientation and chromosome instability.* Nat Cell Biol, 2009. **11**(8): p. 994-1001.

62. Kurban, G., et al., *Collagen matrix assembly is driven by the interaction of von Hippel-Lindau tumor suppressor protein with hydroxylated collagen IV alpha 2.* Oncogene, 2008. **27**(7): p. 1004-12.

63. Hsu, T., et al., *Endocytic function of von Hippel-Lindau tumor suppressor protein regulates surface localization of fibroblast growth factor receptor 1 and cell motility.* J Biol Chem, 2006. **281**(17): p. 12069-80.

64. Chitalia, V.C., et al., *Jade-1 inhibits Wnt signalling by ubiquitylating beta-catenin and mediates Wnt pathway inhibition by pVHL.* Nat Cell Biol, 2008. **10**(10): p. 1208-16.

65. Mikhaylova, O., et al., *The von Hippel-Lindau tumor suppressor protein and Egl-9-Type proline hydroxylases regulate the large subunit of RNA polymerase II in response to oxidative stress.* Mol Cell Biol, 2008. **28**(8): p. 2701-17.

66. Xie, L., et al., *Oxygen-regulated beta(2)-adrenergic receptor hydroxylation by EGLN3 and ubiquitylation by pVHL.* Sci Signal, 2009. **2**(78): p. ra33.

67. Yang, H., et al., *pVHL acts as an adaptor to promote the inhibitory phosphorylation of the NF-kappaB agonist Card9 by CK2.* Mol Cell, 2007. **28**(1): p. 15-27.

68. Mandriota, S.J., et al., *HIF activation identifies early lesions in VHL kidneys: evidence for site-specific tumor suppressor function in the nephron.* Cancer Cell, 2002. **1**(5): p. 459-68.

69. Raval, R.R., et al., *Contrasting properties of hypoxia-inducible factor 1 (HIF-1) and HIF-2 in von Hippel-Lindau-associated renal cell carcinoma.* Mol Cell Biol, 2005. **25**(13): p. 5675-86.

70. Fu, L., et al., *Generation of a mouse model of Von Hippel-Lindau kidney disease leading to renal cancers by expression of a constitutively active mutant of HIF1alpha.* Cancer Res, 2011. **71**(21): p. 6848-56.

71. Shen, C., et al., *Genetic and functional studies implicate HIF1alpha as a 14q kidney cancer suppressor gene.* Cancer Discov, 2011. **1**(3): p. 222-35.

72. Koh, M.Y., et al., *The hypoxia-associated factor switches cells from HIF-1alpha- to HIF-2alpha-dependent signaling promoting stem cell characteristics, aggressive tumor growth and invasion.* Cancer Res, 2011. **71**(11): p. 4015-27.

73. Toschi, A., et al., *Differential dependence of hypoxia-inducible factors 1 alpha and 2 alpha on mTORC1 and mTORC2.* J Biol Chem, 2008. **283**(50): p. 34495-9.

74. Mathew, L.K., et al., *Restricted expression of miR-30c-2-3p and miR-30a-3p in clear cell renal cell carcinomas enhances HIF2alpha activity.* Cancer Discov, 2014. **4**(1): p. 53-60.

75. Xu, J., et al., *Epigenetic regulation of HIF-1alpha in renal cancer cells involves HIF-1alpha/2alpha binding to a reverse hypoxia-response element.* Oncogene, 2012. **31**(8): p. 1065-72.

76. Keith, B., R.S. Johnson, and M.C. Simon, *HIF1alpha and HIF2alpha: sibling rivalry in hypoxic tumour growth and progression.* Nat Rev Cancer, 2012. **12**(1): p. 9-22.

77. Schodel, J., et al., *High-resolution genome-wide mapping of HIF-binding sites by ChIP-seq.* Blood, 2011. **117**(23): p. e207-17.

78. Kaelin, W.G., Jr., *The von Hippel-Lindau tumour suppressor protein: O2 sensing and cancer.* Nat Rev Cancer, 2008. **8**(11): p. 865-73.

79. Lau, K.W., et al., *Target gene selectivity of hypoxia-inducible factor-alpha in renal cancer cells is conveyed by post-DNA-binding mechanisms.* Br J Cancer, 2007. **96**(8): p. 1284-92.

80. Shen, C. and W.G. Kaelin, Jr., *The VHL/HIF axis in clear cell renal carcinoma.* Semin Cancer Biol, 2013. **23**(1): p. 18-25.

81. Haase, V.H., *Renal cancer: oxygen meets metabolism.* Exp Cell Res, 2012. **318**(9): p. 1057-67.

82. Papandreou, I., et al., *HIF-1 mediates adaptation to hypoxia by actively downregulating mitochondrial oxygen consumption.* Cell Metab, 2006. **3**(3): p. 187-97.

83. Zhang, H., et al., *HIF-1 inhibits mitochondrial biogenesis and cellular respiration in VHL-deficient renal cell carcinoma by repression of C-MYC activity.* Cancer Cell, 2007. **11**(5): p. 407-20.

84. Christofk, H.R., et al., *Pyruvate kinase M2 is a phosphotyrosine-binding protein.* Nature, 2008. **452**(7184): p. 181-6.

85. Maroto, P. and B. Rini, *Molecular biomarkers in advanced renal cell carcinoma.* Clin Cancer Res, 2014. **20**(8): p. 2060-71.

86. Ngo, T.C., C.G. Wood, and J.A. Karam, *Biomarkers of renal cell carcinoma.* Urol Oncol, 2014. **32**(3): p. 243-51.

87. Li, L., et al., *DNA methylation in peripheral blood: a potential biomarker for cancer molecular epidemiology.* J Epidemiol, 2012. **22**(5): p. 384-94.

88. Ganti, S. and R.H. Weiss, *Urine metabolomics for kidney cancer detection and biomarker discovery.* Urol Oncol, 2011. **29**(5): p. 551-7.

89. Wykoff, C.C., et al., *Hypoxia-inducible expression of tumor-associated carbonic anhydrases.* Cancer Res, 2000. **60**(24): p. 7075-83.

90. Zhao, A., et al., *Serum miR-210 as a novel biomarker for molecular diagnosis of clear cell renal cell carcinoma.* Exp Mol Pathol, 2013. **94**(1): p. 115-20.

91. Jacobsen, J., et al., *Expression of vascular endothelial growth factor protein in human renal cell carcinoma.* BJU Int, 2004. **93**(3): p. 297-302.

92. Schraml, P., et al., *VHL mutations and their correlation with tumour cell proliferation, microvessel density, and patient prognosis in clear cell renal cell carcinoma.* J Pathol, 2002. **196**(2): p. 186-93.

93. Lidgren, A., et al., *Hypoxia-inducible factor 1alpha expression in renal cell carcinoma analyzed by tissue microarray.* Eur Urol, 2006. **50**(6): p. 1272-7.

94. Bui, M.H., et al., *Prognostic value of carbonic anhydrase IX and KI67 as predictors of survival for renal clear cell carcinoma.* J Urol, 2004. **171**(6 Pt 1): p. 2461-6.

95. Wu, X., et al., *Identification of a 4-microRNA signature for clear cell renal cell carcinoma metastasis and prognosis.* PLoS One, 2012. **7**(5): p. e35661.

96. Michigan, A., T.V. Johnson, and V.A. Master, *Preoperative C-reactive protein level adjusted for comorbidities and lifestyle factors predicts overall mortality in localized renal cell carcinoma.* Mol Diagn Ther, 2011. **15**(4): p. 229-34.

97. Thompson, R.H., et al., *Tumor B7-H1 is associated with poor prognosis in renal cell carcinoma patients with long-term follow-up.* Cancer Res, 2006. **66**(7): p. 3381-5.

98. Tollefson, M.K., et al., *Ki-67 and coagulative tumor necrosis are independent predictors of poor outcome for patients with clear cell renal cell carcinoma and not surrogates for each other.* Cancer, 2007. **110**(4): p. 783-90.

99. Byun, S.S., et al., *Expression of survivin in renal cell carcinomas: association with pathologic features and clinical outcome.* Urology, 2007. **69**(1): p. 34-7.

100. Zigeuner, R., et al., *Biologic significance of fascin expression in clear cell renal cell carcinoma: systematic analysis of primary and metastatic tumor tissues using a tissue microarray technique.* Urology, 2006. **68**(3): p. 518-22.

101. Gibney, G.T., et al., *c-Met is a prognostic marker and potential therapeutic target in clear cell renal cell carcinoma.* Ann Oncol, 2013. **24**(2): p. 343-9.

102. Hoffmann, N.E., et al., *External validation of IMP3 expression as an independent prognostic marker for metastatic progression and death for patients with clear cell renal cell carcinoma.* Cancer, 2008. **112**(7): p. 1471-9.

103. Boysen, G., et al., *Identification and functional characterization of pVHL-dependent cell surface proteins in renal cell carcinoma.* Neoplasia, 2012. **14**(6): p. 535-46.

104. Croft, M., *The role of TNF superfamily members in T-cell function and diseases.* Nat Rev Immunol, 2009. **9**(4): p. 271-85.

105. Goodwin, R.G., et al., *Molecular and biological characterization of a ligand for CD27 defines a new family of cytokines with homology to tumor necrosis factor.* Cell, 1993. **73**(3): p. 447-56.

106. Grewal, I.S., *CD70 as a therapeutic target in human malignancies.* Expert Opin Ther Targets, 2008. **12**(3): p. 341-51.

107. Peitsch, M.C. and J. Tschopp, *Comparative molecular modelling of the Fas-ligand and other members of the TNF family.* Mol Immunol, 1995. **32**(10): p. 761-72.

108. Watts, T.H., *TNF/TNFR family members in costimulation of T cell responses.* Annu Rev Immunol, 2005. **23**: p. 23-68.

109. Hishima, T., et al., *CD70 expression in thymic carcinoma.* Am J Surg Pathol, 2000. **24**(5): p. 742-6.

110. Laouar, A., et al., *CD70+ antigen-presenting cells control the proliferation and differentiation of T cells in the intestinal mucosa.* Nat Immunol, 2005. **6**(7): p. 698-706.

111. Tesselaar, K., et al., *Expression of the murine CD27 ligand CD70 in vitro and in vivo.* J Immunol, 2003. **170**(1): p. 33-40.

112. Sanchez, P.J., et al., *Combined TLR/CD40 stimulation mediates potent cellular immunity by regulating dendritic cell expression of CD70 in vivo.* J Immunol, 2007. **178**(3): p. 1564-72.

113. Lens, S.M., et al., *Antigen-presenting cell-derived signals determine expression levels of CD70 on primed T cells.* Immunology, 1997. **90**(1): p. 38-45.

114. Hintzen, R.Q., et al., *Characterization of the human CD27 ligand, a novel member of the TNF gene family.* J Immunol, 1994. **152**(4): p. 1762-73.

115. Loenen, W.A., et al., *The CD27 membrane receptor, a lymphocyte-specific member of the nerve growth factor receptor family, gives rise to a soluble form by protein processing that does not involve receptor endocytosis.* Eur J Immunol, 1992. **22**(2): p. 447-55.

116. Lens, S.M., et al., *Control of lymphocyte function through CD27-CD70 interactions.* Semin Immunol, 1998. **10**(6): p. 491-9.

117. Nolte, M.A., et al., *Timing and tuning of CD27-CD70 interactions: the impact of signal strength in setting the balance between adaptive responses and immunopathology.* Immunol Rev, 2009. **229**(1): p. 216-31.

118. Hamann, D., et al., *Evidence that human CD8+CD45RA+CD27- cells are induced by antigen and evolve through extensive rounds of division.* Int Immunol, 1999. **11**(7): p. 1027-33.

119. Akiba, H., et al., *CD27, a member of the tumor necrosis factor receptor superfamily, activates NF-kappaB and stress-activated protein kinase/c-Jun N-terminal kinase via TRAF2, TRAF5, and NF-kappaB-inducing kinase.* J Biol Chem, 1998. **273**(21): p. 13353-8.

120. Prasad, K.V., et al., *CD27, a member of the tumor necrosis factor receptor family, induces apoptosis and binds to Siva, a proapoptotic protein.* Proc Natl Acad Sci U S A, 1997. **94**(12): p. 6346-51.

121. Arens, R., et al., *Signaling through CD70 regulates B cell activation and IgG production.* J Immunol, 2004. **173**(6): p. 3901-8.

122. Omasits, U., et al., *Protter: interactive protein feature visualization and integration with experimental proteomic data.* Bioinformatics, 2014. **30**(6): p. 884-6.

123. Junker, K., et al., *CD70: a new tumor specific biomarker for renal cell carcinoma.* J Urol, 2005. **173**(6): p. 2150-3.

124. Adam, P.J., et al., *CD70 (TNFSF7) is expressed at high prevalence in renal cell carcinomas and is rapidly internalised on antibody binding.* Br J Cancer, 2006. **95**(3): p. 298-306.

125. Law, C.L., et al., *Lymphocyte activation antigen CD70 expressed by renal cell carcinoma is a potential therapeutic target for anti-CD70 antibody-drug conjugates.* Cancer Res, 2006. **66**(4): p. 2328-37.

126. Jilaveanu, L.B., et al., *CD70 expression patterns in renal cell carcinoma.* Hum Pathol, 2012. **43**(9): p. 1394-9.

127. Held-Feindt, J. and R. Mentlein, *CD70/CD27 ligand, a member of the TNF family, is expressed in human brain tumors.* Int J Cancer, 2002. **98**(3): p. 352-6.

128. Agathanggelou, A., et al., *Expression of immune regulatory molecules in Epstein-Barr virus-associated nasopharyngeal carcinomas with prominent lymphoid stroma. Evidence for a functional interaction between epithelial tumor cells and infiltrating lymphoid cells.* Am J Pathol, 1995. **147**(4): p. 1152-60.

129. Diegmann, J., et al., *Immune escape for renal cell carcinoma: CD70 mediates apoptosis in lymphocytes.* Neoplasia, 2006. **8**(11): p. 933-8.

130. Wang, Q.J., et al., *Distinctive features of the differentiated phenotype and infiltration of tumor-reactive lymphocytes in clear cell renal cell carcinoma.* Cancer Res, 2012. **72**(23): p. 6119-29.

131. Claus, C., et al., *CD27 signaling increases the frequency of regulatory T cells and promotes tumor growth.* Cancer Res, 2012. **72**(14): p. 3664-76.

132. Arens, R., et al., *Cutting edge: CD95 maintains effector T cell homeostasis in chronic immune activation.* J Immunol, 2005. **174**(10): p. 5915-20.

133. Oflazoglu, E., et al., *Potent anticarcinoma activity of the humanized anti-CD70 antibody h1F6 conjugated to the tubulin inhibitor auristatin via an uncleavable linker.* Clin Cancer Res, 2008. **14**(19): p. 6171-80.

134. Ryan, M.C., et al., *Targeting pancreatic and ovarian carcinomas using the auristatin-based anti-CD70 antibody-drug conjugate SGN-75.* Br J Cancer, 2010. **103**(5): p. 676-84.

135. Jeffrey, S.C., et al., *A potent anti-CD70 antibody-drug conjugate combining a dimeric pyrrolobenzodiazepine drug with site-specific conjugation technology.* Bioconjug Chem, 2013. **24**(7): p. 1256-63.

136. Tannir, N.M., et al., *Phase I dose-escalation study of SGN-75 in patients with CD70-positive relapsed/refractory non-Hodgkin lymphoma or metastatic renal cell carcinoma.* Invest New Drugs, 2014. **32**(6): p. 1246-57.

137. Jiang, H., et al., *Demethylation of TNFSF7 contributes to CD70 overexpression in CD4+ T cells from patients with systemic sclerosis.* Clin Immunol, 2012. **143**(1): p. 39-44.

138. Lu, Q., A. Wu, and B.C. Richardson, *Demethylation of the same promoter sequence increases CD70 expression in lupus T cells and T cells treated with lupus-inducing drugs.* J Immunol, 2005. **174**(10): p. 6212-9.

139. Ma, L., et al., *Increased expressions of DNA methyltransferases contribute to CD70 promoter hypomethylation and over expression of CD70 in ITP.* Mol Immunol, 2011. **48**(12-13): p. 1525-31.

140. Yin, H., et al., *Hypomethylation and overexpression of CD70 (TNFSF7) in CD4+ T cells of patients with primary Sjogren's syndrome.* J Dermatol Sci, 2010. **59**(3): p. 198-203.

141. Zhao, M., et al., *Epigenetics and SLE: RFX1 downregulation causes CD11a and CD70 overexpression by altering epigenetic modifications in lupus CD4+ T cells.* J Autoimmun, 2010. **35**(1): p. 58-69.

142. Yu, S.E., S.H. Park, and Y.K. Jang, *Epigenetic silencing of TNFSF7 (CD70) by DNA methylation during progression to breast cancer.* Mol Cells, 2010. **29**(2): p. 217-21.

143. Petrau, C., et al., *CD70: A Potential Target in Breast Cancer?* J Cancer, 2014. **5**(9): p. 761-4.

144. Casagrande, S., et al., *The protein tyrosine phosphatase receptor type J is regulated by the pVHL-HIF axis in clear cell renal cell carcinoma.* J Pathol, 2013. **229**(4): p. 525-34.

145. Beleut, M., et al., *Integrative genome-wide expression profiling identifies three distinct molecular subgroups of renal cell carcinoma with different patient outcome.* BMC Cancer, 2012. **12**: p. 310.

146. Herrmann, E., et al., *Prognostic factors of papillary renal cell carcinoma: results from a multi-institutional series after pathological review.* J Urol, 2010. **183**(2): p. 460-6.

147. Sika-Paotonu, D., et al., *Nucleolar grade but not Fuhrman grade is applicable to papillary renal cell carcinoma.* Am J Surg Pathol, 2006. **30**(9): p. 1091-6.

148. Moch, H., et al., *Prognostic utility of the recently recommended histologic classification and revised TNM staging system of renal cell carcinoma: a Swiss experience with 588 tumors.* Cancer, 2000. **89**(3): p. 604-14.

149. Wischhusen, J., et al., *Identification of CD70-mediated apoptosis of immune effector cells as a novel immune escape pathway of human glioblastoma.* Cancer Res, 2002. **62**(9): p. 2592-9.

150. Blom, N., et al., *Prediction of post-translational glycosylation and phosphorylation of proteins from the amino acid sequence.* Proteomics, 2004. **4**(6): p. 1633-49.

151. Rechsteiner, M.P., et al., *VHL gene mutations and their effects on hypoxia inducible factor HIFalpha: identification of potential driver and passenger mutations.* Cancer Res, 2011. **71**(16): p. 5500-11.

152. Worth, C.L., R. Preissner, and T.L. Blundell, *SDM--a server for predicting effects of mutations on protein stability and malfunction.* Nucleic Acids Res, 2011. **39**(Web Server issue): p. W215-22.

153. Russell, R.C. and M. Ohh, *The role of VHL in the regulation of E-cadherin: a new connection in an old pathway.* Cell Cycle, 2007. **6**(1): p. 56-9.

154. Singaravelu, K. and B.J. Padanilam, *p53 target Siva regulates apoptosis in ischemic kidneys.* Am J Physiol Renal Physiol, 2011. **300**(5): p. F1130-41.

155. Hintzen, R.Q., et al., *A soluble form of the human T cell differentiation antigen CD27 is released after triggering of the TCR/CD3 complex.* J Immunol, 1991. **147**(1): p. 29-35.

156. Nilsson, A., et al., *Expression of CD27-CD70 on early B cell progenitors in the bone marrow: implication for diagnosis and therapy of childhood ALL.* Exp Hematol, 2005. **33**(12): p. 1500-7.

157. Yoshino, K., et al., *Expression of CD70 in nasal natural killer/T cell lymphoma cell lines and patients; its role for cell proliferation through binding to soluble CD27.* Br J Haematol, 2013. **160**(3): p. 331-42.

158. Chahlavi, A., et al., *Glioblastomas induce T-lymphocyte death by two distinct pathways involving gangliosides and CD70.* Cancer Res, 2005. **65**(12): p. 5428-38.

159. Aulwurm, S., et al., *Immune stimulatory effects of CD70 override CD70-mediated immune cell apoptosis in rodent glioma models and confer long-lasting antiglioma immunity in vivo.* Int J Cancer, 2006. **118**(7): p. 1728-35.

160. Tesselaar, K., et al., *Lethal T cell immunodeficiency induced by chronic costimulation via CD27-CD70 interactions.* Nat Immunol, 2003. **4**(1): p. 49-54.

161. Wherry, E.J., *T cell exhaustion.* Nat Immunol, 2011. **12**(6): p. 492-9.

162. Quigley, M., et al., *Transcriptional analysis of HIV-specific CD8+ T cells shows that PD-1 inhibits T cell function by upregulating BATF.* Nat Med, 2010. **16**(10): p. 1147-51.

163. Crespo, J., et al., *T cell anergy, exhaustion, senescence, and stemness in the tumor microenvironment.* Curr Opin Immunol, 2013. **25**(2): p. 214-21.

164. Gatza, C.E., S.Y. Oh, and G.C. Blobe, *Roles for the type III TGF-beta receptor in human cancer.* Cell Signal, 2010. **22**(8): p. 1163-74.

165. Yuen, J.S., et al., *Inhibition of angiogenic and non-angiogenic targets by sorafenib in renal cell carcinoma (RCC) in a RCC xenograft model.* Br J Cancer, 2011. **104**(6): p. 941-7.

166. Herman, J.G., et al., *Silencing of the VHL tumor-suppressor gene by DNA methylation in renal carcinoma.* Proc Natl Acad Sci U S A, 1994. **91**(21): p. 9700-4.

167. Lai, Y., et al., *Proteomic dissection of the von Hippel-Lindau (VHL) interactome.* J Proteome Res, 2011. **10**(11): p. 5175-82.

168. Cai, Q. and E.S. Robertson, *Ubiquitin/SUMO modification regulates VHL protein stability and nucleocytoplasmic localization.* PLoS One, 2010. **5**(9).

169. Wouters, B.G. and M. Koritzinsky, *Hypoxia signalling through mTOR and the unfolded protein response in cancer.* Nat Rev Cancer, 2008. **8**(11): p. 851-64.

170. Fu, L., et al., *Activation of HIF2alpha in kidney proximal tubule cells causes abnormal glycogen deposition but not tumorigenesis.* Cancer Res, 2013. **73**(9): p. 2916-25.

171. Gordan, J.D., et al., *HIF-alpha effects on c-Myc distinguish two subtypes of sporadic VHL-deficient clear cell renal carcinoma.* Cancer Cell, 2008. **14**(6): p. 435-46.

172. Hedrich, C.M. and T. Rauen, *Epigenetic patterns in systemic sclerosis and their contribution to attenuated CD70 signaling cascades.* Clin Immunol, 2012. **143**(1): p. 1-3.

173. Liu, N., et al., *Increased CD70 expression is associated with clinical resistance to cisplatin-based chemotherapy and poor survival in advanced ovarian carcinomas.* Onco Targets Ther, 2013. **6**: p. 615-9.

174. Bertrand, P., et al., *The costimulatory molecule CD70 is regulated by distinct molecular mechanisms and is associated with overall survival in diffuse large B-cell lymphoma.* Genes Chromosomes Cancer, 2013. **52**(8): p. 764-74.

175. Huang, J., et al., *Soluble CD27-pool in humans may contribute to T cell activation and tumor immunity.* J Immunol, 2013. **190**(12): p. 6250-8.

176. Hendriks, J., Y. Xiao, and J. Borst, *CD27 promotes survival of activated T cells and complements CD28 in generation and establishment of the effector T cell pool.* J Exp Med, 2003. **198**(9): p. 1369-80.

177. Keller, A.M., et al., *Expression of costimulatory ligand CD70 on steady-state dendritic cells breaks CD8+ T cell tolerance and permits effective immunity.* Immunity, 2008. **29**(6): p. 934-46.

178. Roberts, D.J., et al., *Control of established melanoma by CD27 stimulation is associated with enhanced effector function and persistence, and reduced PD-1 expression of tumor infiltrating CD8(+) T cells.* J Immunother, 2010. **33**(8): p. 769-79.

179. Arens, R., et al., *Tumor rejection induced by CD70-mediated quantitative and qualitative effects on effector CD8+ T cell formation.* J Exp Med, 2004. **199**(11): p. 1595-605.

180. Riether, C., C. Schurch, and A.F. Ochsenbein, *Modulating CD27 signaling to treat cancer.* Oncoimmunology, 2012. **1**(9): p. 1604-1606.

181. Ciccarelli, B.T., et al., *Soluble CD27 is a faithful marker of disease burden and is unaffected by the rituximab-induced IgM flare, as well as by plasmapheresis, in patients with Waldenstrom's macroglobulinemia.* Clin Lymphoma Myeloma, 2009. **9**(1): p. 56-8.

182. De Milito, A., et al., *Plasma levels of soluble CD27: a simple marker to monitor immune activation during potent antiretroviral therapy in HIV-1-infected subjects.* Clin Exp Immunol, 2002. **127**(3): p. 486-94.

183. Thomas, L.J., et al., *Targeting human CD27 with an agonist antibody stimulates T-cell activation and antitumor immunity.* Oncoimmunology, 2014. **3**(1): p. e27255.

184. Conti, A., et al., *Progress of Molecular Targeted Therapies for Advanced Renal Cell Carcinoma.* Biomed Res Int, 2013. **2013**: p. 419176.

185. Schildknecht, A., et al., *Priming of CD8+ T cell responses by pathogens typically depends on CD70-mediated interactions with dendritic cells.* Eur J Immunol, 2007. **37**(3): p. 716-28.

186. Kellie, S., et al., *The tyrosine phosphatase DEP-1 induces cytoskeletal rearrangements, aberrant cell-substratum interactions and a reduction in cell proliferation.* J Cell Sci, 2004. **117**(Pt 4): p. 609-18.

187. Trapasso, F., et al., *Restoration of receptor-type protein tyrosine phosphatase eta function inhibits human pancreatic carcinoma cell growth in vitro and in vivo.* Carcinogenesis, 2004. **25**(11): p. 2107-14.

188. Keane, M.M., et al., *The protein tyrosine phosphatase DEP-1 is induced during differentiation and inhibits growth of breast cancer cells.* Cancer Res, 1996. **56**(18): p. 4236-43.

189. Tarcic, G., et al., *An unbiased screen identifies DEP-1 tumor suppressor as a phosphatase controlling EGFR endocytosis.* Curr Biol, 2009. **19**(21): p. 1788-98.

190. Dong, M., et al., *The type III TGF-beta receptor suppresses breast cancer progression.* J Clin Invest, 2007. **117**(1): p. 206-17.

191. Hempel, N., et al., *Loss of betaglycan expression in ovarian cancer: role in motility and invasion.* Cancer Res, 2007. **67**(11): p. 5231-8.

192. Turley, R.S., et al., *The type III transforming growth factor-beta receptor as a novel tumor suppressor gene in prostate cancer.* Cancer Res, 2007. **67**(3): p. 1090-8.

193. Gordon, K.J., et al., *Loss of type III transforming growth factor beta receptor expression increases motility and invasiveness associated with epithelial to mesenchymal transition during pancreatic cancer progression.* Carcinogenesis, 2008. **29**(2): p. 252-62.

194. Finger, E.C., et al., *Endocytosis of the type III transforming growth factor-beta (TGF-beta) receptor through the clathrin-independent/lipid raft pathway regulates TGF-beta signaling and receptor down-regulation.* J Biol Chem, 2008. **283**(50): p. 34808-18.

195. Mythreye, K. and G.C. Blobe, *The type III TGF-beta receptor regulates epithelial and cancer cell migration through beta-arrestin2-mediated activation of Cdc42.* Proc Natl Acad Sci U S A, 2009. **106**(20): p. 8221-6.

196. Hempel, N., et al., *Expression of the type III TGF-beta receptor is negatively regulated by TGF-beta.* Carcinogenesis, 2008. **29**(5): p. 905-12.

197. Vicencio, A.G., et al., *Regulation of TGF-beta ligand and receptor expression in neonatal rat lungs exposed to chronic hypoxia.* J Appl Physiol (1985), 2002. **93**(3): p. 1123-30.

198. Lopez-Casillas, F., et al., *Structure and expression of the membrane proteoglycan betaglycan, a component of the TGF-beta receptor system.* Cell, 1991. **67**(4): p. 785-95.

199. Ingold, B., et al., *Renal cell carcinoma marker reliably discriminates central nervous system haemangioblastoma from brain metastases of renal cell carcinoma.* Histopathology, 2008. **52**(6): p. 674-81.

200. Wyler, L., et al., *Brain metastasis in renal cancer patients: metastatic pattern, tumour-associated macrophages and chemokine/chemoreceptor expression.* Br J Cancer, 2014. **110**(3): p. 686-94.

201. Dahinden, C., et al., *Mining tissue microarray data to uncover combinations of biomarker expression patterns that improve intermediate staging and grading of clear cell renal cell cancer.* Clin Cancer Res, 2010. **16**(1): p. 88-98.

202. Staller, P., et al., *Chemokine receptor CXCR4 downregulated by von Hippel-Lindau tumour suppressor pVHL.* Nature, 2003. **425**(6955): p. 307-11.

203. Hergovich, A., et al., *Priming-dependent phosphorylation and regulation of the tumor suppressor pVHL by glycogen synthase kinase 3.* Mol Cell Biol, 2006. **26**(15): p. 5784-96.

204. Pawlowski, R., et al., *Loss of PBRM1 expression is associated with renal cell carcinoma progression.* Int J Cancer, 2013. **132**(2): p. E11-7.

205. Metzen, E., et al., *Regulation of the prolyl hydroxylase domain protein 2 (phd2/egln-1) gene: identification of a functional hypoxia-responsive element.* Biochem J, 2005. **387**(Pt 3): p. 711-7.

# 12 Curriculum vitae

**Melanie Ruf**
* 28.06.1986
Illnauerstrasse 13
CH-8307 Effretikon
+41 (0) 786231121
Melanie.Ruf@usz.ch
Nationality: german

## Education and Research Experience

| | |
|---|---|
| 08.2011 - Spring 2015 | **PhD thesis at University Hospital Zurich, Institute of Surgical Pathology, Zurich Switzerland** with Holger Moch, MD, Graduate student of the Cancer Biology PhD Program, Life Science Graduate School Zurich, University Zurich<br>"Characterization of the RCC protein surfaceome for clinical applications." |
| 07. 2009 - 03.2011 | **Master of BioSciences, Division of Cell Biology, University of Kaiserslautern, Germany**<br>Major: Cell Biology, Practical courses: Proteomics / Protein Function, Functional Protein Expression, Cellular Physiology/ Membrane Transport, Average Grade 1.0 (very good) |
| 06.2010 – 03.2011 | **Master thesis**: "Redox dynamics of human Mia40 - Glutathione and ALR are the main determinants of the redox state of Mia40", Grade: 1.0 (very good) |
| 10.2006 - 06.2009 | **Bachelor of BioSciences, Division of Cell Biology, University of Kaiserslautern, Germany**<br>**Bachelor thesis**: "Identification of potential mitochondrial glutathione carriers" with grade 1.0 (very good). Average grade 2.0 (good) |
| 09.1997 – 06.2006 | **University entrance exam (Abitur), Friedrich-Hecker-Gymnasium, Radolfzell a. B, Germany**<br>Mathematics: 13 credits; Biology: 12 credits (with 15 credits being the best). Average grade 2.2 (with grade 1.0 being the best). |

## Work experience

08.2011 - Spring 2015 **Research assistant, Institute of Surgical Pathology, University Hospital Zurich, Switzerland**

- PhD research project: Clinical applicability of renal cell carcinoma biomarkers
- Collection and biobanking renal cell carcinoma patients' blood, Urology Department
- Teaching assistant in a genetics course
- Coordination of lab meetings

03.2011 - 06.2011 **Student research assistant, Division of Cell Biology, University of Kaiserslautern, Germany**

- Assisting a PhD project on redox-biology

11.2009 - 03.2010 **Lab rotation, Centre of Molecular Biology Heidelberg (ZMBH), Heidelberg University, Germany**

- Assisting a PhD project on intramembrane proteolysis

11.2008 - 01.2009 **Student research assistant, Division of Animal Physiology, University of Kaiserslautern, Germany**

- Assisting a PhD project on neurodegenerative diseases

07.2008 - 08.2008 **Industrial placement, Laboratory Medicine Singen am Hohentwiel, Germany**

- Bacteriological analyses

## Extra-curricular activities

**Organization of the Cancer Network Zurich Student Retreat 2014, April 12- 14, 2014, CH-Filzbach**

- Organizing international guest speakers, funding and designing a meeting booklet

**Students Representative of the Cancer Network Zurich since April 2014**

- PhD recruitment weeks, (twice a year), getting PhD students with new candidates together
- Organizing social activities for the Cancer Biology PhD students (Christmas event, barbeque)
- Attending meetings of the steering committee Cancer Network Zurich

## Language skills

Native: German

Fluent: English

Basic: Italian and French

## IT skills

MS Office, Corel Draw, SPSS, Graph Pad Prism

## Personal interests

Hiking, snowboarding; climbing;

## Publications

pVHL/HIF-regulated CD70 expression is associated with infiltration of $CD27^+$ lymphocytes and increased serum levels of soluble CD27 in clear cell renal cell carcinoma. Ruf M, Mittmann C, Nowicka AM, Hartmann A, Hermanns T, Poyet C, van den Broek M, Sulser T, Moch H, Schraml P. Clin Cancer Research, 2014 Dec.

The protein tyrosine phosphatase receptor type J is regulated by the pVHL/HIF axis in clear cell renal cell carcinoma. Casagrande S, **Ruf M**, Rechsteiner M, Morra L, Brun-Schmid S, von Teichman A, Krek W, Schraml P, Moch H. J Pathol. 2013 Mar;229(4):525-34.

## Awards and Scholarships

| | |
|---|---|
| May 2013, Heidelberg, Germany | **German Society of Pathology Poster Price** (rewarded with 1000 €), 97. Annual meeting |
| December 2013, Zurich | **Hartmann Müller Stiftung Travel Grant** (1000 CHF) for Keystone Symposium |
| January 2013, Zurich | **Cancer Network Zurich Travel Grant** (1000 CHF) for AACR conference |
| December 2012, Zurich | **Hartmann Müller Stiftung Travel Grant** (1000 CHF) for AACR conference |

## Attendance of Conferences

| | |
|---|---|
| January 2015, Zurich | **12th Charles Rodolphe Brupbacher Symposium**: Breakthroughs in Cancer Research and Therapy |
| January 2014, Breckenridge, CO | **Keystone Symposium**: Hypoxia: Sensing and Signaling |
| May 2013, Heidelberg, Germany | 97. Annual meeting of the **German Society of Pathology e. V.** |
| February 2013, Maui, HI | **AACR/JCA Joint Conference**: Breakthroughs in Basic and Translational Cancer Research |
| January 2013, Zurich | **11th Charles Rodolphe Brupbacher Symposium**: Breakthroughs in Cancer Research and Therapy |
| June 2012, Venice, IT | **Leopoldina Symposium**: Molecular Diagnostics – Today and Tomorrow |

# 13 Acknowledgements

My sincere thanks to Prof. Holger Moch for giving me the opportunity and support to work on this exciting project for my PhD in his research group.

In addition I would like to thank the remaining members of my committee, Prof. Burkhard Becher, Prof. Lukas Sommer, Prof. Bernd Wollscheid and Dr. Peter Schraml for the fruitful discussions and valuable suggestions during our meetings.

Many thanks go to Dr. Peter Schraml for supervising my projects and for his advice throughout my PhD.

The collaboration with Dr. Cédric Poyet, Dr. Thomas Hermanns and Alexandra Veloudios from the department of Urology was of great value for my project.

I also appreciate the collaborations with Prof. Maries van den Broek and Prof. Arndt Hartmann.

My thanks for technical assistance in the lab go to Christiane Mittmann, Martina Storz, Adriana von Teichmann, Sonja Brun-Schmid, Annette Bohnert, Peggy Tzscheetzsch, André Fitsche, Marcel Glönkner, André Wethmar, Monika Bieri, Norbert Wey and especially to Susanne Dettwiler for taking care about everything in the lab and beyond.

I would like to thank Dr. Markus Rechsteiner for his advice and the other lab members of the whole Institute, namely Dorothee Pflüger, Caroline Razafinjatovo, Anna M. Nocwicka, Claudia Corrò, Magda Lukamowics-Rajska, Marion Bawohl, Timo Böge, Friedericke Böhm, Monika Wolf, Mohsen Malehmir, Renaud Maire, Maria Zimmermann-Dours, Dieter Zimmermann, Ruben Casanova, Elisa Bianchi, Adi Kashyap, Alex Soltermann, Nadja Valtcheva, Christine Fritz, Ed Fritz, Qing Zhong and Uli Wagner for creating such a nice working atmosphere. I hope that the friendships will last for years to come.

I also like to thank my dear friend Hella Bolck I have spent a nice time with in Zurich.

I am very thankful for the loving care of my mum, my dad, my brother and my grandmother which well prepared me for my path of life.

My biggest thank goes to Matze for realizing our dreams.